Design of a 3D-Printed Soft Robotic Hand with Distributed Tactile Sensing for Multi-grasp Object Identification

Oliver Shorthose

St. Hugh's College, University of Oxford

Supervisor: Perla Maiolino

A thesis submitted for the degree of

Doctor of Philosophy

December 15, 2023

Abstract

Tactile object identification is essential in environments where vision is occluded or when intrinsic object properties such as weight or stiffness need to be discriminated between. The robotic approach to this task has traditionally been to use rigid-bodied robots equipped with complex control schemes to explore different objects. However, whilst varying degrees of success have been demonstrated, these approaches are limited in their generalisability due to the complexity of the control schemes required to facilitate safe interactions with diverse objects. In this regard, Soft Robotics has garnered increased attention in the past decade due to the ability to exploit *Morphological Computation* through the agent's body to simplify the task by conforming naturally to the geometry of objects being explored. This exists as a paradigm shift in the design of robots since Soft Robotics seeks to take inspiration from biological solutions and embody adaptability in order to interact with the environment rather than relying on centralised computation.

In this thesis, we formulate, simplify, and solve an object identification task using Soft Robotic principles. We design an anthropomorphic hand that has human-like range of motion and compliance in the actuation and sensing. The range of motion is validated through the Feix GRASP taxonomy and the Kapandji Thumb Opposition test. The hand is monolithically fabricated using multi-material 3D printing to enable the exploitation of different material properties within the same body and limit variability between samples. The hand's compliance facilitates adaptable grasping of a wide range of objects and features integrated distributed tactile sensing. We emulate the human approach of integrating information from multiple contacts and grasps of objects to discriminate between them. Two bespoke neural networks are designed to extract patterns from both the tactile data and the relationships between grasps to facilitate high classification accuracy.

Acknowledgments

My deepest thanks go to my supervisor Perla. It has been an honour to be your first student and I hope to have done you proud through such a unique explorative journey. Without your unerring encouragement and energy, there is no doubt I would not have reached this stage.

To everyone at the ORI, thanks for fostering such a positive, diverse and supportive atmosphere. There's no end to the talent that walks through these doors and I have learnt so much about a bizarrely broad range of topics. To Ale and Liang, thank you for the support throughout my degree and the great experiences all over the world. To Nick, your positivity and kindness comes from the top and radiates through the ORI. To Chris, Simon, Matt and Wayne, thanks for giving me pointers on anything hardware related and helping to get my work off the ground. Owen, Lara, Rowan, Jack, Marc, Frank, Efimiya, Yao and Gi, it's always a pleasure to have friendly faces around, and thanks for always lending an ear when needed. To the SRL, you're in good hands and I'm excited to watch the lab's development in years to come.

To Professors Hills and Howey, thank you for your kindness, patience and support during my period of concussion.

Outside of work, an enormous amount of gratitude goes to the clubs that have given me innumerable memories and friends. OURFC, OUHC and Vinnies, whilst I may have spent far too much time away from work on the extracurricular scene, having that outlet and meeting so many people make that time invaluable. To all the Vinnies members in particular, and Gonz especially, thank you for making the last nine years so fun.

To Marston Kitchen, Lucy and Shona, whilst we didn't quite become the influencers we dreamt of, I wouldn't replace you for anyone. Thanks for putting up with me over the years and here's to many more.

Finally, the most important foundation in my life, my family. To my best friend and brother, Matt, thank you for everything you do for me and for always being there. I count myself so lucky to have a constant source of sage advice and guidance in you. To my extended family, aunts, uncles and cousins, thanks for always giving me a positive boost at any occasion and all your continued support.

Mum and Dad, I cannot encapsulate the immense gratitude I have for you both in just this space. Thank you for everything that you have done and continue to do for Matt and me. This work is dedicated to you.

Contents

List of Acronyms and Abbreviations

CNN	Convolutional Neural Network
DEAP	Dielectric Electroactive Polymers
DIP	Distal Interphalangeal (Joint)
DOF	Degrees of Freedom
EDAMS	Encoder-Decoder Architecture for Multi-grasp Soft Sensing
ED	Encoder-Decoder
ER	Electro-rheological (fluid)
FDM	Fused Deposition Modelling
FEA	Fluidic Elastomer Actuator
FEM	Finite Element Method
FFNN	Feed Forward Neural Network
GRU	Gated Recurrent Unit
ICRA	International Conference on Robotics and Automation
IEAP	Ionic Electroactive Polymer
KNN	K-Nearest Neighbours
LSTM	Long Short-Term Memory
RA-L	Robotics and Automation Letters
ROM	Range of Motion
MCP	Metacarpophalangeal (Joint)
ML	Machine Learning
MPC	Model Predictive Control
MR	Magneto-rheological (fluid)
PIP	Proximal Interphalangeal (Joint)
RNN	Recurrent Neural Network
RCNN	Recurrent Convolutional Neural Network
ROSE-Net	Recurrent cOnvolutional Spatial Embedding Network
SLA	Stereolithography
SLS	Selective Laser Sintering
SMA	Shape Memory Alloy
SMM	Shape Memory Material
STT	Scaphotrapeziotrapezoidal (Joint)
SVM	Support Vector Machine
TAROS	Conference Towards Autonomous Robotic Systems
UV	Ultraviolet

List of Figures

1

Introduction

1.1 Motivation

There are many seemingly trivial tasks undertaken by humans that continue to escape the capabilities of robots. One such example is the task of blindly reaching into a bag of distinct objects with the intention of selecting one and retrieving it. From the human perspective, in order to select and subsequently grasp the desired object from the bag successfully, the task can be broken down into the following set of challenges:

1. Entering the bag and approaching the objects without the affordance of visual information.

2. Physically exploring the unstructured contents of the bag without risk of damaging either the objects or the person whilst acquiring tactile information from contact with the objects.

3. Executing a stable grasp of any object in the bag despite complex dynamic interactions in the unstructured environment.

4. Manipulating the object either to achieve a more stable grasp or to explore salient features around the object's body and then using multiple grasps to form, develop, and reinforce beliefs over the object's classification, comparing with the representation in memory.

Over millenia, humans have evolved to exploit *Morphological Computation* throughout our body to approach and achieve a task like this. Morphological computation is the concept that the body's morphology can be used to simplify and inform interactions with the environment whilst reducing the amount of explicit central computation required [1]. Fig. 1.1 illustrates the implications of this concept, whereby the transfer of information and stimuli exists between each system, rather than simply between the central controller (the brain) and the mechanical/sensory systems. Specifically, the body dynamics enable *sensory-motor coordination* such that the way in which the *mechanical* system interacts with the environment directly shapes how the *sensory* system perceives it [2, 3]. For humans, these body dynamics arise in a multitude of ways when undertaking the posed task, including but not limited to: the specific morphologies of the 4 main tactile receptors in the skin, that are each specialised to detect different stimuli for contact discrimination [4]; the natural filtering and passive compliance in the epidermis, dermis, and hypodermis to modulate the signals reaching the receptors [5]; the compliance in the joints and skin to conform naturally to the geometry and stiffness of objects being grasped and reduce incident impulses for safe interaction during contact [6, 7]; the ability to selectively stiffen the joints from soft contact for surface detection and safe exploration to output greater forces for grasping [8]; and the synergies between the 21 degrees of freedom (DOFs) in the hand to simplify and generalise the control of the motions and poses of the hand [9–11]. These features provide us

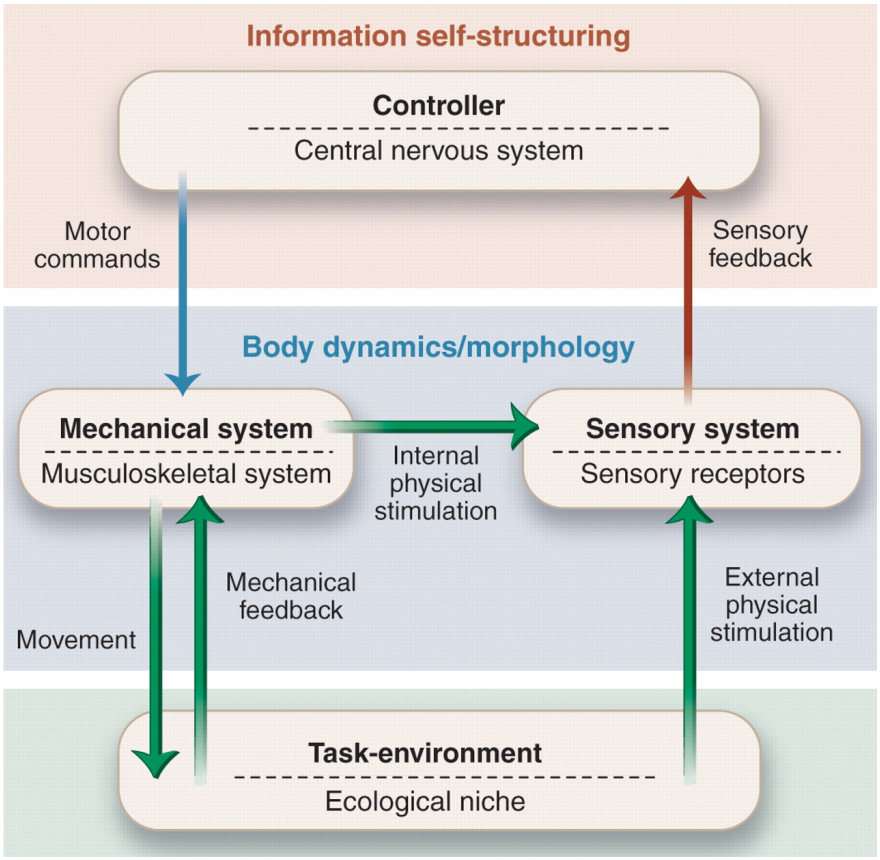

Figure 1.1: The implications of embodiment on the interaction between a robot and its environment. Taking into account the body's dynamics with the environment and the effect of the mechanical system on the sensory system represents a paradigm shift in robotic design. This design approach allows for sensory-motor coordination where the morphology of the body structures and shapes the sensors' response. From [12]. Reprinted with permission from AAAS.

with a high degree of confidence in the safety of interactions, the ability to classify between objects, and the adaptability to conform naturally to the shape of any object, ensuring a stable grasp. Furthermore, humans practise and perfect tasks such as these over many years as we develop. There is a vast difference between an adult's ability to exploit these morphological features compared to an infant.

Even with the benefits afforded by the hand's morphology, tactile sensing is inherently a local process and single contacts are rarely sufficient to distinguish between objects. In this case, humans will adapt the hand's pose and take repeated touches of the object to seek

out and detect variations between objects [13]. We use the sensory-motor coordination to modify the contacts with the objects for specific somatosensory receptor triggering whilst integrating the signals to build up a representation of the contact, which is compared to stored representations in memory to identify the object [5, 14–16].

Whilst humans' development has exploited compliance and body dynamics to enable us to simplify the approach towards complex tasks such as the one proposed, development of robotic systems has traditionally focussed on the deployment of rigid-linked agents with discrete joints. To approach the same task, these agents require complex control schemes to manipulate each joint's DOFs precisely. While some elements of the proposed task have been achieved in traditional robotics, their lack of generalisability and safety stems from the necessity of explicit control.

Due to the rigidity in traditional robotic arms and hands, they are most commonly kept remote from unstructured environments due to the risk posed and the precision required in their safe deployment [17]. Indeed, they have to approach cluttered environments timidly, since unpredicted impact can easily damage either the robot or its environment [18]. In this regard, the task of grasping diverse objects stably in any given pose presents a complex challenge for robots, demanding an end-effector with high dexterity or adaptability to accommodate the diverse geometries involved. Here, dexterous is used to refer to designs with a high number of DOFs and extensive range of motion in the joints. For highly dexterous designs, achieving a stable grasp on any object in any presented pose necessitates complex solutions that utilise a constant feedback loop between sensing and actuation to conform to the specific object's shape and material properties [19]. Typically, these designs are applied to grasping tasks within constrained environments, such as only having a narrow range of objects to grasp or grasping objects in a single pose [20]. Only recently has the diversification of a graspable object set been achieved [21]. For the grasp planning in these instances, an object is localised and/or identified using vision before an explicit planner formulates the

reach, pose, and grasp posture [22]. However, whilst the use of vision in this application has demonstrated widespread success, oftentimes, we are faced with environments with visual occlusion. In this regard, the problem of contact and feature detection is well-motivated for the application of tactile sensing [23].

Tactile sensing unveils the potential to attain richer information about an object's properties, such as its weight, stiffness and friction [24]. Indeed, a number of factors significantly affect the likelihood of success in this task. Primarily, the gripper has to be able to interact with any object in any pose. Whilst this is indeed possible with rigid-linked end-effectors, it relies on the integration and sychronisation of positional or force feedback to detect contact and precisely adapt the effector pose accordingly to ensure both safety in contact and successful grasping [25]. For example, limited solutions have demonstrated success by taking feedback from positional encoders and force/torque sensors at the discrete joints [26]. This proprioceptive feedback can be applied both to the control of the grasp and the object identification itself. However, the control of many DOFs is not trivial and introduces complexity to ensure successful grasps are achieved for a variety of objects, limiting the generalisability of the application. Secondly, tactile object identification is inherently contingent on the amount and type of physical contact between two parties, such as normal or shear forces [22]. In this regard, contact between two rigid surfaces restricts sensory stimulation and requires precise alignment between contact faces to enable successful detection.

Whilst there has been over 100 years of designs presented for anthropomorphic hands with recent application towards object identification, the vast majority are limited in their generalisability by the requirement for complex control schemes as discussed [27]. In contrast, with the advent of Soft Robotics, recent work has looked to target adaptability over dexterity. This paradigm shift is motivated by taking inspiration from biological solutions to implement the *Morphological Computation* that was discussed previously to focus more on how the

characteristics of the body can be used to simplify tasks by embodying the intelligence and allowing the morphology to shape the sensory input and the mechanical output [28–31].

Soft materials and compliant joints are intrinsically connected to adaptability since designers can exploit the passivity of their design to conform to the shape of the environment with minimal control complexity [32]. This concept enables the agent to offload control from central computation and, rather, to embody it within the agent's materials and geometry to achieve greater conformability, and perception in the environment [2]. Through this embodiment, deployment in unstructured environments without prior knowledge becomes possible, as it enables leveraging physical interactions for favorable object-environment interactions instead of solely relying on rejecting or avoiding external disturbances [33, 34]. Bonilla et al. [18] explored this concept in the context of a manipulation paradigm and how the exploitation of structural softness enables complex interactions with the environment as shown in Fig. 1.2; by using soft materials in anthropomorphic hands, robots can use the contact with the environment favourably rather than having to avoid it timidly.

In the initial exploration process, exploiting the passive compliance of soft materials allows for energy dissipation when in contact with objects [29, 35]. The dissipation leads to intrinsically safe designs that ensure the risk of damage to either party is naturally reduced [36]. In this regard, the implementation of soft joints or linkages provides a significant advantage over traditional robotic end-effectors in facilitating safety during exploration, as they do not require the same precise adaptations during contact for safe interactions.

Once safe contact has been made with the object, the next step is to be able to perform a static and stable grasp of a diverse set of objects. Enhancing the dexterity of an end-effector with the compliance of soft materials enables this object diversification, from greater geometric variability to including a range of stiffness [27, 37, 38]. The passive compliance allows the hand to conform naturally to the shape of the object and solutions using soft end-effectors have shown that, in the framework of a static relationship between agent, object,

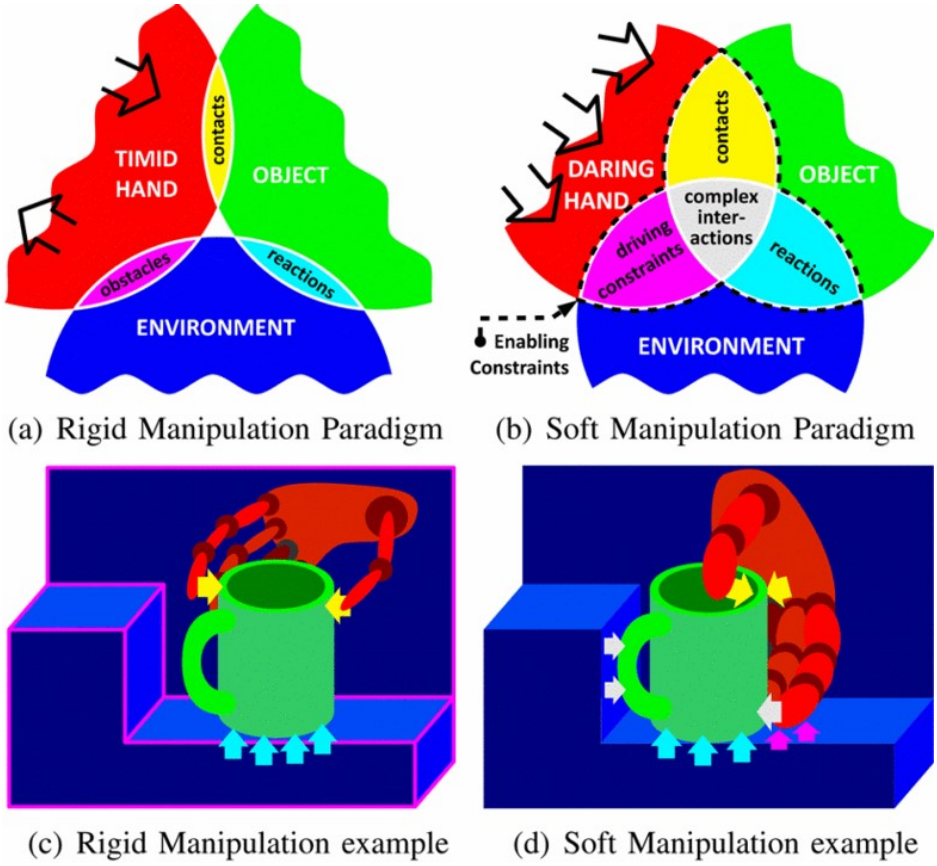

Figure 1.2: The manipulation paradigm highlighting the difference between *rigid* and *soft* manipulators. The colours in (a) and (b) are reflected respectively in (c) and (d). A rigid-bodied hand has to approach manipulation timidly and plan only to contact where a good quality grasp can be achieved. Conversely, a soft daring hand actively seeks out contact with the environment to exploit information from complex interactions and passively shape the hand. Reproduced with permission from [18] ©2014 IEEE.

and environment, they can grasp a wide range of objects with only open-loop control [39]. By extension, objects can be presented in a variety of poses or centre offset positions and the soft end-effector is still able to execute a successful grasp without control or positional adjustments [40]. Furthermore, the softness of the material allows for a greater surface area of contact between the gripper and the object, increasing the friction in the grasp and therefore improving the likelihood of grasp success.

Within the context of tactile sensing and utilising softness at the point of contact, as

stated before, maximising physical contact between two parties is crucial for acquiring comprehensive tactile data for object identification. The amount of contact can be understood in terms of two aspects:

1. The surface area between the end-effector and the object. By designing a system that naturally conforms to the shape of the object under scrutiny, the surface area between the agent and object can be increased [41]; this is achieved within a Soft Robotic design by the bulk conformability in the contact and the compliance between the sensors and the object.

2. The spatial distribution of sensors on the end-effector. In this case the distribution of the sensors relates to the number and density of sensors placed around the end-effector; by distributing the sensors across the entire surface area in contact, a greater number are likely to be stimulated for data acquisition at any given contact [42–44].

Furthermore, the combination of these two factors, conforming to the object and detecting the surface across that contact, facilitates the acquisition of patterns in the tactile data that would be otherwise missed by rigid-bodied agents. In effect, the adaptability of the end-effector to the object's geometry shapes the data to simplify the inference for object recognition [45–48].

Although sensing in compliant grippers can provide a solid foundation for accurate object identification, tactile sensing inherently only provides local information. Relying solely on one grasp risks missing salient features necessary for accurate identification or confusing sets of similar geometry for one another [49]. While using distributed sensing rather than purely tip sensing can mitigate this issue to some extent [50, 51], the human approach can be emulated by integrating information from multiple grasps across the surface of the body. This holds even greater promise for improving accuracy rates as the knowledge of the object morphology is developed. However, achieving this goal requires developing a Bayesian framework capable of integrating subsequent information to build upon prior

knowledge, as well as a physical system that is able to adapt to any pose that the object is presented in as discussed previously.

This thesis seeks to explore and develop the abilities of Soft Robots to exploit morphological computation to simplify the task of tactile object identification. Inspiration is taken from the human approach of using compliance in the joints and skin to conform naturally to the objects under scrutiny and ultimately formulate a multi-grasp identification procedure. Two overarching questions are formed to be answered and to structure the thesis:

1. How can the principles of Soft Robotic actuation and sensing be implemented to design a hand that combines human-like dexterity with a high degree of adaptability to grasp a wide range of objects with just a simple control scheme and tactile feedback? This is addressed in Chaps. 2 and 3, in exploring actuation and fabrication methodologies, and designing a soft anthropomorphic hand with integrated distributed tactile sensing.

2. How can the embodied intelligence afforded by the adaptability within that hand be exploited to formulate, simplify and solve a multi-grasp tactile object identification task? This is addressed in Chaps. 4 and 5, in the application of the soft hand to grasping a set of objects from all poses and developing two neural networks for object identification based on the tactile data from those grasps.

1.2 Thesis Structure and Contributions

Chapter 2: Preliminary Investigations and Soft Actuator Design

For the design of a hand that can be applied to the complex task that was outlined in Sec. 1.1, the work in this thesis seeks to design an actuator that demonstrates inherent compliance, is easily fabricable with high repeatability, can be simply controlled, and achieves comparable

actuation speed to a human finger. This will allow for the levels of adaptability that facilitate simplifying grasping the diverse set of objects.

The field of Soft Robotics has rapidly expanded over the last decade, producing a wide range of new actuation methodologies that have the potential to be applied to the design of the hand [52, 53]. The preliminary work in Chap. 2 examines the new and diverse approaches that have been presented in the field [37, 54]. The approaches are compared and contrasted and pneumatic actuation is chosen as it suits this design criteria most closely.

Having chosen pneumatic actuation for the actuator, this thesis then explores the properties of the novel materials and fabrication methodologies that can best facilitate the behaviours that are desired in the actuator. In particular, it is desirable to be able to incorporate multiple materials within the same body to enable hybrid rigid-soft designs with carefully chosen material behaviours through the body [55]. Furthermore, this works also seeks to simplify the overall fabrication and component integration process, and maximise the repeatability between samples.

Through these preliminary investigations, multi-material polyjet 3D-printing and pneumatic actuation were identified as best-suited for the overall task [56]. The concepts were applied to develop a bi-directional actuator. The contributions of this work compared with the state of the art are:

1. The application of multi-material polyjet printing to the fabrication of an actuator, achieving simplified manufacturing and improved repeatability.

2. The easily implemented variable stiffness and tunable force output that enables greater force output and multiple control modes.

The chapter concludes with the presentation of the paper that was published in conference proceedings at TAROS 2021.

Chapter 3: Soft Hand Design

For the purpose of grasping a diverse range of objects, the work in this thesis seeks to produce a gripper that can combine both dexterity and adaptability [38]. In this regard, human hands are well known for their ability to perform a wide range of tasks, from fine manipulation to heavy lifting, and so are well suited towards this task [27, 57]. In Chap. 3, the kinematics required for human-like dexterity are justified, which, in part, is derived from the opposability of the thumb, and motivates the inclusion of an active palm [58–61]. This dexterity is then combined with the adaptability contributed by the soft materials and actuation methodology investigated in the previous chapter (Chap. 2) to produce a soft anthropomorphic hand.

In addition to the structure and motion of the hand, the thesis investigates the integration of soft sensing systems that will form the basis for the object identification task that is formulated in Chap. 4. As with the actuation, this work seeks to develop an inherently compliant sensing scheme that is easily integrated into the body of the hand [41]. As discussed in Sec. 1.1, distributing the sensing around the hand enables greater tactile information to be gained from each object interaction, and inspiration is taken from human behaviour to determine the sensor placement [62].

The combination of the hand and sensing system culminates in the overall design of a monolithic 3D-printed hand with integrated distributed tactile sensing. The contributions of the hand are:

1. A monolithic multi-material 3D-printed body, which facilitates the exploitation of the different selected materials and significantly reduces fabrication complexity.

2. Integrated, distributed soft pneumatic tactile sensing for large-scale contact detection across the surface of the hand.

3. An active palm to achieve human-like dexterity through enhanced thumb opposition.

This work was published in RA-L 2022 and the paper is included.

Chapter 4: Multi-Grasp Tactile Object Identification

As humans, we take multiple touches and grasps of an object to develop a tactile profile of an object, especially in the case that local information may not be sufficient to discern between similar object classes. In Chap. 4, the thesis first reviews how soft grippers and hands can be applied to tactile object identification and subsequently investigate how they can mimic the multiple grasps that humans use to improve on those solutions [26, 39, 63, 64]. The thesis then looks into how machine learning and neural networks have been applied to classify objects based on tactile data from soft robotic grippers and hands. The complex interrelations that emerge within the acquired data in tactile object identification can be well evaluated with the analysis provided by these tools [26, 65].

The adaptability of the hand developed in Chap. 3, enabled it to grasp a set of objects from any presented pose and gain tactile information from these grasps using the integrated sensing. The morphology and compliance of the hand helps to shape the tactile data that is acquired by conforming to the geometry of the object to enable accurate identification. The tactile data from these grasps is passed through an encoder-decoder architecture and, importantly, the grasp order in the data is randomised to prevent any reliance from forming in the identification process.

The contributions of this identification methodology are:

1. Object classification based on information gained from multiple grasps that achieves higher accuracy than single-grasp identification solutions.

2. A data structure and architecture (EDAMS) that enforces geometric separation in the latent space.

3. Pose-invariant identification, where each object can be identified in any presented position.

This work was presented at Robosoft 2023 and the corresponding paper is provided.

Chapter 5: Bayesian Framework for Open-Ended Object Identification

In Chap. 5 this thesis develops upon the object identification work in the previous chapter in two significant ways. Firstly, the work seeks to develop an open-ended classification procedure whereby any number of grasps can be taken to inform the identification process. Secondly, a 2D embedding for subsequent vision-analogous classification is implemented to improve the accuracy at a low number of grasps.

To allow for any number of grasps to be input, rather than the limited number in the prior methodology, the chapter explores how Recurrent Neural Networks (RNNs) have been implemented across a range of applications to use a form of short-term memory [66]. This memory enables us to maintain a running update of the classification output and implement a Bayesian framework for object classification, influenced by the output of the network on the previous grasp [67, 68]. The prior prediction is concatenated into the network and data is sequentially acquired until satisfactory belief in the output of the classification is achieved.

Whilst the shortcomings of actual visual identification have been recognised, the means of feature extraction from images have been studied in depth and are well documented in the literature [69–71]. Tactile identification can use these methods analogously since object features can also trigger across proximal taxels leading to similar distinguishable patterns [24]. Chap. 5 looks to exploit these similarities by using convolutional layers to extract local features from an embedded 2D representation of the tactile data.

Chap. 5 develops a new model for the analysis of the data acquired in Chap. 4. By using an RCNN-based network (ROSE-Net), it is shown that the prior classification belief

distribution can be concatenated with the innovation data to inform future predictions and form a 2D embedding for vision-analogous spatial feature extraction. The contributions of this methodology are:

1. A novel recursive network that leverages on work developed in visual object identification.

2. An open-ended framework that is capable of processing any number of grasps sequentially with monotonically increasing classification accuracy.

3. Improved accuracy in pose-invariant object identification compared to the previous work.

This work has been submitted to Science Advances and is currently under review.

1.3 Publications

The following publications were based on the work presented in this thesis:

- O. Shorthose, L. Scimeca, A. Albini and P. Maiolino, "Exploiting Deep Learning to Achieve Multi-Grasp Pose-Invariant Object Recognition with a Soft Hand", *Under review in Science Advances*

- O. Shorthose, A. Albini, L. Scimeca, L. He and P. Maiolino, "EDAMS: An Encoder-Decoder Architecture for Multi-grasp Soft Sensing Object Recognition", in IEEE 5th International Conference on Soft Robotics (RoboSoft). 2023

- O. Shorthose, A. Albini, L. He and P. Maiolino, "Design of a 3D-Printed Soft Robotic Hand With Integrated Distributed Tactile Sensing", in IEEE Robotics and Automation Letters, 7(2), 3945-3952. 2022

- O. Shorthose, L. He, A. Albini, and P. Maiolino, “Design of a Multimaterial 3D-Printed Soft Actuator with Bi-directional Variable Stiffness”, in Annual Conference Toward Autonomous Robotics Systems: Vol. 13054 LNAI (pp. 238-248). Springer. 2021

2

Preliminary Investigations and Soft Actuator Design

The rapid emergence of Soft Robotics in the last decade has been largely enabled by the development of novel fabrication and actuation methodologies [30]. These methodologies have paved the way for a whole host of material and actuator behaviours that were previously unachievable. Specifically within these behaviours, this work seeks to exploit the compliance that facilitates safe and adaptable actuation.

Sec. 2.1 discusses the Soft Robotic actuation methodologies that have the potential to be applied to the further design of the soft hands. After identifying pneumatic actuation as being best suited, Sec. 2.2 then explores the methods of fabricating soft pneumatic actuators. Variable stiffness methodologies that are used to increase the output force of an actuator are identified in Sec. 2.3. The paper that was presented at TAROS 2021 is given in Sec. 2.4

with further information about the undertaken work given in Sec. 2.5. The chapter finishes with a brief discussion of the limitations of the actuator and modifications that were made for the later design of the soft hand in Sec. 2.6.

2.1 Actuation Methodologies

There has been a wide range of methodologies proposed for Soft Robotic actuation [37, 38, 54, 72]. Each one aims to exploit soft materials to build robotic bodies that conform to the environment, and are robust, safe, and impact resistant [73–75]. In this work, the primary focus in design is on a methodology that allows for a high degree of compliance, will provide inherent adaptability in deployment, has comparable speed to human fingers [59], and is simple and repeatable to fabricate. The most commonly employed techniques are broken down in [72] and the main methods can be summarised as follows:

Methodology	Induced Stress	Frequency	Fabrication	Benefits	Limitations	References
Magnetic	0.1MPa	100Hz	Difficult	Hardware commonly available off-shelf, field permeates most materials	Bulky hardware required, high currents to achieve desired force output cause significant ohmic heating	[76–78]
Tendon	1MPa	1-10Hz	Medium	Hardware commonly available off-shelf, high force output, efficient	Bulky hardware and motors required, most designs use inextensible tendons (reduced compliance), extra control schemes for variable impedance required	[38, 54, 79]
SMA/SMPs	>1000MPa	1Hz	Medium	High force output, large stroke	Requires external heating, lossy, very slow, low strain-rate, must be antagonistically designed	[80–83]
DEAPs	1MPa	1000Hz	Difficult	High efficiency, high speed, silent	High activation voltages can cause material breakdown and they have low stroke length	[84–86]
IEAPs	0.1MPa	10Hz	Medium	Large displacement, low excitation voltage	Low force output, risk of electrolysis breakdown	[84, 85, 87]
FEAs	0.1MPa	10Hz	Easy	Large displacement, easily designed, cheap, high compliance	Low force output, small perforations prevent operability	[56, 88–92]

Table 2.1: Comparison of the different actuation methodologies. Induced stress and frequency are presented as orders of magnitude rather than extracting specific values from the literature to allow for easier comparison. The measure of fabrication is taken from qualitatively comparing the steps required to fabricate actuators.

As a result of evaluating these design criteria, pneumatic FEAs were implemented in the work presented in this thesis. A deeper review into the state of the art within the field of FEAs is presented in the paper in Sec. 2.4.

2.2 Fabrication Methodologies

2.2.1 Enabling Soft Robotic Design

Whilst multiple fabrication methodologies have been proposed for FEAs, the majority of designs are fabricated using casting and/or 3D printing. Casting is the process of pouring a liquid material into a mould, which is then left to cure before the mould is either removed physically or chemically [89, 93]. This process is commonly used in the production of silicone rubber parts but also allows for the integration of other components such as sensors between fabrication steps [94]. It shows great promise within Soft Robotics because the materials can be cheaply acquired and easily implemented. However, it has a number of drawbacks. The fine margins in the ratios of the materials that are mixed for curing, along with the imperfections from degassing the solution and the use of moulds requiring fine alignment, can lead to high variability between samples [95]. Additionally, it has been shown that a component manufactured with casting and 3D printing has higher performance in the printed sample when using the same material for both methods [96].

3D printing had its advent in the mid-1980s and involves layer-by-layer fabrication of a body based on a digital model [97, 98]. Within Soft Robotics, FDM, SLA, SLS and polyjet have been used, each with their own respective advantages and disadvantages [55, 99].

FDM is the most common method used in Soft Robotics due to its low cost and ease of use [100, 101]. It works by heating and extruding a thermoplastic through a nozzle, which sets upon cooling [102, 103]. However, it is limited in the materials that can

be used, and the resolution of the printed parts is often low [104]. Furthermore, FDM components often experience delamination, which may not be a critical issue for many mechanical applications. However, in pneumatic applications, delamination can quickly lead to leakages, rendering the component useless. SLA and SLS have both received much less attention as the costs of production and complexity of fabrication significantly reduce the accessibility of the manufacturing techniques. A few solutions have been presented, but they are only capable of producing single material components [105], which severely limits the ability to exploit different material behaviours without relying on post-fabrication integration of different bodies.

Polyjet printing is a relatively new technology that has been used in Soft Robotics to produce monolithic multi-material components. Photopolymers are jetted onto a build tray, blended and cured with UV light for high-resolution printing [99, 103]. Through this process, the printers are able to achieve high-resolution printing ($16\mu m$ [106]). Typically, the mix of photopolymers is between a rigid and a soft material and, by specifying the ratio of these, the shore hardness of the material can be chosen. By corollary, the stiffness, tensile strength, and other material properties can be chosen. These materials can then be seamlessly blended to allow for the exploitation of complex material behaviours [107]. Furthermore, the high accuracy and dissolvable support material allow for the integration of complex internal geometries that are not possible with other methods of additive manufacturing. This enables the design of the cavities for fluidic actuation and pneumatic sensing which will be detailed in subsequent sections.

Due to the benefits listed above, polyjet printing was chosen to develop the pneumatic actuator. However, because the available materials have only recently been developed, at the time of the start of this project, they were not well characterised in the literature. Therefore, in order to be able to use the materials in simulations and actuator design, tensile testing of the catalogue of available polyjet materials was undertaken. The factors affecting material

properties are presented in Sec. 2.2.2 and the testing is detailed in Appendix 6.

2.2.2 Polyjet Material Characterisation

Polyjet printing was invented in 1998 by Objet Geometries Ltd., which was subsequently acquired by Stratasys in 2012. Due to the relatively recent advent of the technology, there is little characterisation of the materials in the literature and the material properties between papers and manufacturer's documentation are not consistent [107–111]. Through the work that has been done, it has been discovered that polyjet materials are highly variable depending on a set of factors.

Firstly, the layout of the pieces in the print bed has been shown to vary the elastic modulus, tensile strength, and visco-hyperelasticity. Primarily, the orientation of the components affects these factors - specimens printed in the X-direction have the highest tensile strength and elastic modulus, Y-direction components were comparable but lower, but those printed in the Z-direction were significantly weaker in all tests [112–114]. The orientations of the pieces are shown in Fig. 2.1 from Abayazid et al. [113] and the print head moves primarily in the X-direction. The streaks shown in the inlay are characteristic of polyjet printing and are indicative of material property differences based on orientation. Additionally, the proximity of the printed pieces to each other in the Y-direction affects the material properties [106, 115]. The closer the pieces are to each other in the Y-direction, the higher the elastic modulus. This is primarily due to the UV dispersion between pieces when they are closer together curing the same component multiple times per layer. These factors can generally be controlled by the user, but further complex reasons to do with the printer's jetting algorithms that cannot be easily modified are discussed in the literature [115].

Beyond these factors, the material properties vary over time and with increased exposure to UV. Of course, UV is required to cure the materials initially, but as the material ages,

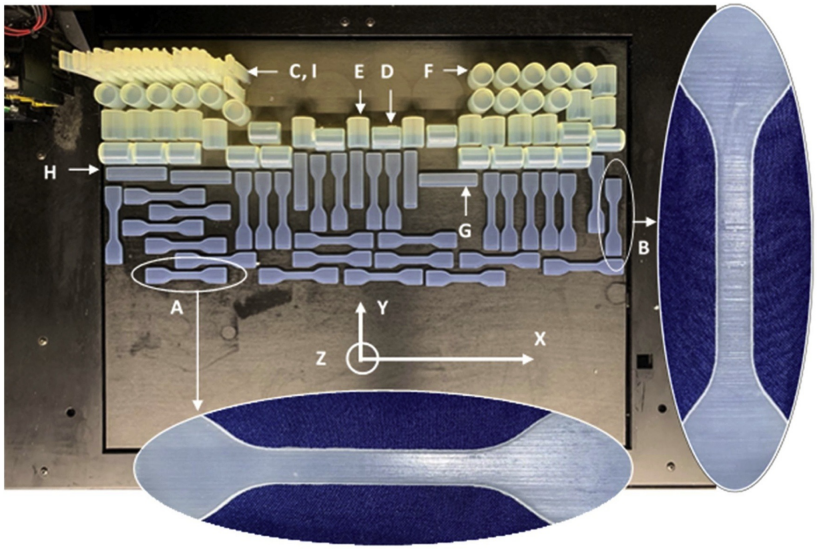

Figure 2.1: Layout of test samples in tensile testing undertaken to characterise polyjet printed samples. Reproduced with permission from Abayazid et al. [113].

the material loses its elastic properties and increases in tensile strength [114]. This is a significant problem for the materials as this makes long-term utility unpredictable and parts must be stored out of direct light.

Whilst polyjet printing enables monolithic multi-material printing, the interfacial relationships between different materials are complex. For a designer, it is important to know whether to design abrupt material changes or to implement gradation between them. Mueller et al. [107] found that the material mixing is at the micro-scale rather than the molecular scale and therefore can be viewed akin to a conventional composite material with strengthening fibres distributed through the body. Additionally, they showed that local anisotropy has to be considered when designing the material interfaces to prevent warping. Lumpe et al. [116] showed that there is great variability and unpredictability when measuring the tensile properties of interfaces. Solutions to this have been proposed as including a transition zone between materials or embedding the materials within each other at the transition.

Due to the conflicting material properties' data, tensile testing of the materials was undertaken to characterise some of their basic mechanical properties. Standard ASTM D638

protocols were followed for the tests. These are presented in Appendix 6 and were used to form the basis of the simulations in this chapter and the next.

2.3 Variable Stiffness

As stated in Sec. 2.1, FEAs have been utilised to great effect within Soft Robotics designs but are often limited to a low force output. However, simply increasing the internal pressure to increase the force may cause perforations in the soft casing materials. To solve this shortfall, variable stiffness can be implemented in a variety of ways [117, 118]. The application of variable stiffness can be generally split into using semi-active actuators that vary their elasticity or fully active actuators to achieve antagonism. These can further be split into combinations of the same methodologies presented in Sec. 2.1 which are presented in Table 2.2. This work seeks to increase the force output whilst maintaining the simplicity of fabrication.

	Actuation Technology		Speed of Stiff.	Depending on	Speed of Destiff.	Depending on
ACTIVE (antagonistic arrangement)	**Active-Active**	EAP & EAP	++	Voltage amplifier	++	Discharge
		Fluidics & fluidics	+	*Fluidic inflow*	o	*Fluidic outflow*
		Tendons & fluidics	o	Motor's velocity and fluidic inflow	o	Motor's velocity and fluidic outflow
	Active-Passive Structure	Fluidics & braided sleeves	+	Fluidic inflow	o	Fluidic outflow
		SMA & braided sleeve	+	Electric power	-	Thermal conditions
		SMA & flexible layers	-	Electric power	-	Thermal conditions
		EAP & flexible layers	+	Voltage amplifier	++	Discharge
SEMI-ACTIVE (intrinsic rigidity tuning)	**Jamming-based**	*Granular jamming*	+	*Vacuum pump outflow*	o	*Vacuum pump inflow*
		Layer jamming	+	*Vacuum pump outflow*	o	*Vacuum pump inflow*
	ER and MR materials	MR fluids	++	Magnetic field	++	Magnetic field
		MREs	++	Magnetic field	++	Magnetic field
		EREs	++	Electric field	++	Discharge
	Low melting point materials	Wax	- -	Thermal conditions	-	Heat source
		Polymers	- -	Thermal conditions	o	Heat source
		Alloys	- -	Electric power	-	Thermal conditions
	Glass transition-based		- -	Thermal conditions	o	Heat source
	SMMs	Polymers	- -	Heat source	-	Thermal conditions
		Alloys	- -	Electric power	-	Thermal conditions
	Conductive polymer		- -	Thermal conditions	-	Electric popup
	Chemical-based		- -	Drying conditions	-	Hydration speed

Table 2.2: Qualitative comparison of variable stiffening. Evaluation scale: ++, +, o, -, - -. The most suitable methods for the purpose of this work have been italicised. Reproduced with permission from Manti et al. [118] ©2016 IEEE.

Jamming-based semi-active actuators have been proposed by incorporating extra material into the body of the actuator to modulate their mechanical properties upon variation of the internal pressure of the chamber [119]. This concept was brought to the forefront of Soft Robotics designs by Brown et al. [120] with the Universal gripper. The concept works by reversibly removing the free space around the jamming media to force them together, thereby increasing the shear forces between them and increasing the stiffness of the body. This process is illustrated in Fig. 2.2. Since Brown's work, it has commonly been applied to granular, layer and fibre jamming [121]. The main benefit of these actuators is that they have been shown to increase the output force of the system significantly without modifying the original shape of the actuator, which makes them well suited to a range of Soft Robotics applications. Furthermore, the control required to vary the stiffness is straightforward and does not increase the complexity of the system substantially. However, they require the integration of additional components which can complicate the fabrication process, and (especially in granular jamming) the behaviour can be unpredictable depending on the initial state of the particles [122].

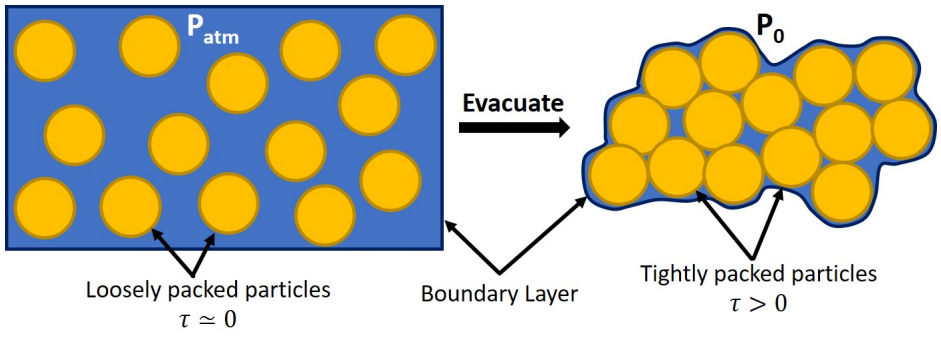

Figure 2.2: The concept behind jamming actuators as the internal cavity is evacuated. τ is the shear force between particles.

Active actuators for FEAs generally take the form of collinear or parallel actuators that work in partnership or opposition to each other to modify the bending and stiffness of the actuators [123–125]. Whilst these are not able to achieve the considerable increase

in force output that is demonstrated by jamming actuators, they do not require additional components and are therefore simpler to fabricate. Additionally, through the manipulation of each independent chamber, various control schemes can be achieved to diversify the application of the actuator. Further down the line, this diversity has the potential to enable different behaviours in the soft hand's fingers, for example, increasing the force output or stiffening a straight finger. The control schemes are presented within the contributed paper and discussed further in Sec. 2.5.

2.4 Contributed manuscript

The manuscript in this chapter was published in the proceedings of TAROS 2021. It utilises pneumatic actuation, multi-material 3D printing, and parallel actuation to create a monolithic variable stiffness actuator with multiple output control capabilities [126]. The main contribution is the ability to exploit variable stiffness for increased force output and multiple control modes in a monolithic body without requiring a complicated fabrication methodology, ensuring repeatability between samples. This work provides the basis for the actuation and fabrication methodologies used for the soft hand.

Design of a Multimaterial 3D-printed Soft Actuator with Bi-directional Variable Stiffness *

Oliver Shorthose[1], Liang He[1], Alessandro Albini[1], and Perla Maiolino[1]

Oxford Robotics Institute, University of Oxford, Oxford OX1 2JD, UK
{ollies,liang,ale,perla}@robots.ox.ac.uk
https://ori.ox.ac.uk/

Abstract. A multi-material 3D printed soft actuator is presented that uses symmetrical, parallel chambers to achieve bi-directional variable stiffness. Many recent soft robotic solutions involve multi-stage fabrication, provide variable stiffness in only one direction or lack a means of reliably controlling the actuator stiffness. The use of multi-material 3D printing means complex monolithic designs can be produced without the need for further fabrication steps. We demonstrate that this allows for a high degree of repeatability between actuators and the ability to introduce different control behaviours into a single body. By independently varying the pressure in two parallel chambers, two control modes are proposed: complementary and antagonistic. We show that the actuator is able to tune its force output. The differential control significantly increases force output with controllable stiffness enabled within a safe, low-pressure range ($\leq$ 20 kPa). Experimental characterisations in angular range, repeatability between printed models, hysteresis, absolute maximum force, and beam stiffness are presented. The proposed design demonstrated a maximum bending angle of 102.6°, maximum output force 2.17N, and maximum beam stiffness 0.96mN m^2.

1 Introduction

Soft and compliant materials have been increasingly implemented into robotics research in the last decade. These soft robots have shown benefits over their rigid counterparts with regards to higher levels of safety and the ability to adapt to unknown environments or tasks [1, 2]. However, the compliance of the materials and non-linear behaviour limit precise position control and the force that can be applied to the environment [1, 3].

Various research works have proposed solutions to solve the above issues. In particular, to increase the force that can be applied, variable stiffness actuators have been proposed based on several methods [4, 5]. These solutions, based on composite materials, introduce challenges in the actuator fabrication and control because they require the integration of extra systems into the soft actuators. In contrast, antagonistic pneumatic actuators, composed of parallel chambers,

* We gratefully acknowledge support by EPSRC Programme Grant 'From Sensing to Collaboration' (EP/V000748/1)

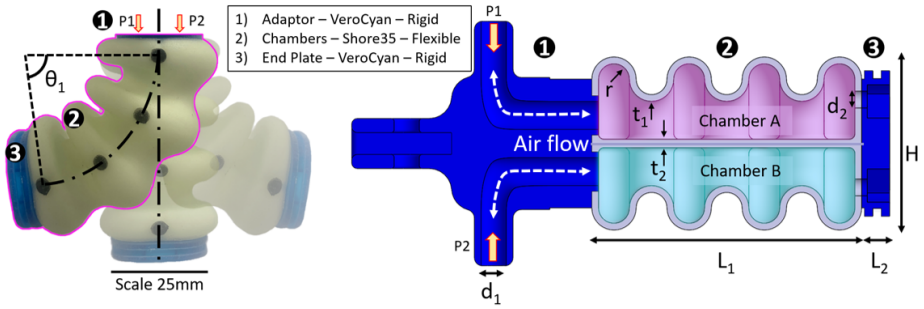

Fig. 1: Left: The multi-material actuator bent in both directions and at the neutral position. P1 and P2 are the independently applied driving pressures. θ_1 is the output angle. Right: Section view of the actuator showing the two chambers and the different regions utilising multi-material fabrication. Geometric properties are presented in mm: $r_i = 2.75$; $t_1 = 1.2$; $t_2 = 1.5$; $d_1 = 4.5$; $d_2 = 3$; $L_1 = 48$; $L_2 = 5$; $H = 31$.

achieve variable stiffness behaviour whilst avoiding the need for extra internal parts [6–8]. Many of these designs excel in one-directional bending stiffening to improve force output but are limited in having a one-sided active region [8, 9]. Bi-directional variable stiffness actuators have successfully improved the bending performance with a larger workspace [6]. However, fabricating multiple chambers in the actuator is challenging with moulding and casting methods, where multiple stages of assembly or lost-wax casting are typically needed [6, 10].

Recent advances in soft material 3D printing have provided an effective solution to quickly fabricate soft actuators precisely with high repeatability [11–13]. Compared to conventional silicone moulding methods, actuators fabricated via 3D printing can also have higher design freedom. Complex internal geometries that can optimise the bending motions can be introduced into the design [14,15]. Furthermore, recent advances in additive manufacturing have provided the ability to use multi-material printing. By introducing a variety of materials into a fully-integrated monolithic actuator, designs can be extended to exploit complex material behaviours [9, 16].

In this work, we present the design of a multi-material 3D printed soft monolithic actuator which incorporates parallel symmetrical chambers to achieve bi-directional variable stiffness. The actuator is experimentally characterised to demonstrate its performance improvements compared to the state of the art. Fig. 1 shows the printed actuator in both neutral and bent poses. The two parallel chambers can be actuated independently with two modes: complementary and antagonistic. Complementary control is the method of applying positive pressure to one chamber whilst exerting negative pressure in the other, and antagonistic control applies the same pressure in both chambers. Currently available 3D printed soft materials are still limited in the range of elongation at break compared to conventional silicone polymers. For instance, Ecoflex 00-

30 (Smooth-on [17]) has elongation at failure of 900% compared to Agilus 30 (Stratasys [18]), which exhibits a range of 220-270%. This limitation implies that 3D printed bending actuators are more prone to failure when only driven with positive pressures. To address this issue, we have proposed the two control modes, which increase the actuator workspace and force output while maintaining the capability of tunable stiffness. Crinkles are also integrated into the design to mitigate the limited material elongation where structual compliance is explored predominantly instead of material compliance.

2 Design and Fabrication of the Actuator

The actuator consists of two parallel bellow-shaped flexible chambers connected by a common midlayer. By regulating the pressure variation between the two chambers, bidirectional bending motions with tunable stiffness can be achieved. The design utilises novel 3D printing technology to maximize the ease and precision of fabrication and significantly reduces the time between design-fabrication cycles. Fig. 1 shows the schematics of the actuator with design specifications in the chambers, end plate, and base attachment.

The design consists of two expanding chambers bonded to an inextensible central layer. The compliant region expands to enforce a bending motion about the central layer with the increase of driving pressure. A bellows shape design has been incorporated to reduce the chamber's strain during expansion and facilitate easy extension/contraction of the chambers [19]. The Shore 35 Agilus/VeroCyan blend was used in the fabrication of the actuator to ensure maximum compliance. The bellow structure design further reduces the stress concentration on the material during the inflation, where a smaller principal strain is required for the material during bending. When the bellows expand, there is little tensile stress induced in the material compared to a design without bellows [13].

The parallel chambers enable variable stiffness control of the actuator without requiring the addition of granules or extra internal layers through antagonistic behaviour. Furthermore, a higher force output than a single-sided chamber (with the same driving pressure) can be achieved through complementary control behaviour. The end plate is designed to be rigid (VeroCyan) to prevent ballooning at the end which wouldn't contribute to the curvature of the body and would increase local bending strains. The surface area between the end plate and chambers was maximised to reduce warping or delamination at multi-material interfaces. Similarly to the end plate, the base is designed to be rigid to prevent unfavourable displacements when pressurised.

The relationship between bending angle, stiffness and pressure cannot simply be presented in analytical form and so optimum parameters have to be determined through simulation. A parametric analysis was run in CAD to determine the optimum geometry for the chambers. The thickness of the chamber and the inner radius of the crinkle were identified as critical parameters governing the bending behaviour of the actuator and were applied to a grid search optimisation algorithm. The body's principal stresses and tip displacement were allocated as

the key metrics. An internal pressure of 10kPa was applied to the model whilst the thickness of the material was varied between 1mm and 3mm, and the inner radius of the crinkle pattern was varied between 1.5mm and 2.75mm. These ranges were chosen to satisfy printing constraints for minimum feature size, and to ensure the overall length of the actuator was less than 50mm.The optimised design parameters are illustrated in Fig 1. The normalised simulated results of the displacement and stress were weighted towards prioritising the maximisation of the displacement over minimising the stress at a weighting ratio 5:4. The difference of the weighted values was minimised to find the optimal combination of thickness and inner radius, which was found when the chamber thickness was 1.2mm and the inner radius was 2.75mm. The overall length of the chambers is 48mm, the height is 31mm, and the weight is 35g. The central layer was empirically set to be 1.5mm.

Polyjet technology (Stratasys J735 printer) was used for multi-material printing of the actuator (VeroCyan and Agilus30). VeroCyan is a rigid plastic that has a quoted tensile strength of 50-65MPa and Shore hardness 83-86D. Agilus30 is a compliant and rubber-like material, which has a quoted tensile strength of 2.1-2.6MPa and a Shore hardness of 30A.

3 Control Setup

In this section, the performance of the proposed actuator was physically tested as the bending angle versus driving pressure, hysteresis, and the effect of increased force output and tunable stiffness via complementary and antagonistic control. To evaluate differences in the printed actuators' performance, a total of 3 actuators were tested under identical experimental conditions. The actuators were tested 5 times for each test category with time between each test of more

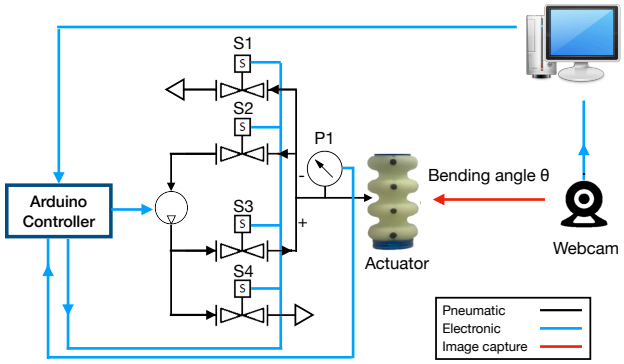

Fig. 2: Control architecture for one chamber of the soft actuator. The Arduino controls the pumps and valves, responding to real-time pressure values from the pressure sensor. The data from the Arduino and webcam is stored and post-processed to plot.

than 5 minutes to allow any residual strain energy to fully dissipate. Chambers A and B are indicated in Fig. 1 and used interchangeably between tests to validate the bi-directionality.

The actuator was controlled by an Arduino. The pneumatic setup used one Delaman air pump, four Yosoo1210 solenoid valves, and one Panasonic ADP5101 pressure sensor per chamber. The pressures were sampled at 50Hz. A 30Hz HD Webcam was used to acquire a video stream for angle detection. The setup is shown in Figs. 2 and 3. For the actuator characterisation, closed-loop PI (proportional-integral) control was used to compare the internal pressure value against a target value. The output of the PI control governed a pulse-width modulated (PWM) pump input, and the inflate and deflate valves. The angle of the actuator was acquired by identifying black markers down the centre of the actuator (shown in Fig. 1) and fitting them to a circular profile using a constant curvature approximation.

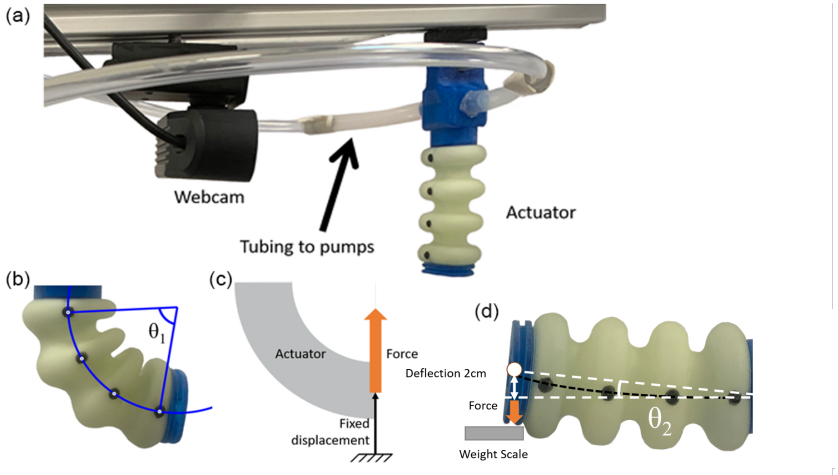

Fig. 3: (a) Experimental setup: the webcam is used for angle acquisition. (b) A circular profile is fitted to identify markers from the webcam stream to determine the angle, θ_1. (c) Complementary force test: the actuator is attached to a weight and inflated/deflated to change the force output. (d) Antagonistic stiffness test: the deflection was set at 2mm as the chambers were inflated and the force was recorded. θ_2 indicates the angle used in the small angle approximation.

4 Testing

Pressure versus Angle This test is used to evaluate the repeatability of the actuators' performance. Using PI control, Chamber A was inflated at a continuous rate of 0.5kPa/sec to a maximum target pressure of 16kPa with Chamber

B maintained at atmospheric pressure. Although the chamber was empirically found to withstand pressures up to 22.3kPa, the targeted range was chosen to be 0-16kPa. This is to examine mid-range performance without risking breaking the actuator. Fig. 4 shows the results for a single chamber being actuated. Across all 15 tests for the 3 actuators, the single chamber actuation test shows that, at the target pressure of 16kPa, the mean angle is 44.8°, with a standard deviation of 1.3°. This translates to only a 2.9% variation compared to the full range of the test, which validates the repeatability of the fabrication method. It is also worth noting that the actuator requires lower pressures than other comparable designs [7, 9, 13].

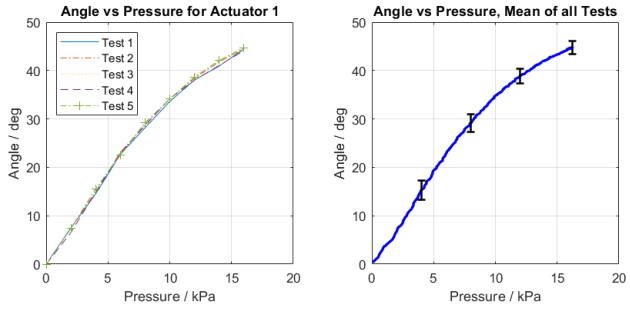

Fig. 4: Result of the single chamber pressure versus angle test. (a) 5 tests on one actuator. (b) average of 15 tests across 3 actuators.

Hysteresis The amount of hysteresis in a design can complicate the control of the system by adding a reliance on the historic behaviour of the actuator. The tests were undertaken by increasing the pressure in Chamber A by 0.5kPa/sec with PI control up to 16kPa target, holding the pressure steady for 2 seconds, and then decreasing the pressure by the same rate until the actuator returned to the neutral pose. Fig. 5 is shown with the lower curve indicating the inflation sequence and the higher curve indicating the deflation sequence. The amount of hysteresis is presented as the percentage difference between the area under the curves for the increasing and decreasing pressure cycles. This value was calculated to be 24.7%.

Complementary/Antagonistic control Using two parallel chambers, the force output and beam stiffness of the actuator can be tuned. The force output was tested for both complementary and antagonistic control.

The actuator's performance (Complementary control) with respect to stiffness variation was tested in terms of the actuator's maximum force. In this regard, a thread was wound around the end plate of the actuator and attached to digital weight with displacement constrained. By measuring the change in weight on a set of scales, the exerted force was deduced (Fig. 3c). For each change in pressure, the pressure was held constant for 5 seconds to ensure a static force was recorded. Chamber A was inflated to a maximum pressure of

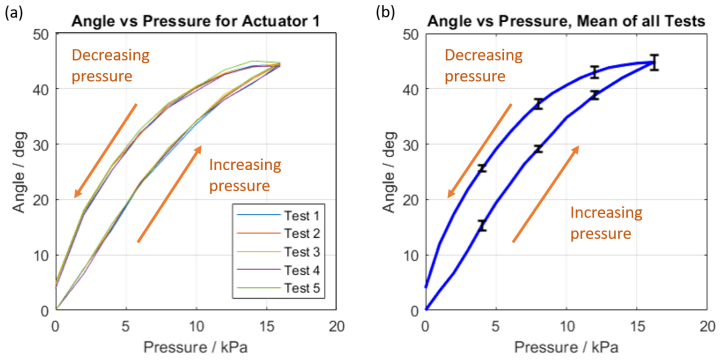

Fig. 5: Hysteresis test results. The pressure was increased/decreased at 0.5kPa/s for the inflation and deflation phases. 16kPa was the maximum targeted pressure in Chamber A before deflation. (a) 5 tests on one actuator. (b) average of 15 tests across 3 actuators.

Table 1: Complementary/Antagonistic control

		Chamber A	
		Positive Pressure	Negative Pressure
Chamber B	Positive Pressure	Antagonistic	Complementary
	Negative Pressure	Complementary	Antagonistic

20kPa to achieve a bent position and provide a reference force before Chamber B was depressurised to increase the force output. The depressurisation was done in 5 decrements between 0 and -22.5kPa.

The actuators' resistance to deflection (Antagonistic control) was tested by enforcing a tip deflection, pressurising the chambers, and measuring the imposed lateral force as shown in Fig. 3d. The tip was deflected by 2mm to ensure that the force being applied is normal to the end of the actuator under a small angle approximation ($\sin\theta \approx \theta$). The chambers were equally pressurised in 2kPa increments up to 20kPa with 5 seconds wait to ensure static force acquisition. Classical beam theory was applied to calculate the beam stiffness of the actuator at each pressure increment. The actuator was approximated to be a cantilever, fixed at one end, with stiffness $k = 3EI/L^3$. By applying this to Hooke's law, the beam stiffness (EI) was deduced.

To acquire a maximum force output for the actuator that can be used for benchmarking the actuator within the literature, Chamber A was pressurised to 20kPa and Chamber B was completely evacuated before the force measurement was made.

When only one chamber was actuated, the force output was 0.56N. The complementary variable force plot (Fig. 6b) shows that the design is able to increase the output force linearly by 1.56N by reducing the pressure in Chamber B. This behaviour provides an overall maximum force output of 2.17N. The

antagonistic variable force plot (Fig. 6a) demonstrates that the beam stiffness of the actuator can be increased by 0.64mN m^2, which corresponds to more than a 300% increase. Whilst this is a low absolute stiffness output, it is comparable to similar work at a considerably lower pressure and validates the use of the control modes to improve the force and output of the actuator [6].

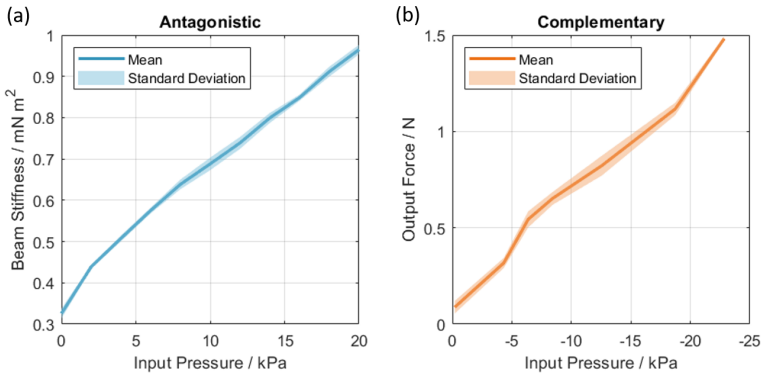

Fig. 6: (a) Result of the antagonistic actuator force test. Both chambers were inflated simultaneously from 0-20kPa in 2kPa increments. (b) Result of the complementary control force test. Chamber A was pressurised to 20kPa before starting this test and the presented data is the difference in force recorded as Chamber B was depressurised from 0 to -22.5kPa in 5kPa increments.

Effect of stiffness variation on angle The effect of independently varying the pressure in the parallel chambers leads to a change in the output angle. To enact precise position control, it is important to understand the extent of this effect for the complementary control mode. Chamber A was inflated to a single target pressure, the valves were closed, and then Chamber B was deflated. The target pressure in Chamber A was set at 13kPa and the target pressure in Chamber B was set at -10kPa. Both target pressures were, again, chosen to demonstrate the mid-range performance. The test was then used to determine a value for the maximum angle of the actuators, which can be used for easily benchmarking the design within the literature, by inflating Chamber A to 22.5kPa and deflating Chamber B to -20kPa.

The results are presented in Fig. 7 with a common x-axis to indicate the timing for the test. The test presents the effect of the change of stiffness on the actuator's angle. By actuating the second chamber, the angle is increased from 33.1° to 85.7° over the pressure change of -10kPa. This indicates that the stiffness variation has a significant effect on the output angle. This variation can be accounted for by mapping the pressure in each chamber to the output angle. The mean maximum angle across 15 samples is 85.5°, with a standard deviation

of 2.9°. This corresponds to a 3.4% variation compared to the full range of the test, which further demonstrates the repeatability of the fabrication process.

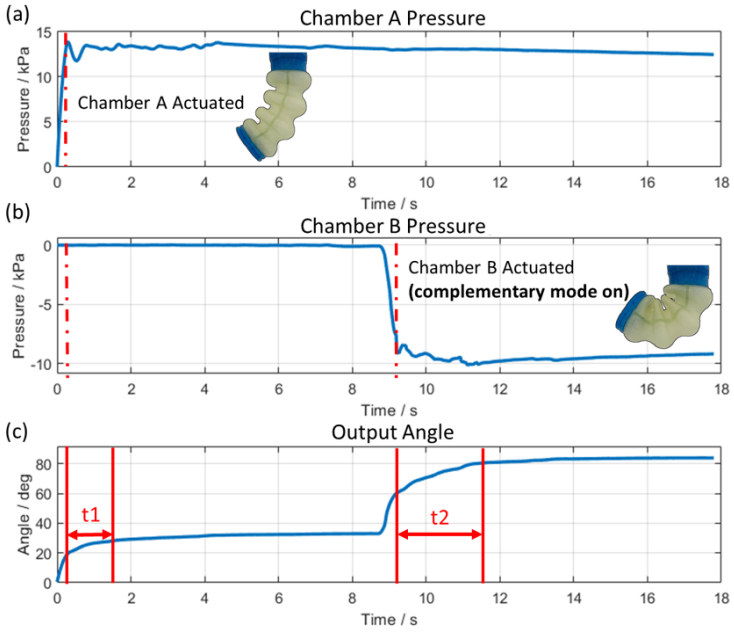

Fig. 7: Results of the two chamber pressure versus angle test. (a) Pressure in Chamber A. (b) Pressure in Chamber B. The rise times are calculated as: t1: 1.5 sec, t2: 1.9 sec. The pressure in Chamber A continues to drop over time as the volume is affected by the contraction in Chamber B. (c) Angle subtended by the actuator.

The maximum values of the actuators' input pressure, force, and angle are -25 to 22.3 kPa, 2.17 N, and 102.6°, respectively. The maximum pressure value was acquired by applying pressure until the actuator failed; the minimum pressure was determined by completely evacuating the actuator; the force and angle measurements were taken at slightly lower pressure values than the extremes (-24.5kPa and 22kPa) and measured in accordance with Fig. 3b and c.

5 Conclusion

This paper presents a multi-material 3D printed soft monolithic actuator that incorporates parallel symmetrical bellow chambers to implement bi-directional variable stiffness. Complementary and antagonistic control modes were proposed and implemented in the design while the two chambers can work collaboratively with either positive pressure or negative pressure. For pneumatic actuators that

operate in the low-pressure region (< 20 kPa), output force and bending angle performance is always a challenge. Compared to actuators that can only be actuated in a single mode with either positive or negative pressure, the presented design achieves higher output force, larger bending angle, or tunable stiffness without the need to increase the driving pressure.

3D printing rather than silicone moulding introduces quicker prototyping, better reproducibility, and stronger interfacial bonds to the actuator. The test results confirm the high level of reproducibility with low deviation between test results. The actuator was fully physically characterised under two-chamber PI control. The results show that the proposed complementary and antagonistic control method is promising for future work in bi-directional bending actuators. The key metrics to take from the studies are: maximum angle of curvature 102.6°; maximum output force 2.17N; controlled force variability 1.56N; and maximum beam stiffness 0.96mN m^2. With the proposed complementary/antagonistic control modes, this design achieves a higher output force and comparable bending angles to the similar designs [6, 13] at a fraction of the driving pressure.

Future work plans to further explore the potential of this actuator design and investigate the possible applications in grasping and in-hand manipulation. The authors will investigate variations on this preliminary design: increasing the stiffness to improve force output; adding modularity; scaling down the size of the actuator; and adding tactile sensing as a means of feedback.

Supplementary video: `https://youtu.be/F-ANfUwE0XY`

References

1. Kim, S., Laschi, C., Trimmer, B.: Soft robotics: A bioinspired evolution in robotics (may 2013)
2. Abondance, S., Teeple, C.B., Wood, R.J.: A Dexterous Soft Robotic Hand for Delicate In-Hand Manipulation. IEEE Robotics and Automation Letters **5**(4), 5502–5509 (2020)
3. Iida, F., Laschi, C.: Soft robotics: Challenges and perspectives. In: Procedia Computer Science. vol. 7, pp. 99–102. Elsevier B.V. (jan 2011)
4. Manti, M., Cacucciolo, V., Cianchetti, M.: Stiffening in Soft Robotics: A Review of the State of the Art. IEEE Robotics & Automation Magazine **23**(3), 93–106 (sep 2016)
5. He, L., Leong, F., Dulantha Lalitharatne, T., de Lusignan, S., Nanayakkara, T.: A haptic mouse design with stiffening muscle layer for simulating guarding in abdominal palpation training. In: 2021 IEEE International Conference on Robotics and Automation (ICRA). IEEE (2021)
6. Babu, S.P.M., Sadeghi, A., Mondini, A., Mazzolai, B.: Antagonistic pneumatic actuators with variable stiffness for soft robotic applications. In: 2019 2nd IEEE International Conference on Soft Robotics (RoboSoft). pp. 283–288 (2019)
7. Suzumori, K., Wakimoto, S., Miyoshi, K., Iwata, K.: Long bending rubber mechanism combined contracting and extending fluidic actuators. In: IEEE International Conference on Intelligent Robots and Systems. pp. 4454–4459 (2013)
8. Chen, Y., Chung, H., Chen, B., Sun, Y.: A lobster-inspired bending module for compliant robotic applications. Bioinspir. Biomim **15**(5), 56009 (jul 2020)

9. Zhu, M., Mori, Y., Wakayama, T., Wada, A., Kawamura, S.: A Fully Multi-Material Three-Dimensional Printed Soft Gripper with Variable Stiffness for Robust Grasping. vol. 6, pp. 507–519 (2019)
10. Yirmibesoglu, O., Morrow, J., Walker, S.: Direct 3D printing of silicone elastomer soft robots and their performance comparison with molded counterparts. In: 2018 IEEE International Conference on Soft Robotics, RoboSoft 2018. pp. 295–302. Institute of Electrical and Electronics Engineers Inc. (jul 2018)
11. Sachyani Keneth, E., Kamyshny, A., Totaro, M., Beccai, L., Magdassi, S.: 3D Printing Materials for Soft Robotics. Advanced Materials (2020)
12. Yap, H.K., Ng, H.Y., Yeow, C.H.: High-Force Soft Printable Pneumatics for Soft Robotic Applications. Soft Robotics **3**(3), 144–158 (sep 2016)
13. Peele, B.N., Wallin, T.J., Zhao, H., Shepherd, R.F.: 3D printing antagonistic systems of artificial muscle using projection stereolithography. Bioinspiration and Biomimetics **10**(5), 055003 (sep 2015)
14. He, L., Tan, X., Suzumori, K., Nanayakkara, T.: A method to 3d print a programmable continuum actuator with single material using internal constraint. Sensors and Actuators A: Physical **324**, 112674 (2021)
15. Gul, J.Z., Sajid, M., Rehman, M.M., Siddiqui, G.U., Shah, I., Kim, K.H., Lee, J.W., Choi, K.H.: 3D printing for soft robotics–a review (dec 2018)
16. Zolfagharian, A., Mahmud, M.A., Gharaie, S., Bodaghi, M., Kouzani, A.Z., Kaynak, A.: 3D/4D-printed bending-type soft pneumatic actuators: fabrication, modelling, and control. Virtual and Physical Prototyping **15**(4), 373–402 (2020)
17. Smooth-On: Ecoflex 00-30 product information, `https://www.smooth-on.com/products/ecoflex-00-30/`
18. Stratasys: Agilus 30, `https://www.stratasys.com/materials/search/agilus30`
19. Dammer, G., Gablenz, S., Hildebrandt, A., Major, Z.: Design and shape optimization of PolyJet bellows actuators. In: 2018 IEEE International Conference on Soft Robotics (RoboSoft). pp. 282–287. IEEE (apr 2018)

2.5 Supporting Information

This section provides further information about the parametric study that was used to determine the design parameters for the actuator in the contributed manuscript, and the multiple control modes that are possible with the parallel symmetric design. The detail for both was not included in the original manuscript due to space constraints.

Parametric Study The contributed manuscript presents a design study formulated to determine the optimum design parameters for the actuator using the material properties determined in Sec. 2.2.2. The thickness of the actuator and the radius of the crinkle were chosen as governing parameters for the actuator behaviour. The internal pressure is -10kPa in chamber A and +10kPa in chamber B. Fig. 1 in the contributed paper shows the cross-section of the actuator with the indicated parameters and the result of the simulation with the final version of the actuator is shown in Fig. 2.3.

To simplify the simulation, the actuator adaptor was omitted and symmetry was exploited through the actuator. The cross-section used for the simulations can be seen in Fig. 1 of the contributed manuscript. Doing this reduces the number of nodes requiring solving through the FEM process, speeding up the process considerably. The adaptor was replaced with a *fixed* fixture which prevents any movement in the x, y, or z directions at this end of the actuator and the second half of the actuator was replaced with a *symmetry* fixture which mirrors the body and fixtures about the central plane. A *bonded* global contact was enforced which prevents relative displacement at the interfaces between bodies in the study.

The results of the design study are shown in Fig. 2.4. As can be seen in Fig. 2.4a, the output displacement increases with crinkle radius but reduces with chamber wall thickness. This trend isn't particularly of note because crinkles with larger radii will more readily flatten to enforce displacement and, when the chamber walls are thickened, they will provide greater

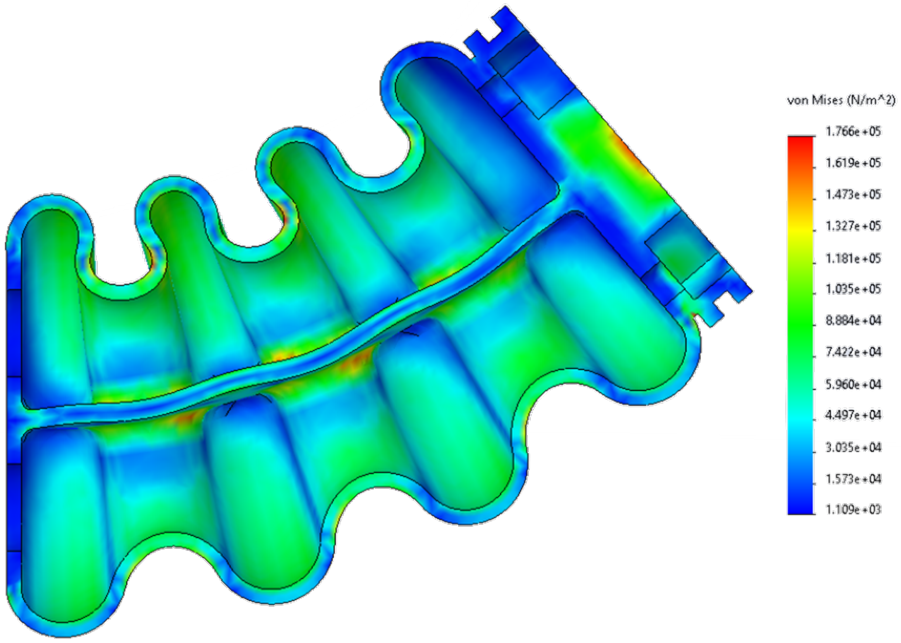

Figure 2.3: FEA of the actuator with the parameters used in the parametric study. The Von Mises stress is presented here to highlight the stress concentrations around the midlayer.

resistance to extension. For the stress analysis, only the stress in the chambers is examined, rather than the rigid end pieces because the failure stress in the two materials used is greater than an order of magnitude different and so it can be safely adjudged that the rigid end pieces will not fail (see Appendix Table A1 for more detailed information). In Fig. 2.4b, the data demonstrate that wall thickness has a much less significant effect on the Von Mises stress than the radius of the crinkles. The reason for this trend can be found in Fig. 2.3, where the high-stress concentration regions can be found at the intersection of the mid-layer and the sides. The thickness of the material does not affect this because the stress is not through-thickness, rather it is concentrated in these 'soft hinge' regions. The crinkle radius, however, does affect the peak stress because the effective moment about the bending point increases with the crinkle radius. In other words, the force applied to enforce bending is further from the soft 'joint' region and therefore greater stress is imparted. It can be seen in both Figs. 2.4a and 2.4b that when the crinkle radius reaches 3mm, there is significant noise

in the results. This is largely due to well-known meshing limitations in Solidworks when calculating results of soft materials with large deformations. However, up to this point, the results are consistent and the trends are clear to be used in informing design choices.

The optimum design parameters for the actuator were calculated by first normalising the stress and displacement data to allow for direct comparison and applied to the formula:

$$p = \ argmax\ (5 \cdot x - 4 \cdot \sigma) \tag{2.1}$$

Where x is the greatest displacement and σ is the greatest stress in the chambers of the actuator. The stress term is negative since the goal is to minimise it. Fig. 2.4c shows each of the normalised datapoints with the value that maximises this equation highlighted.

Control Schemes The actuator in [126] is capable of three separate modes of control:

1. Single chamber actuation, where only one chamber is pressurised and the other is left open to the atmosphere. This mode is used to generate a single direction of actuation, either extension or contraction.

2. Complementary control, where both chambers are pressurised in opposite polarities. This mode is used to increase both the force and output angle of the actuator.

3. Antagonistic control, where both chambers are pressurised in the same polarity. This mode is used to increase the stiffness of the actuator.

The three modes are shown in Fig. 2.5. Using the complementary control increases the force and output angle of the actuator; this could be applied to a gripper capable of lifting heavier objects or in exploration capacity where the increased output angle enables an improved range of motion. In the other control scheme, the antagonistic control increases the stiffness of the actuator; by modulating the stiffness of the actuator and attaching exteroceptive

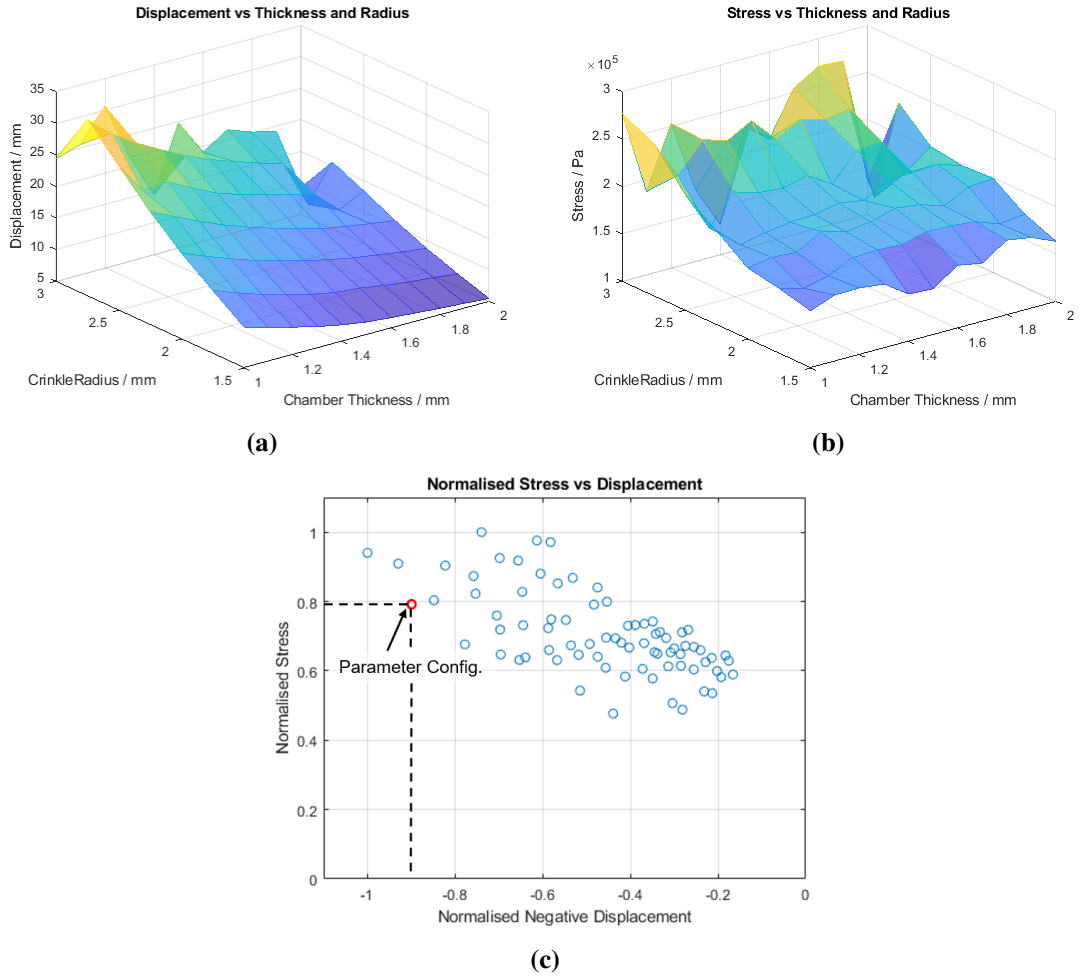

Figure 2.4: (a) Displacement results of the parametric study (b) Stress results of the parametric study (c) Normalised values of the displacement and stress results with the chosen configuration highlighted.

sensing, material or friction detection can be enabled by detecting the vibration frequencies as the actuator is dragged along a surface.

Further discussion points over the process used to fit the shape of the actuator have been added to Appendix A.2.

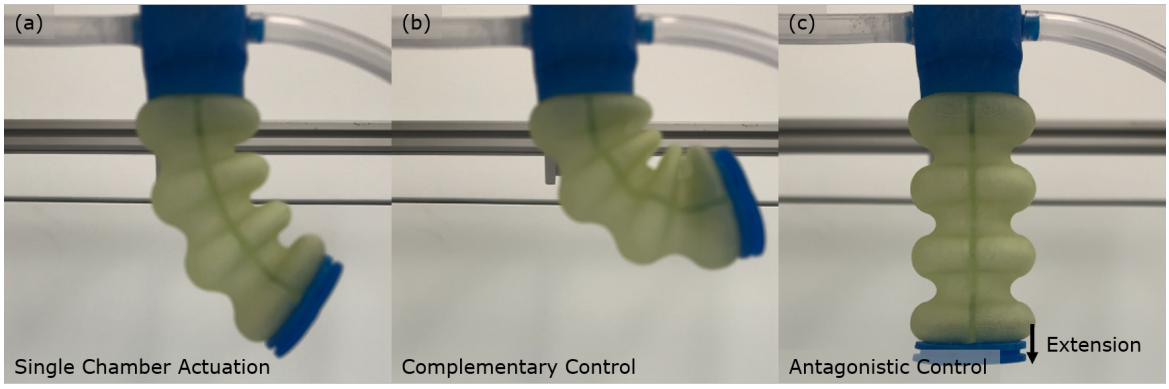

Figure 2.5: Three control modes for the bi-directional actuator. (a) Single chamber actuation. (b) Complementary control, to increase force and angle output. (c) Antagonistic control, to increase beam stiffness.

2.6 Limitations and Further Work

Force output The primary limitation of the presented actuator is its force output. Whilst using complementary control facilitated a near four-fold increase in the force output, the maximum output was still only 2.17N. This is comparable with other pneumatically actuated work in the literature but low compared to actuators with alternate actuation methodologies. An obvious next step, in this regard, would be to use different materials from the printer portfolio or to consider a different method of achieving variable stiffness such as particle jamming through the core. However, both of these methods would likely reduce the range of motion, which is paramount for the kinematic range of the actuation towards the design of the fingers in the next chapter.

Reliability With regard to the reliability, as indicated in Sec. 2.2.2, the materials provided by the polyjet printer can demonstrate high variability depending on the conditions they are printed in and stored in. The effect of that is they can be unpredictable if not handled identically between specimens. During the work, it was found empirically that some samples

would perforate at lower pressures if left in direct light for too long or in the cleaning solution. For the actuators presented in the contributed paper, they were produced and stored identically which is reflected in the results. This performance variability is a problem that is not with the actuator itself but with the nascent materials. Essentially, the materials are not yet ready for use in a general production environment with long-term variable storage conditions but the techniques developed in this chapter show great promise for future applications for 3D printed photopolymers. Therefore, as material science continues to develop, it can be expected that the reliability of similarly fabricated actuators will improve.

With the risk of actuator failure in mind, actuators with small perforations were found to still be able to function successfully under vacuum actuation since the failure mechanism/hole tends to close in this configuration. This discovery was used to inform the design of the joints presented in the following chapters and chose to use only single-chamber actuation.

Uniform vs. Multi-Segment Actuation The presented actuator shows promise towards being used as a uniformly actuated finger in the design of the hand. Indeed, in follow-up work, a simple three-finger gripper was designed for use in a pick-and-place task with simple open-close control and a diverse range of objects. However, uniform actuators are limited to being able only to present a power grasp, with poor performance when trying to execute a precision grip [40, 127]. This has been shown to limit the range and size of objects that can be grasped by a gripper. Therefore, for the design of the hand, multi-segment fingers were chosen to facilitate the pinch grasp. This is discussed in more detail in the next chapter, in combination with the requirements posed by the GRASP taxonomy posed by Feix et al. [128].

Statement of Authorship for joint/multi-authored papers for PGR thesis

To appear at the end of each thesis chapter submitted as an article/paper.

The statement shall describe the candidate's and co-authors' independent research contributions in the thesis publications. For each publication there should exist a complete statement that is to be filled out and signed by the candidate and supervisor **(only required where there isn't already a statement of contribution within the paper itself).**

Title of Paper	Design of a Multimaterial 3D-printed Soft Actuator with Bi-directional Variable Stiffness
Publication Status	☒Published ☐ Accepted for Publication ☐ Submitted for Publication ☐ Unpublished and unsubmitted work written in a manuscript style
Publication Details	Shorthose, O., He, L., Albini, A., & Maiolino, P. (2021). Design of a Multimaterial 3D-Printed Soft Actuator with Bi-directional Variable Stiffness. In *Annual Conference Toward Autonomous Robotics Systems: Vol. 13054 LNAI* (pp. 238–248). Springer. https://doi.org/10.1007/978-3-030-89177-0_25

Student Confirmation

Student name:	Oliver Shorthose		
Contribution to the paper:	I developed the idea for the actuator with Professor Maiolino I developed the design of the actuator and undertook the characterisation I led the write-up with support from the other authors		
Signature: 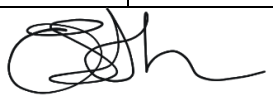		Date	19th July 2023

Supervisor Confirmation

By signing the Statement of Authorship, you are certifying that the candidate made a substantial contribution to the publication, and that the description described above is accurate.

Supervisor name and title:	Professor Maiolino		
Supervisor comments:	I confirm that the student made a substantial contribution to this publication and the contribution of the other authors is as described above		
Signature: 		Date	19/07/23

3

Soft Hand Design

As humans, we use our hands from a young age to explore the world around us. They facilitate complex and wide-ranging interactions with the environment, from grasping and manipulating objects to sensing and interpreting a plethora of stimuli [129]. However, this combination of dexterous actuation and a highly sensitive nervous system presents an intricate design challenge for engineers to replicate [19]. This chapter takes the actuation and fabrication methodologies developed in the previous chapter and apply them to the design of a soft robotic hand. The compliance afforded by pneumatic actuation is combined with the kinematics of the human hand to achieve human-like dexterity in grasping and simplify fabrication relative to comparable works by using multi-material 3D printing. An active palm is included to increase the range of motion of the thumb and achieve thumb opposability, a key feature of human grasping [61]. Furthermore, the work looks to embed distributed tactile sensing into the body of the hand to enable exteroceptive sensing across the entire surface.

Sec. 3.1 discusses the grasp taxonomies that have been developed to understand the dexterity of the human hand and how they have been applied to the design of anthropomorphic robotic hands. Then, a discussion is presented over how soft materials can be used to simplify the required control whilst demonstrating strong performance in grasping challenges. Sec. 3.2 explores the role of sensing for informed interactions between soft robotic end-effectors and the environment. The paper that was published in RA-L 2022 and presented at ICRA 2022 is presented in Sec. 3.3. Sec. 3.4 provides further information over the kinematic analysis that was undertaken before finishing with a discussion of the limitations of the hand and proposed modifications for the future application towards object identification in Sec. 3.5.

3.1 Anthropomorphic Robotic Hands

Solutions to the formidable task of designing anthropomorphic hands have ranged widely, culminating in applications across a host of fields, ranging from prosthetics to industrial manipulation and, more recently, human-robot interaction [25, 27, 130]. However, to date, most examples are designed to be applied to a single application and the versatility of the human hand is yet to be realised. This is largely due to traditional solutions attempting to control each of the DOFs explicitly, leading to highly complex control schemes that are prohibitively difficult to generalise [131].

In order to achieve human-like grasping and manipulation, it is first necessary to comprehend the behaviour and movement of the hand. With its 21 DOFs, the hand is capable of presenting a wide range of postures, requiring detailed analysis into those most implemented [9]. Classification of these is made challenging by the innumerable permutations of individual finger poses. Therefore, simplification and reduction to the most commonly used grasps have been presented by work done by Feix et al. [128]. The authors reviewed previously proposed taxonomies and filtered them down to 33 unique prehensile grasps

that are then grouped according to the type of grasp (power, precision or intermediate) and the use of the thumb in the grasp (adducted or abducted). The set of grasps provides a baseline dexterity for designers to target when working towards anthropomorphic dexterity. By extension, the role of the thumb in grasping has been extensively researched both in the context of human grasping and in robotic biomimetic grasping [132]. The evidence clearly indicates that the adduction-abduction behaviour of the thumb contributes significantly to successful grasping and in-hand manipulation. Commonly, this behaviour in robots is measured through application to the Kapandji opposition test to compare it with the human range of motion [60]. The work takes the dexterity of the thumb as a paramount requirement for the design of the hand in this work and this is reflected in the contributed paper in Sec. 3.3.

Developing upon the Feix Taxonomy and Kapandji opposition test has resulted in an array of promising and impressive anthropomorphic hands with highly dexterous capabilities. However, as reported by Piazza et al. [27], when applied to benchmarking competitions such as the Amazon Picking Challenge [133], DARPA Robotics Challenge [134] or the Robotic Grasping and Manipulation Competition [135], solutions with simplified control and designs performed best. Indeed, although a high level of dexterity can offer certain advantages, when aiming for generalisability, as is the case in these competitions, adaptability and simplification is often found to be more desirable. In this regard, the inclusion of soft materials into hands has achieved that goal with previous designs successfully grasping a wide range of objects with just simple control schemes [42, 136–139]

This work draws inspiration from the dexterity and extensive range of motion achieved by human hands and combine it with the adaptability afforded by soft joints to design a soft robotic hand. Through this combination, it is possible to produce a soft hand that is capable of grasping a wide range of objects. This design allows for versatile control, offering the option of a simple underactuated scheme or a more complex one, where each DOF can be individually controlled if desired. This soft robotic hand serves as the foundation for the

subsequent chapters in this thesis, whereby the hand is applied to object identification tasks.

3.2 Tactile Sensing Methodologies

Sensing most commonly applied to robotic hands can be broken down into proprioception and exteroception. Proprioception, or kinaesthesia, refers to the means of sensing that provides an understanding of the agent's pose and movement at any given time. It can also be used to monitor internal forces applied through the body of the agent whereas exteroception refers to sensing that provides information about stimuli external to the agent. This work explores the application of both sensing methodologies and their role in the context of grasping and, ultimately, how they can be applied towards object identification in Chaps. 4 & 5.

3.2.1 Proprioception

Humans rely on proprioception, sometimes known as the "sixth sense," consciously and subconsciously to monitor and update their body position and motion [140]. Analogously, robotic solutions leverage proprioceptive sensing for state estimation during object and environmental interactions. For traditional robots, the joint angles and torques are often provided by positional encoders and torque sensors that are placed at the discrete joints of the robot [131]. For the purpose of grasping diverse objects, this data is essential (often in combination with exteroceptive sensing) in order to inform control schemes for successful grasping and avoidance of damage to the object [23, 141].

Some designs within Soft Robotics have exploited proprioception to inform structural reconstruction, object identification, grasp stability estimation, and surface feature identification [142–146]. Whilst proprioception is significantly more difficult with Soft Robotics because of the near infinite DOFs within soft actuators, it has been achieved through a range of flex sensors such as using conductive fluids, stretchable strain sensors, capacitive

sensors, waveguides or other methodologies [41]. However, the integration of these sensors often jeopardises the softness or range of motion of the actuator [146], and, within object identification, proprioception is limited in the range of objects that can be identified beyond discriminating between sizes and stiffnesses within a similar object class [147]

3.2.2 Exteroception

Exteroception provides us with the means to perceive the surrounding environment, whether that is the weight of an object, the smell of a perfume, or myriad other stimuli. For robotic agents, sight and touch specifically are of paramount importance for informed interactions both initially when predicting what interaction to expect and subsequently interpreting an incident contact. This work focusses on utilising sensing to enhance the capabilities of the hand toward in-hand object identification and therefore visual exteroception is out of the scope of the work.

In particular, this project explores sensing solutions that can maintain the softness that has been achieved in the actuation phase of design as detailed in Sec. 3.1 to ensure compliance in the grasp whilst forming the foundation of sensing for object detection. Within the paradigm of exteroceptive sensing, softness at the point of contact enables greater surface area between the parties, increasing the force distribution to improve safety in contact, increase friction in the grasp and facilitate greater sensor stimulation [41, 148]. Previous solutions have achieved this through two main methods: soft skins and discrete sensors (distributed and localised).

Soft skins are comprised of a thin layer that can be wrapped around intricate geometries and achieve contact detection through sensors that are distributed across the layer [149]. These skins are designed to be lightweight, flexible, and often elastic so they can conform to the shape of the host body without restricting movement or adding bulkiness [150]. Most commonly, the sensors within the skin are barometric, resistive, capacitive, magnetic or

optical. They have demonstrated strong performance in the context of large-area tactile sensing applied to anthropomorphic hands and robotic grippers [23, 151, 152]. However, soft skins require the integration of additional components onto the body of the hand, complicating fabrication, and their thin structure is liable to damage through repeated or forceful contacts [41]. Therefore, with the goal of simplifying fabrication for repeatable production, the decision was made to explore sensors that can be embedded within the hand or individually attached to mitigate the potential tearing of or damage to the skins.

Sensors placed on or embedded within the hand are often localised, whereby they are placed in the fingertips for detection during pinch grasping, or they can be distributed around the hand to provide a wider scope of contact between the object and environment. Tip detection has been used successfully in closed-loop force control and rudimentary shape detection [138, 153–156]. However, it is limited to a small area of sensing that requires specific object placement for successful operation. Conversely, using distributed sensing allows for contact detection across a larger area, enabling both precision and power grasping, but increases the complexity of both the fabrication and the signal processing [42, 43, 50]. In this work, the primary target is the application of grasping a wide range of objects from any pose and, therefore, being able to acquire tactile data and thus detect salient features across the entire hand is desirable.

For the purpose of undertaking grasping and manipulation tasks, twinning the incoming tactile stimulus and the outgoing planned action has been shown to be beneficial for successful interactions [3]. This is known as sensory-motor coordination (SMC) and involves the close integration of input, processing and output. Rather than relying on an explicit mapping between input and output, SMC allows the user to embody that mapping and significantly reduce the complexity of the control model [157, 158]. Furthermore, by physically coordinating the contact detection with the subsequent reaction actuation, a synergistic relationship is created whereby the input-output inherently affect each other

directly; for humans, this relationship is learned through development to achieve simplified control for in-hand manipulation [16]. Within the context of soft robotic hands, SMC can be achieved most effectively by situating the sensors and actuators in proximity to one another, and by embedding the sensors within the body of the agent rather than integrating separate systems [159, 160]. By distributing the sensors around the body of the hand, the distance between each sensor and its corresponding closest actuators can be further reduced, which will enhance the hand's ability for manipulating objects in future work.

Through this analysis of the potentials and limitations across proprioception and exteroception, the decision was made to design embedded, distributed, pneumatic, tactile sensing into the hand in this work. By exploiting a multi-material monolithic design for the distributed sensors, the sensory system is coupled closely with the output actuation for close sensory-motor coordination. Furthermore, by using pneumatic sensing, the softness of the grasping contact is maintained with simple fabrication, whilst being able to detect contact across the entire surface.

3.3 Contributed Manuscript

The contributed manuscript in this chapter was published in the Robotics and Automation Letters 2022 and presented at ICRA 2022. The paper takes the findings from this chapter and uses multi-material 3D printing to achieve a highly repeatable design that exploits an active palm and vacuum actuation to emulate the human range of motion in the hand to fulfil the Feix grasp taxonomy and Kapandji thumb opposition task, and demonstrate adaptive grasping. Integrated distributed tactile sensing is implemented to achieve exteroception across the entire surface of the hand [161].

Erratum: In Section IV B (4) of the published version of the paper, it states "100 cycles have been isolated to show the detail of the test's results in Fig. 8". This is misplaced and

should be in Section IV B (3). The figure represents the *Dynamic Sensor Output* rather than the *Dynamic Finger Output*.

IEEE ROBOTICS AND AUTOMATION LETTERS, VOL. 7, NO. 2, APRIL 2022 3945

Design of a 3D-Printed Soft Robotic Hand With Integrated Distributed Tactile Sensing

Oliver Shorthose, *Graduate Student Member, IEEE*, Alessandro Albini, *Member, IEEE*, Liang He, *Member, IEEE*, and Perla Maiolino, *Member, IEEE*

***Abstract*—Humans rely on distributed tactile sensing in their hands to achieve robust and dexterous manipulation of delicate objects. Soft robotic hands have received increased attention in recent years due to their adaptability to unknown objects and safe interactions with the environment. However, the integration of distributed sensing in soft robotic hands is lacking. This is largely due to the complexity in the integration of soft sensing solutions with the hands. This letter proposes a novel soft robotic hand that incorporates an active palm and distributed pneumatic tactile sensing in both the fingers and the palm. Multi-material 3D printing allows the tactile sensors to be directly printed on the hand, whereas conventional tactile approaches require the sensors to be attached as part of multiple fabrication procedures. Active degrees of freedom are introduced in the palm to achieve increased dexterity. The proposed hand successfully performed 32 of the 33 Feix taxonomy grasps and all 11 Kapandji thumb opposition poses.**

***Index Terms*—Soft robot applications, soft sensors and actuators, multifingered hands, additive manufacturing.**

I. Introduction

RESEARCH into soft robotics has increased over the last decade introducing soft, compliant materials to improve the safety and adaptability of robotic designs. The compliance allows for interaction with objects that vary in geometry and stiffness without requiring sophisticated control strategies. Specifically, robotic hands have received ample focus due to the interest in combining anthropomorphism with soft materials to achieve safe interaction and human-like dexterity [1]–[3].

Unlike many robotic hands that focus solely on finger and thumb actuation, humans use the degrees of freedom (DOFs) in the palm to achieve a wide range of grasp poses [4]. The adaptability of the human palm and the flexibility in creating contact configurations also increases the ability to ensure a robust grasp through uncertainty. This is compounded by the utilisation of passive compliance to interact with more diverse environments and establish greater dexterity [5]. Recently, soft robotic hand designs have been presented that incorporate active palms and passive compliance to improve their dexterity in manipulation [6]–[8]. Specifically, by mimicking the kinematics and softness of the human hand and implementing extra DOFs in the palm, soft robotic hands can interact with a wider variety of objects and achieve safer in-hand manipulation. For example, in [6], the authors proposed a 3 finger soft gripper with an active palm. The active palm allows the gripper to successfully grasp a wide variety of objects with different geometries and stiffnesses. Furthermore, the gripper compliance enables robust grasping with simple open-loop control. A soft humanoid hand with an active palm was proposed in [7]. The design demonstrated high compliance whilst grasping, thus avoiding damaging the grasped objects. Additionally, it was shown to be capable of performing a high number of different grasps from the Feix taxonomy [4]. In [8], the soft robotic hand design is inspired by a human hand model and it is composed of 26 independent DOF. The authors showed the possibility of achieving highly dexterous in-hand manipulation tasks. However, although the compliance of the hand has been successfully shown to be a key feature in achieving safe interaction with objects, these solutions lack a means of tactile sensing feedback to properly regulate the contact forces applied to the object and undertake precise in-hand manipulation [9]–[11]. Therefore, a lot of effort has been dedicated to the development of solutions providing soft robots with exteroceptive sensing [12].

In particular, tactile sensing has been shown to be essential in partnership with soft robotic hands or grippers to achieve safe and delicate object grasping and manipulation [9], [13]–[15].

For example, in [7] tactile sensors were integrated in the tips of a soft prosthetic hand enabling closed loop control of the grasping force. In [15] authors proposed a novel soft sensor that can be integrated on the tips of existing grippers to sense contact forces and the curvature of objects in their grasp. A monolithic soft robotic finger with an embedded tactile sensor in the tip was presented in [14]. In this solution, a soft pneumatic chamber was directly 3D-printed on the finger to detect tactile forces. The letter presented in [10] proposed a novel soft fingertip with embedded air cavities that can be used as a sensing element and actively change the shape of the fingertip, thus achieving a robust grasp while manipulating delicate objects. Although, these solutions have demonstrated the benefits of introducing tactile feedback to a soft gripper or finger, they allow to retrieve lumped contact information only. A more complete spatial information of the contact events can be attained from a distributed sensing network.

Manuscript received September 9, 2021; accepted January 24, 2022. Date of publication February 7, 2022; date of current version February 18, 2022. This letter was recommended for publication by Associate Editor R. MacCurdy and Editor K.-J. Cho upon evaluation of the reviewers' comments. This work was supported by EPSRC Programme Grant From Sensing to Collaboration under Grant EP/V000748/1. *(Corresponding author: Oliver Shorthose.)*

The authors are with the Oxford Robotics Institute, University of Oxford, Oxford OX26NN, U.K. (e-mail: oliver.shorthose@eng.ox.ac.uk; alessandro@robots.ox.ac.uk; liang.he@eng.ox.ac.uk; perla.maiolino@eng.ox.ac.uk).

Digital Object Identifier 10.1109/LRA.2022.3149037

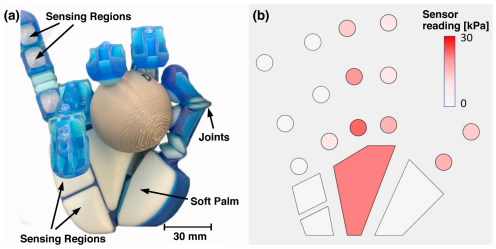

Fig. 1. The proposed soft hand with the active palm and distributed tactile sensing. (a) The soft robotic hand grasping a sphere. The sensing regions and joints consist of 3D printed air chambers. (b) The corresponding sensor output from the distributed pneumatic sensing. In this visualisation, the color is related to the detected change in internal pressure.

In particular, [16] provided distributed contact sensing capabilities on the fingers of a pneumatically actuated soft hand. An array of 4 flexible piezoresistive force sensors was integrated on each finger. The contact data were then used to train a neural network to classify a set of different grasping poses. Beyond the sensorisation of the fingers, [17] extended soft tactile sensing capabilities to the palm of a Shadow Hand (Shadow Robot Company, U.K.). Distributed contact sensing measurements were then exploited to classify objects' properties while performing in-hand manipulation. However, this integration cannot be easily performed on soft hands. Additionally, although [16] and [17] showed the advantages of having a soft tactile sensing array in manipulation tasks, they still rely on an a posteriori integration procedure required to embed tactile sensors onto an existing hand. This can increase the risk of human error in the fabrication process or reduce the durability of the system.

The contribution of this letter is the novel design of a multi-material 3D printed soft robotic hand with an active palm, fully integrated with distributed tactile sensing capabilities. Fig. 1 shows the proposed hand. It contains 18 tactile sensing regions, consisting of 3D printed soft chambers. The soft pneumatic joints achieve controllable actuation for the active degrees of freedom. This is combined with passive compliance provided by the soft material to demonstrate successfully 32 out of the 33 required Feix taxonomy poses and all of the Kapandji opposition test poses. The designs proposed in [6]–[8] rely on silicone casting, thus requiring multi-step fabrication. Conversely, our design is monolithic and can therefore be fully 3D printed without requiring further integration of the parts, simplifying the fabrication of the hand. The solutions provided in [7], [10], [14], [15] have successfully integrated soft tactile sensors on robotic grippers or hands, however the sensing is limited to fingertips. Our design utilises distributed sensing to provide information over the contact locations and pressures applied on the hand. Additionally, by incorporating soft pneumatic pads, the design integrates an inherent compliance, allowing for greater adaptability to objects. The range of motion of each finger as well as the maximum grasping force have been characterised. Furthermore, the Feix Taxonomy and Kapandji Score [4], [18] have been evaluated to benchmark the dexterity of the whole hand.

The structure of the letter is as follows: Section II presents the design of the hand; Section III details the fabrication process; Section IV reports the experiments performed to characterise the system; The result of the Feix Taxonomy and Kapandji Score are reported in Section V; the Conclusion follows.

II. Hand Design and Actuation

The soft robotic hand is designed to attain dexterity comparable to a human hand in the fingers and palm. The hand incorporates the following design features: 1) soft actuation of the palm to increase the workspace of the thumb, 2) full coverage of the hand with soft pads to increase its adaptability and safety in grasping, 3) distributed sensing of the surface to provide tactile information of the object-hand interaction.

A. Palm and Hand Design

The geometry of the hand is designed based on human hand anatomy. The palm is introduced so that the soft thumb can reach the same places on the hand as a human thumb can, and the fingers have a comparable range of motion.

Similar to the human hand, the fingers are actuated at the metacarpophalangeal (MCP), proximal interphalangeal (PIP), and distal interphalangeal (DIP) joints, as shown by the actuator regions in Fig. 2. The desired bending range of each joint was determined by examining the mean value of the functional range of motion for the human finger joints [19]. This value was found to be 74°. To simplify the design process, this target was chosen to be identical for each joint.

The thumb was actuated at the scaphotrapeziotrapezoidal (STT), MCP, and interphalangeal (IP) joints. The desired bending angles were similarly deduced from a comparison to the human range of motion: STT abduction 42°; MCP flexion 53°; IP flexion 80° [20].

The positions of the MCP joints of each finger were determined from hand anatomy, taking the joint positions of an average human male [21]. Human fingers have a natural splay, with approximately 6° between the index and middle finger, 5° between middle and ring finger, and 10° between the ring and little finger. These angles were also incorporated into the design. To simplify the overall design, the fingers' joint lengths were constrained to be the same. The overall length of each finger was targeted at the average length of the average human male middle finger (93 mm) [21].

Although the hand is soft, the integration of bone sections and compliant joints leads to a predictable motion of the hand that can be approximated as a set of joints, interconnected by rigid links. With the simplified kinematics, the angle of actuation between the base of the palm and the STT joint, and the axial rotation of the thumb are identified. The angle between the thumb and the base of the palm was determined to be 20°, and the axial rotation of the thumb is 30°. This configuration allows the thumb to come into contact with each fingertip, thereby demonstrating the design's dexterity.

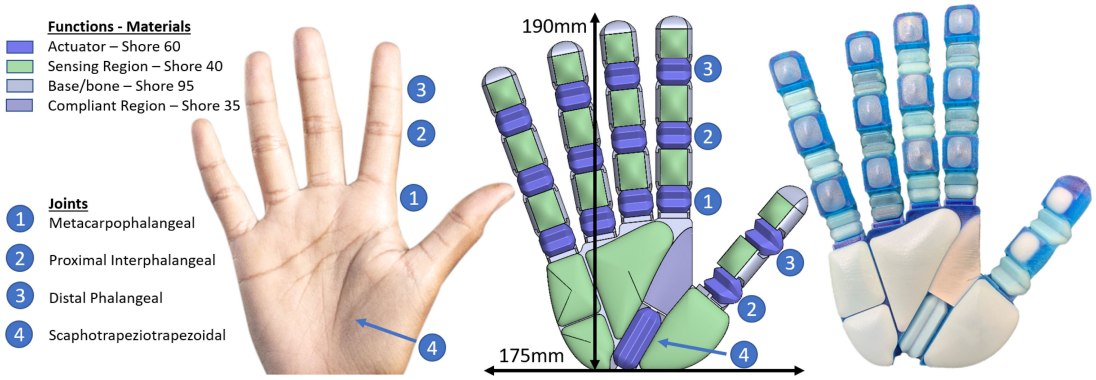

Fig. 2. (Left): Human hand for scale and to indicate where each joint is; (Middle): CAD model of the soft robotic hand. The different regions are indicated in the legend with their respective Shore A hardness as follows: Blue, actuator, Shore A60; Green, sensing region, Shore A40; Grey, base/bones, Shore A95; Blue-grey, compliant region, Shore A35; (Right): The 3D printed hand. The total weight of the hand is 135 g, the height is 190 mm and the width is 175 mm.

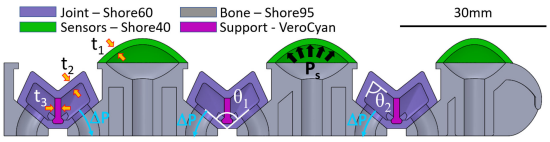

Fig. 3. Cross-section of the finger. The different regions are indicated in the legend. P_s is the internal pressure on the soft pneumatic sensors and ΔP indicates the flow of air to evacuate the chambers. The dimensions are presented in mm: $t_1 = 1.25$; $t_2 = 1.5$; $t_3 = 1.0$; $\theta_1 = 100°$; $\theta_2 = 75°$.

B. Actuation

The fingers have three identical joints, the MCP, PIP and DIP, which can be independently actuated by applying negative pressure to each one of the M-shaped chambers (see Fig. 3). Vacuum actuation was chosen to achieve the required bending angle (74°) over a small region, which allows the kinematic simplification of discrete joints to be validated. Additionally, vacuum actuation was chosen over positive-pressure actuation to reduce the tensile stresses induced in the chambers [22].

Fig. 3 shows a cross-section through the finger, highlighting the different materials and geometries in the design. The design takes inspiration from an origami folding structure and uses a rigid centre support to prevent the chamber from collapsing [23]. The width and height of the fingers were chosen to fit roughly to the same size of a human finger (20 mm).

The thumb and palm joints use the same M-shape design as the fingers. This simplifies the design process and reduces the necessary characterisation.

The fingers were simulated with Finite Element Modelling (FEM) in Ansys software (Ansys, Inc., USA) to validate geometry and design. Static structural tests were carried out using a Neo-Hookean hyperelastic model. The material properties of the Stratasys Digital Materials for the simulation were found in [24]. The shear modulus was computed as $G = \frac{E}{2(1+\nu)}$ where E is the Young's modulus and ν is the Poisson's ratio.

1) To evaluate the material in the joints' performance under pressurisation, a negative pressure was applied to the interior surfaces whilst one of the bone pieces had a fixed boundary condition applied. The negative pressure was set at 10 kPa as a mid-range target that would not cause material failure. The bending angle was taken as the angle between the two bone pieces either side of the joint and was compared between materials.
2) To ensure the finger would not deflect under self-weight, gravity was applied over the body without any other external forces. The tip deflection was recorded for each joint material.

As a result of the simulations, Shore A60 Vero/Agilus blend was selected to fabricate the joints (tensile strength 3.5-4.5 MPa, elongation at break 150-170%). Further details about the materials are also introduced in the Section III. Furthermore, the addition of the central support was simulated. Fig. 4 shows the simulated joint with and without the central support. Without the central support the joint flattened, not causing any bending motion, whereas the central support enforced a bending motion around the centre of the joint as desired.

C. Distributed Tactile Sensing

Pneumatic chambers are chosen as the tactile sensing methodology in the hand design due to the inherent sensor softness, and ease of integration with single-batch 3D printing [10], [14]. In this respect, the sensors are designed as air-filled soft membranes that are raised 4 mm from the surface of the fingers and palm, with 1.5 mm thickness and material stiffness of Shore A40 hardness. The pneumatic sensing units are distributed over the whole hand to capture the contact information of the entire surface area. The softness of the sensing skin provides additional adaptability and safety to the grasp.

In each finger, three soft sensing units cover the bone regions between each joint to ensure that the sensors are not affected as the finger bends (Fig. 3). In the palm, the regions were selected by assessing the most commonly used regions in the human hand

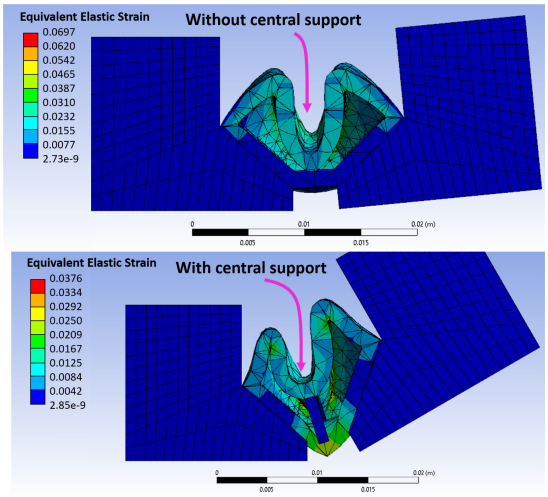

Fig. 4. A comparison of the FEM study: (a) without the central support; (b) with the support. It can be noticed that rigid support in the centre prevents the chamber from collapsing in the undesired direction and supports the bending motion.

for object manipulation [25]. The regions identified are the base of the thumb, and the region below the pinky finger, whereas the central region is used less frequently. The soft sensor above the STT joint is integrated as part of the active palm sensing region. In total, 18 independent sensing regions are introduced to the hand. The detailed distribution is shown in the green regions in Fig. 2.

III. Materials and Fabrication

The soft robotic hand is 3D printed using multi-material polyjet technology (J735, Stratasys Ltd, USA). This allows for monolithic integration of the soft sensing regions and the stiffer bone structures. For this design, a combination of Vero, a rigid plastic, and Agilus30, a rubber-like soft plastic was used [24]. By changing the proportions of the two materials in a blend, the shore hardness of the material can be controlled (ShoreA [30,35,40,50,60,70,85,95]) [24].

The palm and thumb are printed monolithically, whilst the fingers are printed separately and attached via a simple slot connection. This allows for easy replacement of the fingers should they be damaged without having to reprint the entire hand. After printing, the support material is removed by placing the printed piece in a chemical bath (GEMINI SSR-550) filled with chemical support removal solution (0.02 kg/L Sodium Hydroxide and 0.01 kg/L Sodium Metasilicate).

The materials of each region are indicated in Fig. 2. The material of the joints was chosen to be Shore A60 after the simulation as detailed in Section II. The main body was chosen to be Shore A95 to provide a small amount of compliance whilst providing sufficient strength to support the weight of the fingers and objects. The sensors are Shore A40 to allow for a greater

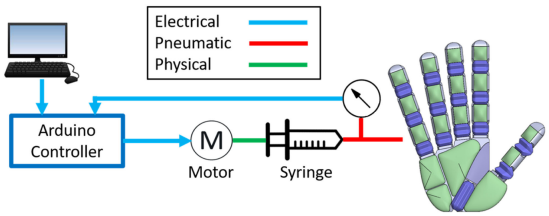

Fig. 5. Control architecture for the soft hand. The Arduino controls the stepper motors, responding to real-time pressure values from the pressure sensors. The data from the Arduino and webcam is stored and post-processed to plot.

degree of compliance whilst not failing under the applied load to compress the sensors.

IV. System Characterisation

This section describes the experimental characterisation of the proposed design. In particular, we focused on the characterisation of 1) the range of motion of the fingers in relation to the pressure applied, 2) the output of the pressure sensors in relation to the applied force, 3) the overall grip strength of the hand where both the fingers and palm are involved in a grasping configuration.

A. Experimental Setup

A closed loop PID control executed on an Arduino board was used to set the desired pressure to actuate the joints. Each joint in the hand is connected using identical length tubes of 1 mm internal diameter (ID) to a pressure sensor (ADP5101) mounted on a PCB, remote from the hand, and connected to the Arduino board which samples the sensors' output at 50 Hz. The Arduino is also responsible for driving a set of stepper motors (Nema 17 Step with A4988 driver) actuating pneumatic syringes as depicted in Fig. 5. This sets the internal pressure of the joints as desired. The number of stepper motors and syringes required is dependant on the number of DOFs being controlled in any particular application. The pneumatic chambers corresponding to tactile sensing elements were also connected via 1 mm ID tubing to 18 different ADP51A11 pressure sensors and the measurements were sampled at 20 Hz using an Arduino.

B. Testing and Results

1) Range of Motion: The fingers' range of motion was tested pseudo-statically by applying negative pressure to the chambers at 5 kPa decrements until full actuation was achieved. The three joints in the finger were actuated concurrently. At each decrement, the pressure was held constant for 15 seconds to reduce any effect of hysteresis. The angle of the joints was recorded through a webcam using image acquisition software, *MATLAB image acquisition toolbox*, identifying markers at each joint and plotting the angle between them. Each characterisation test was repeated 5 times for 3 different printed models to test the repeatability of the fabrication process. Between tests, the

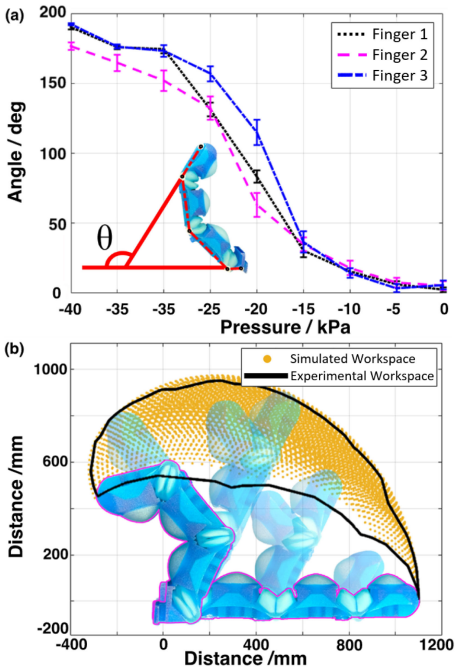

Fig. 6. (a) Results of the range of motion tests for the fingers. The fingers were actuated in 5 kPa decrementing pressure intervals and held for 15 seconds to ensure quasi-static conditions. The angle, θ presented is the angle between the first and last digits in the finger. (b) Range of motion for each finger. The yellow point cloud indicates the final position that the tip can reach depending on the application of pressure in each joint. The black line indicates the outline of the workspace that was observed experimentally.

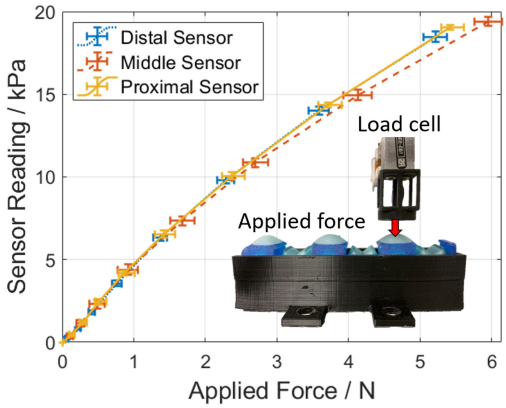

Fig. 7. Results of the static sensor output test. A load cell was brought into contact with the three finger sensing chambers and held statically for 15 seconds before being removed between tests. The displacement was increased by 0.5 mm between tests. Each data point indicates the values read at the 0.5 mm increments.

bodies were returned to a neutral position for 1 minute to allow any residual stresses to dissipate.

Fig. 6 (a) displays the results of the fingers' range of motion. The average maximum bending angle of the individual joints was $70.0°$. The average maximum angle between the first and last joints was $186.3°$. The joints' output angles is slightly lower than the target angle of $74°$ discussed in Section II. However, as shown in the next Section, this does not compromise the whole hand dexterity while performing the Feix and Kapandji tests.

A comparison of the simulated workspace against the real finger's workspace is presented in Fig. 6 (b). The simulated workspace is extrapolated from the kinematic simulation by examining the output position of the finger tip at each proposed output angle. Similarly, the real workspace is composed of the tip position at each angle recorded from the range of motion test. As shown, the workspaces have a considerable overlap, with a 2.7% difference in terms of areas between the simulated and real workspace.

2) Static Sensor Output: The output of the sensors, with respect to the force applied, was characterised by bringing a load cell into contact with the sensor and reading the pressure output. As shown in Fig. 7, the load cell was connected to a flat plate that ensured the whole surface area was depressed. The load was held constant for 15 seconds to allow transient variations to dissipate. The force was increased by displacing the sensors further in 0.5 mm increments and was removed from the sensor surface between increments. The load cell was mounted on a 3-axis Shibaura BA-III cartesian robot. This procedure was repeated 6 times for each chamber on the fingers and three printed specimens were tested. The plot shown in Fig. 7 shows the result of the characterisation. The mean standard deviation across the 30 experiments in the case of the pressure readings was 0.19 kPa. The mean standard deviation for the force readings was 0.09 N instead.

3) Dynamic Sensor Output: To test the sensors' dynamic response and durability, a 0.167 Hz cyclic load was applied to the sensors with 0.5 s pause at the top and bottom of the stroke. The load was applied with the same flat plate used in the static sensor output test, mounted on the Shibaura BA-III cartesian robot. The plate depressed the sensor by 3 mm repeatedly for 1,000 cycles. The small depression was chosen to ensure the material stayed within the linear elastic region. The sensitivity was analysed as the pressure delta over the force delta. The mean was found to be 2.31 kPa/N; the standard deviation was 0.012 kPa/N; the relative variation across the 1000 cycles was 1%.

4) Dynamic Finger Output: To test the fingers' response to cyclic actuation and durability, they were repeatedly actuated 500 times over 3 hours. A syringe was connected to a stepper motor and actuated to increase and decrease the volume of air in the joints by 10 ml. The syringe paused for 7 seconds between tests to ensure the finger was static and residual stresses had subsided. The peak-to-peak pressure is analysed to assess whether any leakages developed or if the material had significantly softened. The mean peak-to-peak pressure was 54.85 kPa, the standard deviation was 0.55 kPa and the greatest difference between two cycles was 2.03 kPa. 100 cycles have been isolated to show the detail of the test's results in Fig. 8.

5) Sensor Hysteresis: To evaluate the amount of hysteresis exhibited by the pressure chambers, a 0.167 Hz sinusoidal load

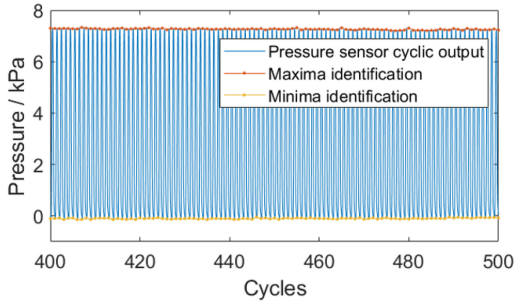

Fig. 8. Results of the dynamic sensor output test. A load cell was cyclically brought into contact with the three finger sensing chambers at 0.167 Hz. A pause of 0.5 seconds was introduced at the top and bottom of each stroke. The maxima and minima are highlighted.

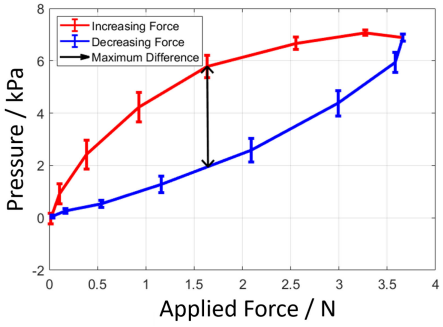

Fig. 9. Results of hysteresis cyclic test. The load cell was depressed and released by 3 mm repeatedly at 0.167 Hz for 20 cycles. The lines show the mean of the increasing and decreasing cycles respectively with the point of maximum difference highlighted.

was applied for 20 cycles. The hardware was the same as for the cyclic sensor output test and the sensor was similarly depressed by 3 mm repeatedly but for 20 cycles. The result is displayed in Fig. 9. The maximum difference at a single applied force value was 3.82 kPa, equating to 54% of the maximum recorded pressure.

6) Grip Strength: The grip strength was characterised similarly to the work presented in [16]. In order to validate the combined strength of the fingers and palm, the hand's grip strength was tested by gripping a cylinder that was mounted to a load cell. In this test, the joints' chambers were connected to each other in the same actuation system (a single syringe as in Fig. 5). The hand was actuated by controlling the overall pressure to -35 kPa in order to grasp the cylinder and to test the maximum grip strength.

The cylinder was then raised at 5 mm/sec until the grasp slipped and the force was reduced. The output of the load cell was recorded throughout and Fig. 10 shows the physical setup for this test. This procedure was repeated 6 times. The load cell is connected to a Shibaura BA-III cartesian which ensures a steady vertical motion. The results of the grip strength test are shown in Fig. 10 with the profile indicating how the force in the load

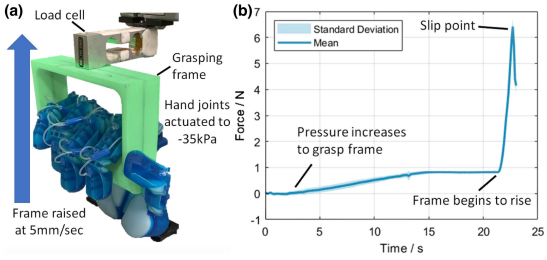

Fig. 10. Results of the grasp strength tests. (a) Physical setup for the grasp strength test. The frame and load cell are connected to a Shibaura BA-III Cartesian robot. (b) Graph of the grasp strength test's results. The pressure was decreased to -35 kPa as the hand came into contact with the frame. The frame was then raised at 5 mm/sec until the the grasp slipped.

cell varies as the grasping frame is raised. The peak indicates the mean maximum grip force among all the 6 experiments, which was found to be 6.42 N with a standard deviation of 0.29 N.

V. Hand Dexterity Validation

A. Feix Taxonomy

The goal of this Section is to validate the kinematic of the hand and its passive compliance by evaluating its performance on the Feix taxonomy poses and the Kapandji opposition test poses.

The Feix taxonomy is a set of 33 grasp poses that aims to encompass the dexterity of the human hand. The tests were undertaken by analysing the relevant DOFs to actuate, the amount of actuation for each DOF, and the objects required to validate the grasp. The object was then placed in the hand and grasped for 30 seconds to ensure stability was achieved. The hand successfully displayed 32 of the 33 grasps, with pose 27, the quadpod, being unsuccessful (see Fig. 11). The pose was categorised as a failure because it could not entirely grasp at the finger tip pads and required the side of the distal joint of the fourth finger to support the object. In future designs of the hand, this failure will be addressed by adding controlled splay to the fingers by increasing the number of DOFs in the MCP of the fingers.

Fig. 11 shows a selection of the grasps that demonstrate: precision grasps (6, 19 and 20), power grasps (4, 10 and 31), a side grasp (16) and the use of passive compliance to achieve a grasp (23). The full list of images representing all the 33 grasps configuration can be found in the attached video, provided as a supplementary material.

B. Kapandji Test

The Kapandji test originates from assessing a patients thumb opposition and ability to reach different regions of the hand and fingers. There are 11 points that need to be reached to achieve the full score. As with the Feix tests, the relevant DOFs were actuated until the desired points were brought into contact. The position was then maintained for 30 seconds to validate controlled motion.

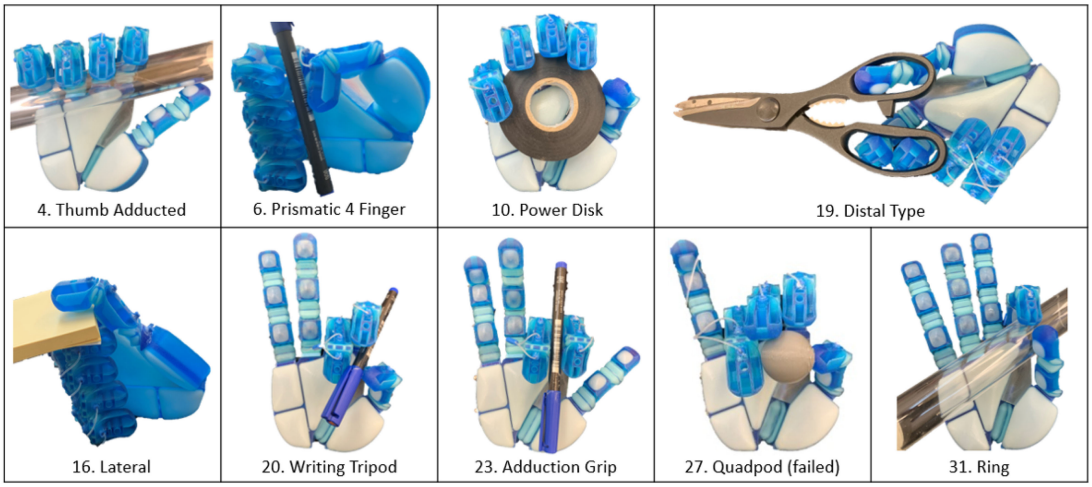

Fig. 11. A selection of the 33 completed grasps from the Feix taxonomy tests used as a dexterity benchmark. Each pose was held for 30 seconds to verify stability. These poses have been selected for presentation as they demonstrate the widest range of grasps in the taxonomy.

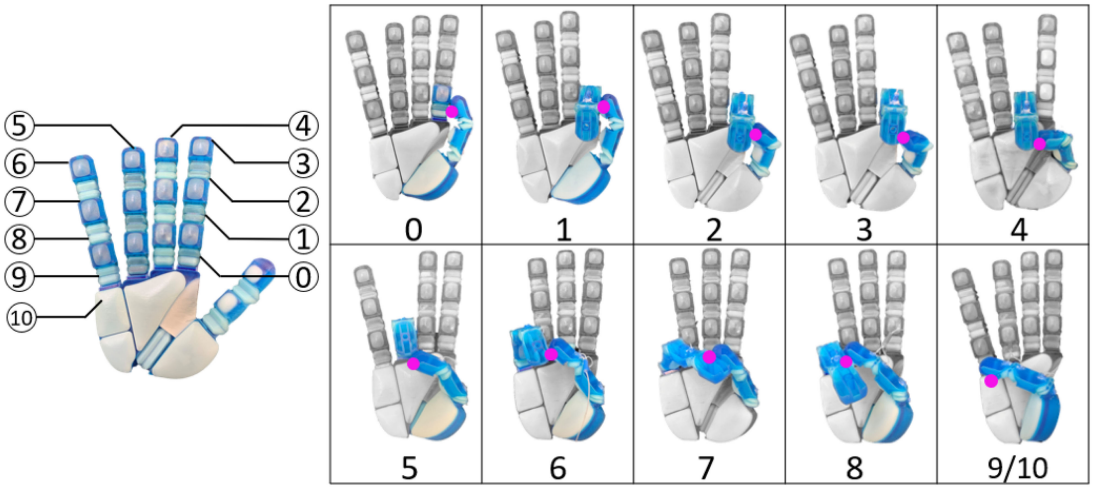

Fig. 12. Results of the Kapandji tests. The thumb was brought into contact with each assigned position on the hand in accordance with the Kapandji thumb opposition test. Each position was held for 30 seconds. The magenta dots indicate the points of contact between the thumb and rest of the hand. The colored regions show the DOFs that are active in each pose.

The hand achieved all 11 of the opposition poses. Therefore, this experiment validates the human-like dexterity of the soft hand. The results are presented in Fig. 12 and demonstrate that the thumb opposition is similar to a human hand.

VI. Conclusion

In this letter, we have presented the design of an anthropomorphic soft robotic hand with distributed tactile sensing. The hand is 3D printed using polyjet technology to simplify the manufacturing process and allow for monolithic multi-material integration. The tactile sensors are designed as compliant pneumatic chambers embedded into the surface.

The finger joints' were characterised and display an average maximum output angle of 70° per joint. The workspace of the fingers is presented with close similarity to a simulated workspace based on a human finger's range of motion.

The whole hand was characterised with a grasping strength test, the Feix Taxonomy test, and the Kapandji Score test. The maximum grasping force was found to be 6.42 N and the hand could achieve 32 of the 33 requisite poses for the Feix test and all of the poses in the Kapandji test.

In future iterations of the hand, the failed Feix taxonomy pose will be addressed by considering the splaying motion of the hand as an extra DOF.

As shown in Fig. 1 the distributed tactile sensing system allows for the monitoring of contact pressures applied by the hand during the interaction with objects. This opens the possibility for further extension of the work exploiting closed loop control algorithms to achieve dexterous in-hand manipulation and fine control of the contact forces. A simple demonstration of the response of the tactile system is included in the video provided as supplementary material.

REFERENCES

[1] J. Hughes, U. Culha, F. Giardina, F. Guenther, A. Rosendo, and F. Iida, "Soft manipulators and grippers: A review," *Front. Robot. AI*, vol. 3, no. 11, p. 1, Nov. 2016. [Online]. Available: www.frontiersin.org

[2] C. Piazza, G. Grioli, M. G. Catalano, and A. Bicchi, "A century of robotic hands," *Robot., Auton. Syst. Annu. Rev. Control Robot. Auton. Syst.*, vol. 22, pp. 1–32, 2019.

[3] Z. Wang *et al.*, "A soft robotic hand based on bellows actuators for dishwashing automation," *IEEE Robot. Automat. Lett.*, vol. 6, no. 2, pp. 2139–2146, Apr. 2021.

[4] T. Feix, J. Romero, H. B. Schmiedmayer, A. M. Dollar, and D. Kragic, "The GRASP taxonomy of human grasp types," *IEEE Trans. Human-Mach. Syst.*, vol. 46, no. 1, pp. 66–77, Feb. 2016.

[5] J. A. Hughes, P. Maiolino, and F. Iida, "An anthropomorphic soft skeleton hand exploiting conditional models for piano playing," *Sci. Robot.*, vol. 3, no. 25, pp. 1–13, 2018.

[6] V. Subramaniam, S. Jain, J. Agarwal, and P. Valdivia y Alvarado, "Design and characterization of a hybrid soft gripper with active palm pose control," *Int. J. Robot. Res.*, vol. 39, no. 14, pp. 1668–1685, Dec. 2020.

[7] H. Wang, F. J. Abu-Dakka, T. N. Le, V. Kyrki, and H. Xu, "A novel design of soft robotic hand with a human-inspired soft palm for dexterous grasping," 2020, *arXiv:2009.00979*.

[8] J. Zhou *et al.*, "A soft-robotic approach to anthropomorphic robotic hand dexterity," *IEEE Access*, vol. 7, pp. 101 483–101 495, 2019.

[9] Q. Lu, L. He, T. Nanayakkara, and N. Rojas, "Precise in-hand manipulation of soft objects using soft fingertips with tactile sensing and active deformation," in *Proc. 3rd IEEE Int. Conf. Soft Robot.*, 2020, pp. 52–57.

[10] L. He, Q. Lu, S.-A. Abad, N. Rojas, and T. Nanayakkara, "Soft fingertips with tactile sensing and active deformation for robust grasping of delicate objects," *IEEE Robot. Automat. Lett.*, vol. 5, no. 2, pp. 2714–2721, Apr. 2020.

[11] S. E. Navarro *et al.*, "A model-based sensor fusion approach for force and shape estimation in soft robotics," *IEEE Robot. Automat. Lett.*, vol. 5, no. 4, pp. 5621–5628, Oct. 2020.

[12] H. Wang, M. Totaro, and L. Beccai, "Toward perceptive soft robots: Progress and challenges," *Adv. Sci.*, vol. 5, no. 9, 2018. [Online]. Available: https://onlinelibrary.wiley.com/doi/full/10.1002/advs.201800541

[13] G. Gu *et al.*, "A soft neuroprosthetic hand providing simultaneous myoelectric control and tactile feedback," *Nature Biomed. Eng.*, 2021. [Online]. Available: http://dx.doi.org/10.1038/s41551-021-00767-0

[14] C. Tawk, H. Zhou, E. Sariyildiz, M. In Het Panhuis, G. Spinks, and G. Alici, "Design, modeling and control of a 3D printed monolithic soft robotic finger with embedded pneumatic sensing chambers," *IEEE/ASME Trans. Mechatronics*, vol. 26, no. 2, pp. 876–887, Apr. 2021.

[15] H. Yang, Y. Chen, Y. Sun, and L. Hao, "A novel pneumatic soft sensor for measuring contact force and curvature of a soft gripper," *Sensors Actuators, A: Phys.*, vol. 266, pp. 318–327, 2017. [Online]. Available: http://dx.doi.org/10.1016/j.sna.2017.09.040

[16] P. M. Khin, J. H. Low, M. H. Ang, and C. H. Yeow, "Development and grasp stability estimation of sensorized soft robotic hand," *Front. Robot. AI*, vol. 8, no. 3, pp. 1–12, 2021. [Online]. Available: https://www.frontiersin.org/articles/10.3389/frobt.2021.619390/full

[17] G. Buscher, M. Meier, G. Walck, R. Haschke, and H. J. Ritter, "Augmenting curved robot surfaces with soft tactile skin," in *Proc. IEEE Int. Conf. Intell. Robots Syst.*, 2015, pp. 1514–1519.

[18] A. Kapandji, "Cotation clinique de l'opposition et de la contre-opposition du pouce," *Annales de Chirurgie de la Main*, vol. 5, no. 1, pp. 67–73, Jan. 1986.

[19] G. I. Bain, N. Polites, B. G. Higgs, R. J. Heptinstall, and A. M. McGrath, "The functional range of motion of the finger joints," *J. Hand Surg.: Eur. Volume,* vol. 40, no. 4, pp. 406–411, 2015.

[20] P. Levangie and C. Norkin, *Joint Structure and Function: A Comprehensive Analysis*, F. A. Davis, Ed., 5th ed. 2011.

[21] A. Buryanov and V. Kotiuk, "Proportions of Hand Segments," *Int. J. Morphol.*, vol. 28, no. 3, pp. 755–758, 2010.

[22] C. Tawk, G. M. Spinks, M. In Het Panhuis, and G. Alici, "3D printable linear soft vacuum actuators: Their modeling, performance quantification and application in soft robotic systems," *IEEE/ASME Trans. Mechatronics*, vol. 24, no. 5, pp. 2118–2129, Oct. 2019.

[23] J.-G. Lee and H. Rodrigue, "Origami-based vacuum pneumatic artificial muscles with large contraction ratios," *Soft Robot.*, vol. 6, no. 1, pp. 109–117, 2019.

[24] Stratasys Ltd., Digital Materials Data Sheet, 2013. [Online]. Available: https://www.stratasys.com/-/media/files/material-spec-sheets/mss_pj_digitalmaterialsdatasheet_0617a.pdf

[25] S. Sundaram, P. Kellnhofer, Y. Li, J.-Y. Zhu, A. Torralba, and W. Matusik, "Learning the signatures of the human grasp using a scalable tactile glove," *Nature*, vol. 569, no. 7758, pp. 698–702, May 2019. [Online]. Available: https://doi.org/10.1038/s41586-019-1234-zhttp://www.nature.com/articles/s41586-019-1234-z

3.4 Supporting Information

3.4.1 Hand Kinematics

In order to validate the kinematics of the proposed hand design before the physical design was formulated, a MATLAB simulation was developed. This was done by simulating discrete joints and rigid links with positions determined by the average hand proportions presented by Ingram et al. [59]. The ROM of the joints was then controlled through sliders that allowed us to verify whether the hand could indeed reach the proposed positions required by the Kapandji Thumb Opposition test [60]. Further detail is provided in Appendix B.1.

3.5 Limitations and Future Work

Force output The primary limitation of the hand in its current state is the grasping force output is only $6.42N$, which limits the wider application of the hand. Whilst the design of the hand allows it to conform to a wide range of objects and grasp them for object identification, the force output is currently not sufficient to lift heavier objects. The reasoning for this is that, once the joints are fully evacuated, the force output is limited by the strength of the joints' materials.

As explored in Sec. 2.3 there are a number of methods of exploiting variable stiffness to increase soft actuators' force output. One of the key facets in the design of the soft hand presented in this work is the simplicity of fabrication for ease of repeatable production. In this regard, many of the methodologies presented would be unsuitable, since they require the further integration of parts onto the 3D-printed body. This introduces the risk of human error in fabrication and therefore variation between specimens. Therefore, future work could propose the exploration of particle or layer jamming across the W-joints which can be printed

within the original monolithic design [162–164]. Comparable works have shown force increases of up to 8 times and thus jamming shows great promise as a means of improving the strength of the hand. For the scope of the work in this thesis, the output force of the hand was sufficient to grasp the desired objects and stimulate sensory responses for the identification tasks and therefore was not the priority for this work.

Sensing surface area Another limitation of this design iteration is the limited sensing surface area. Further empirical examination of the methods of grasping objects indicates that the sides of the fingers are commonly in contact with the objects but there is no sensor coverage in these regions. Two examples of this are shown in Fig. 3.1 where the objects are held in a stable grasp but without contacting a sensor pad. To address this limitation, the sensing capabilities were extended to the sides of the fingers in the following chapter.

Figure 3.1: Two examples of grasping from the Feix taxonomy in [161], where a stable grasp is achieved but without contacting a sensor pad. This informed the extension of the sensing to the sides of the fingers in the following chapter.

Statement of Authorship for joint/multi-authored papers for PGR thesis

To appear at the end of each thesis chapter submitted as an article/paper.

The statement shall describe the candidate's and co-authors' independent research contributions in the thesis publications. For each publication there should exist a complete statement that is to be filled out and signed by the candidate and supervisor **(only required where there isn't already a statement of contribution within the paper itself).**

Title of Paper	Design of a 3D-Printed Soft Robotic Hand With Integrated Distributed Tactile Sensing
Publication Status	☒Published ☐ Accepted for Publication ☐ Submitted for Publication ☐ Unpublished and unsubmitted work written in a manuscript style
Publication Details	Shorthose, O., Albini, A., He, L., & Maiolino, P. (2022). Design of a 3D-Printed Soft Robotic Hand With Integrated Distributed Tactile Sensing. *IEEE Robotics and Automation Letters*, *7*(2), 3945–3952.

Student Confirmation

Student name:	Oliver Shorthose		
Contribution to the paper:	I developed the idea for the hand with Professor Maiolino and Alessandro Albini I developed the design of the joints from simulations and undertook their characterisation. I put the control scheme together with Alessandro Albini and characterised the whole hand I led the write-up with support from the other authors		
Signature: 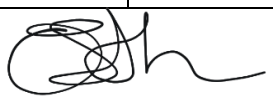		Date	19th July 2023

Supervisor Confirmation

By signing the Statement of Authorship, you are certifying that the candidate made a substantial contribution to the publication, and that the description described above is accurate.

Supervisor name and title:	Professor Maiolino		
Supervisor comments:	I confirm that the student made a substantial contribution to this publication and the contribution of the other authors is as described above		
Signature: 		Date	19/07/23

4

Multi-Grasp Tactile Object Identification

Humans combine vision and touch seamlessly to determine how to interact with objects [165]. Ordinarily, we see an object and begin planning an interaction policy with it before using our hands to reinforce and update that primary policy [166]. However, in many cases, such as an unsighted classification task, visual identification is unsuitable. When presented with this challenge, we as humans will use the multiple receptors in the skin to distinguish blindly between objects based on their specific properties such as material, geometry, surface features, and friction [5]. Our ability to simplify the task of object exploration is greatly facilitated by the morphological computation developed through evolution [2]. This allows us to conform naturally to the shape of the objects we are exploring, leveraging synergies in our muscles and compliance in our skin and soft tissues [6, 7, 10]. To further enhance discrimination between objects, we employ multiple touches and grasps, isolating salient features and identifying similarities [14, 15, 167]. This chapter seeks to take inspiration

from how humans implement compliance and multiple grasps to approach tactile object identification and achieve high-accuracy discrimination.

Sec. 4.1 presents previously implemented solutions to tactile object identification for both traditional and soft robotic end-effectors and explore how taking multiple contacts and grasps can improve identification accuracy. Sec. 4.2 then reviews how machine learning techniques can be applied to tactile achieve object identification in the presence of highly non-linear relationships.

4.1 Tactile Object Recognition

Being able to recognise objects enables tailored control methods for grasping and manipulation, leveraging upon knowledge of their specific properties. Whilst research into object identification has generally focussed on using vision to detect and identify an object before planning an appropriate grasping strategy, it cannot be deployed in conditions with occluded or variable light conditions and requires perspective for sizing the object in a real scene [168]. Furthermore, vision is unable to detect intrinsic object properties such as weight, stiffness, surface features, or even specific heat capacity [169]. In this regard, the sense of touch is essential for being able to discriminate between these characteristics [24].

Touch has been applied to object recognition in a variety of ways using the exteroceptive and proprioceptive sensing methodologies identified in Sec. 3.2. Most commonly, rigid-bodied end-effectors equipped with an array of tactile sensors are used to grasp an object, either with a set maximum applied force, or with sensory feedback to inform a control scheme over the contact dynamics and end-effector positioning [23, 26, 170]. However, these control schemes are not trivial and incorrect application can easily lead to damaging the object. In this regard, solutions with soft joints and surfaces have been deployed to ensure inherent safety in the contact, whilst simplifying the control required to conform to

the object's geometry [41, 171]. Furthermore, softness in sensing at the point of contact allows for greater surface area in contact with the object and can be used to affect and shape the perception of the contact [31, 48].

Many approaches to soft tactile object recognition have used soft sensors placed at the tips of either rigid-bodied or soft grippers and grant detection over a small surface area, sometimes in conjunction with proprioceptive sensing [46, 49, 156]. Whilst these can enable high-resolution feature detection, they are limited to precision grasping and require specific object placement within the hand to identify the object successfully. Conversely, distributing the sensing over the entire hand allows for grasping in a variety of postures, as well as increasing the likelihood of sensor stimulation in any given grasp [23, 149]. However, whilst distributed sensing can mitigate the inherent locality of information provided by tactile sensing to an extent, it is still common to miss salient object features if only single grasps are deployed for identification [50, 51].

To increase the likelihood of detecting salient features and to improve the classification accuracy, multiple grasps can be taken of a single object [49]. Following the definitions from Liu et al. [26], taking multiple grasps to inform object identification can be viewed as either an active, semi-active or passive exploratory procedure. The choice between the type of procedure governs whether the object is presented to the hand, the hand approaches the object which is fixed in place, or the hand explores the object autonomously. Naturally, the complexity of the control scheme required for active exploration with grasping compared to semi-active or passive is far greater. By implementing one of these schemes and taking multiple grasps from different poses, the classification method becomes less reliant on the specific presentation of the object to hand as has been commonly used in previous solutions [146, 147, 172].

The work in this chapter modified the distributed sensing from the previous chapter to increase the surface area as detailed in Sec. 3.5 to increase the surface area by a factor

of 3.7. This significantly increased the likelihood of sensor-object contact during a grasp, thereby maximising the information attained from each grasp. The compliant nature of the hand is used, both in actuation and sensing to enable morphological computation in the contact with the object. This comes in the form of inherent conformability to the shape of the object without an explicit complex control scheme and data acquisition that is shaped by the morphology of the sensors. A semi-active exploration methodology is used whilst data is recorded from the sensors around the hand. Details of the modifications to the hand are covered in the contributed paper and further in the discussion section of this chapter.

4.2 Data Processing and Classification

Contact between a sensorised end-effector and an object intrinsically leads to the emergence of salient patterns between the taxels of the end-effector. To distinguish between these patterns in the data, machine learning techniques have been deployed to classify objects [63, 65]. These include standard ML classification techniques such as SVM, random forest, decision tree, naive Bayes or similar. For example, Homberg et al. [146] used a Bayesian framework and K-nearest neighbours (KNN) to classify objects based on either an enveloping or a pinch grasp of each object; Pannen et al. [50] and Yan et al. [147] compared KNN, decision trees and SVM performances on tactile data acquired from simple grasps of a set of objects; and Ma et al. [156] grasped 10 different stiffness objects from a single pose and applied a Random Forest classifier to distinguish between them. However, all of these approaches exploited a restricted set of object poses, which simplifies the task significantly by reducing the variation in sensing data between samples of the same object. In this regard, the proposed ML classifiers have limitations when confronted with higher complexity data, such as in the case of unknown object pose, greater noise in detection, higher dimensionality data (from greater distribution, multi-modality, or higher resolution), or more object classes [173–175].

To deal with the limitations that exist when classifying higher complexity data, neural networks have been devised. Due to the local spatial relationships that exist between stimulated tactile sensors in a grasp, CNNs can be used to extract features from the tactile data to classify the object [45, 69, 176]. Specifically, CNN autoencoders and encoder-decoder (ED) architectures, which have been successfully applied to visual salient object detection [177], can be deployed to identify the emergent patterns in tactile data [51]. These work by taking high dimensional input data and reducing the dimensionality with feature extraction using encoders such as ResNet, VGGNet, or Inception [178–180]. This lower-dimension latent representation is then decoded back into the original high dimensional space and the reconstruction loss is input to an optimiser to train the network. The reconstruction loss is most often the mean-squared error or cross-entropy between the input and output data from the network. Extracting the latent representation and applying the standard ML classifiers listed above allows for accurate object classification. The general structure for an ED architecture is provided in the contributed paper. The work that has been presented thus far has focussed on using a single grasp of an object to extract features and classify the object. However, this work seeks to take inspiration from the human approach of tactile object identification whereby multiple grasps are taken to build up a representation of the object and the inter-grasp relationships are important for recognition. This requires a network that can extract features from between grasps.

This work implements an ED architecture to extract the features from taking multiple grasps of a set of objects. The network is designed such that features can be extracted across the full set of grasps rather than just from a single grasp as has been presented in prior work. The silhouette score is calculated in the latent space to quantify the geometric separation between object clusters and include that in the loss function to enforce greater separation for ease of classification. A set of standard ML classifiers are compared in the latent space data to distinguish between the presented objects [181].

4.3 Contributed Paper

The contributed manuscript in this chapter was presented at the Robosoft Conference in 2023. It details the modifications made to the soft hand from Chap. 3 to improve grasping kinematics and increase the sensing surface area. The paper presents the application of the soft hand towards a multi-grasp object identification task, where the use of multiple grasps facilitates higher accuracy classification. The compliance in the hand is used to significantly simplify the task with respect to a traditional robotic hand that would require a complex control scheme. The grasps' tactile data is processed through an encoder-decoder architecture for low-dimensional latent space extraction and classification. The dependency on grasp order is also decoupled at the input by augmenting the data sequence [182].

EDAMS: An Encoder-Decoder Architecture for Multi-grasp Soft Sensing Object Recognition

Oliver Shorthose[1], Alessandro Albini, Luca Scimeca, Liang He and Perla Maiolino

***Abstract*— The use of tactile sensing exhibits benefits over visual detection as it can be deployed in occluded environments and can provide deeper information about an object's material properties. Soft hands have increasingly been used for tactile object identification, providing a high degree of adaptability without requiring complex control schemes. In this work, we propose a framework for identifying a range of objects in any pose by exploiting the compliance of a soft hand equipped with distributed tactile sensing. We propose EDAMS, an Encoder-Decoder Architecture for Multi-grasp Soft sensing and an ad-hoc data structure capable of encoding information on multiple grasps, while decoupling the dependency on the pose order. We train the model to map the high-dimensional multi-grasp tactile sensor data into a lower-dimensional latent space capable of achieving the geometrical separation of each object class, and enabling accurate object classification. We provide an empirical analysis of the benefit of multi-grasp perception for object identification, and show its impact on the separation of the objects in sensor space. Notably, we find the classification accuracy to change widely across the number of grasps, ranging from 47.0% for a single grasp, to 99.9% for 10 grasps.**

***Index Terms*— Soft robotic hands, object identification, tactile sensing**

I. Introduction

Object recognition stands as one of the most fundamental capabilities for autonomous robots, leading to successful grasping and manipulation. Beyond the widespread vision-based methods for object recognition, tactile sensing has the potential to provide additional information about the physical properties of objects like surface features, friction, and stiffness [1]–[5]. It can also be utilised in unstructured environments with variable lighting conditions, transparent objects and occlusions [6]. Due to their potential, tactile-based and hybrid methods have seen a rapid development in recent years for object recognition [7], [8].

The majority of works in the relevant literature make use of rigid end-effectors equipped with tactile sensors to perform object recognition. However, these grippers require complex control schemes to manipulate different types of objects and to guarantee accurate and safe interaction [9], [10]. On the other hand, due to their compliance, soft end-effectors can adapt to, and manipulate, a wide range of objects using simpler control strategies [11]–[13]. In this respect, several works have exploited the compliance of soft grippers to perform object recognition using proprioceptive sensing [2], [14] or a combination of proprioceptive and tactile sensors [15], [16] with simple open loop control. Indeed, the compliance allows the grasp configuration to adapt passively to the shape and stiffness of the objects, generating a different tactile response.

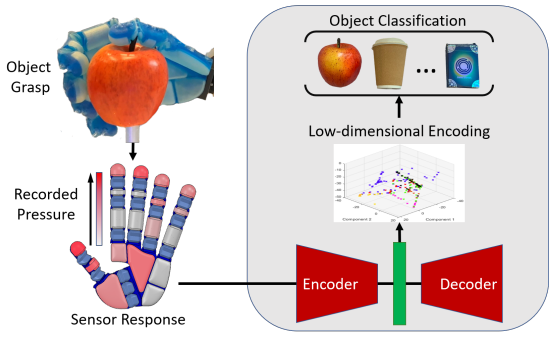

Fig. 1. Overview of the proposed model. Sensor data is recorded from multiple grasps of objects and fed into the EDAMS architecture. Classification is made on the low-dimensional clusters from the bottleneck of the encoder-decoder.

While the aforementioned works only grasp objects from a single posture, different approaches leverage the dexterity provided by an anthropomorphic hand to grasp objects in different orientations, achieving object recognition that is robust to pose uncertainty [17], [18]. For example, the work proposed in [17] combined flex and force sensors to discriminate between 10 different classes of objects, providing variation between the object poses when being grasped. In [18], a high resolution tactile sensor was integrated on a soft robot hand to be exploited for object recognition. The authors show that a high number of tactile sensors is fundamental in recognising object features successfully and the performance of a recognition system rapidly drops when the spatial resolution decreases. Whilst these works show the possibility of performing

We gratefully acknowledge support by EPSRC Programme Grant 'From Sensing to Collaboration' (EP/V000748/1)

O.Shorthose, A.Albini, L.He, and P.Maiolino are with Oxford Robotics Institute, University of Oxford, Oxford, UK. P.Maiolino is also with the University of Genoa, Liguria, IT. L.Scimeca is with Harvard University and Dana Farber, Boston, MA, USA.

[1] corresponding author's email: ollies@robots.ox.ac.uk

object recognition from multi-modal feedback, or from high resolution tactile sensing using a single grasp, they require different types of sensors and flexible PCBs to be embedded in the soft body, thus increasing the complexity of the fabrication and affecting the durability and compliance of the system.

Soft pneumatic tactile sensors can be exploited and embedded to provide tactile feedback, without affecting the overall compliance of the body [19]. Despite this, fabrication methods currently only allow pneumatic sensors with low spatial resolution to be equipped on soft robots, where the information acquired from a single hand grasp may be inadequate for accurate object identification. In addition, tactile sensors can only capture local information leading to discriminative ambiguities. As a consequence, we argue that multiple contacts are often required to perform accurate object recognition via the sense of touch.

This paper addresses the problem of performing tactile object recognition from multiple grasping postures using a soft hand equipped only with pneumatic tactile sensors. This is achieved by using multi-grasp tactile information and employing an Encoder-Decoder Architecture for Multi-grasp Soft sensing (EDAMS) to map the information into a low-dimensional latent space, while enforcing the geometrical separation of different objects [20]. We empirically analysed how the accuracy increases in relation to the number of grasps, further stressing the importance of multi-grasp sensory information for tactile object discrimination.

In this paper, we improve on the hand-design from [21] to increase the contact sensing area and the conformability when grasping. The compliance and kinematics provided by the hand allow for a wide range of objects to be grasped in different orientations without complex control schemes. The objects are chosen from commonly used objects with different features such as a range of stiffness and geometries.

To summarise, the main contribution of this paper is a data structure and learning architecture capable of decoupling the dependency of the grasp pose sequences from sensor data, as well as learning a low level embedding that enforces meaningful geometric separation within object subsets in sensory space (EDAMS). The paper is structured as follows: Section II details the updated design and control scheme of the hand; Section III describes the experimental setup and the data collection procedure. The testing and analysis of the object identification task are presented in Section IV; Section V provides the conclusion of our work and the future direction.

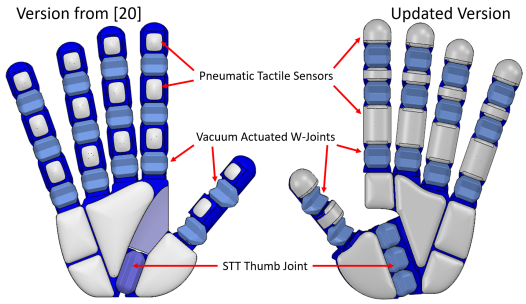

Fig. 2. Comparison of the soft hand presented in [21] (left) against the modified version (right).

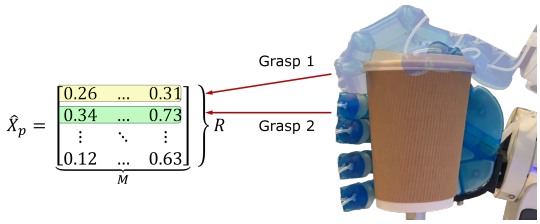

Fig. 3. Structure of the sample $\hat{X}_p$. Tactile responses corresponding to grasps from different postures are laid on separate rows, forming a matrix of multi-grasp sensor data. R is the number of grasps in the sample, and M is the number of sensors in the hand.

II. Methodology

A. Hand Design

The soft anthropomorphic hand's design was first presented in [21] and is shown in Fig. 2. The hand uses vacuum actuated W-joints to achieve human-like dexterity as demonstrated by the Feix taxonomy and Kapandji thumb opposition tests [22], [23]. Up to 15 degrees of freedom (DOFs) can be independently actuated, but to simplify the control for this work, the whole hand was underactuated as a single DOF.

Multi-material 3D printing is utilised to manufacture the hand and to achieve a fully integrated design which includes 19 pneumatic tactile sensors distributed on the fingers and the palm. Specifically, digital materials obtained from a combination of Agilus©, a compliant, rubber-like material, and VeroCyan©, a rigid plastic, are used in different proportions to achieve different shore hardness across the hand. In this respect, the soft joints are made from ShoreA 60, the pneumatic sensor chambers from ShoreA 35 and the structural part of the hand from ShoreA 95. The material proportions are available from the manufacturer.

The passive adaptability of the hand to the shape of the objects is crucial in generating the different sensor responses and simplifying the inference process for the object recognition task. Thus, several changes have been made to the original hand design presented in [21]:

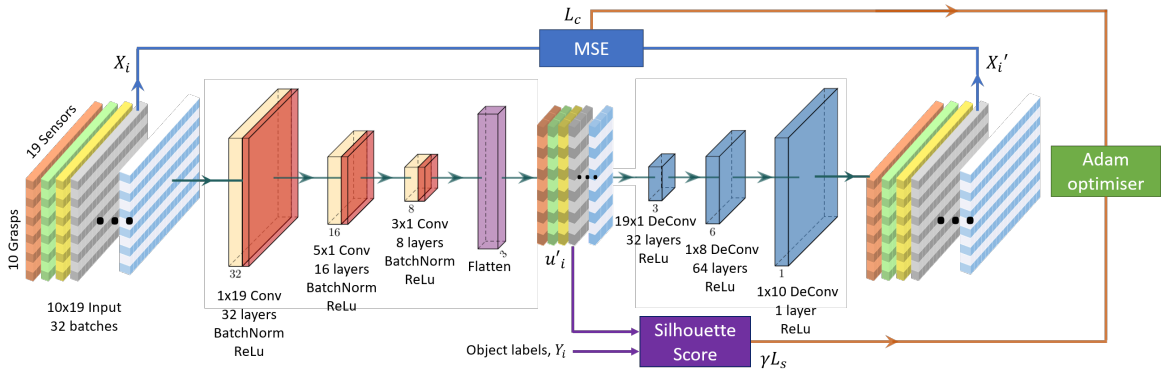

Fig. 4. Architecture of the EDAMS Encoder-Decoder Model. u'_i is the bottleneck data to be classified.

1) The surface area of the sensors has been increased to cover the sides of each finger and the finger tips. This was introduced to ensure that there was contact between the objects and sensors in all poses.
2) The lengths of each finger phalanx have been scaled to mimic the respective distances between joints in the human hand [24]. Specifically, shortening the medial phalanx reduces the contact area of the central sensor, but it increases the surface area of its neighbouring sensors and improves the grasping around objects.
3) The scaphotrapeziotrapezoidal (STT) joint was rotated 10° out of the plane of the palm. In the previous design, we observed that the opposition of the thumb was not into the plane of the hand when the STT joint was actuated. The hand could satisfy the Feix and Kapandji tests as desired, but its grasping strength was limited by this. The increased angle was introduced to ensure the thumb grasps objects into the plane of the hand, increasing the stability of the grasp.

Fig 2 shows how the above modifications to the original design allow the hand to achieve greater conformability and improves the tactile sensors' response (with respect to the number of sensors in contact with the object and higher sensor values). Moreover, we performed a new characterisation of the sensors' responses with respect to applied forces, by following the same procedure explained in [21]. The results of the characterisation tests are presented in the supplementary video attached to the manuscript. The tactile sensor responses are linear in the applied displacement range and show good repeatability across three 3D printed fingers.

B. Model Architecture and Learning

In this Section we first explain how we organised the individual samples and the dataset to: (i) capture the information of multiple grasp poses; (ii) make the classification robust to different sequences of grasping poses; (iii) evaluate the effect of the number of grasps on the classification accuracy. Finally, we describe the structure of the EDAMS model and the training procedure to ensure the separation of objects in the low-dimensional embedding.

1) Dataset Structure: We devise a data-structure that is suitable for learning, and that enables the *decoupling* of the sequence of the order of grasp poses in the data during learning. For each single grasp, we encode the tactile sensor responses as a 1D vector $\in \Re^M$, where M is the number of sensors. We then form a matrix $\hat{X}_p \in \Re^{R\times M}$, with $\{1,\ldots,P\}$ and P the total recorded dataset size, containing the responses of the tactile system to R different grasping postures of the same object, repeated 30 times (Fig. 3).

Since the grasp data in $\hat{X}_p$ follows the grasp pose sequence recorded during experiments, there would normally be a data dependency with respect to the order of the grasps and the object's identity. At the dataset level, we decouple this dependency with data augmentation. In particular we defined new samples X_i, with $i = \{1,\ldots,N\}$, by randomly permuting, $K = 100$ times, the rows of each $\hat{X}_p$. In our case $P = 210$ (see Section III), thus, the total number of samples in the augmented dataset is $N = P \times K = 21000$.

To evaluate how the number of grasps affects object recognition, we replaced the respective number of lower rows in each sample X_i with zeros to simulate 1, 3, 5 and 7 grasps and retrained the model. These number of grasps were chosen to be equally distributed up to 10 grasps.

2) Encoder-Decoder Model: We developed an Encoder-Decoder Architecture for Multi-grasp Soft sensing (EDAMS) to be able to identify features of the grasp data, and produce a (meaningful) lower dimensional latent space that can subsequently be used to classify objects. In the encoder, three convolutional layers with *batch normalisation*

and *ReLu* activation were implemented as shown in Fig. 4. The first convolutional layer contains $1 \times M$ weight filters and can thus read the data from a single grasp at once, then stride across the row dimension to read all other grasps. This design, together with the data structure previously described, allows the model to learn *sensor adjacency* rules within the column dimension, but not the row dimension, thus achieving a decoupling of the order of grasps at the model level. This is followed by stacked convolution and reshape layers for the embedding, and de-convolutions for decoding (Fig. 4).

3) Low-Dimensional Embedding Isolation: For the purpose of our experiments, we wish to learn a low level embedding which enforces meaningful geometrical separation within object subsets in sensory space.

Let X_i be a general tactile data matrix, as previously defined. As per encoder-decoder literature we wish to encode X_i into a subspace u'_i, and then reconstruct the matrix into X'_i while enforcing reconstruction consistency. We implement a simple mean squared error (MSE) consistency loss of the form:

$$L_c = \sum_{i}^{N} \frac{(X_i - X'_i)^2}{N} = \sum_{i}^{N} \frac{(X_i - D(E(X_i)))^2}{N} \quad (1)$$

where E and D are respectively the encoder and decoder networks, and $u'_i = E(X_i)$. We enforce a geometrical separation between each object class within the u subspace by adding a differentiable implementation of the Silhouette Score within our function [25]. The Silhouette Score for any object class is given by:

$$L_s = \frac{a - b}{\max(a, b)} \quad (2)$$

where a is the average intra-cluster distance, and b is the average inter-cluster distance to the closest object class in the projected space [25], [26]. Finally, we train our model on a loss of the form:

$$L = L_c - \gamma L_s \quad (3)$$

where the hyper-parameter γ can modulate the model's *pressure* to find a sub-space enforcing geometrical object class separation. We use a vanilla Adam optimiser to handle the training dynamics [27], and choose to stop training when either $L_s >= 0.99$ on the validation set (suggesting high cluster separation), or when there was no validation loss improvement for more than 100 epochs (early stopping). We further set u to be three-dimensional, to allow for easy plotting and evaluation. We find this low-dimensional sub-space to suffice in representing our set of objects.

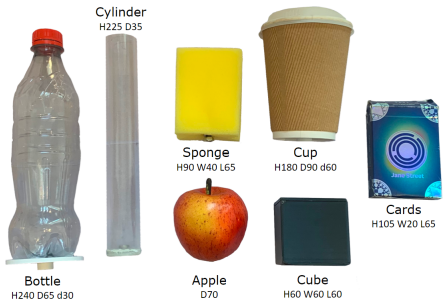

Fig. 5. The selection of objects used for the identification tasks. The figure reports the dimensions in mm: H, height; W, width; L, length; D, max. diameter; d, min. diameter. The objects are presented in the orientation used for data acquisition.

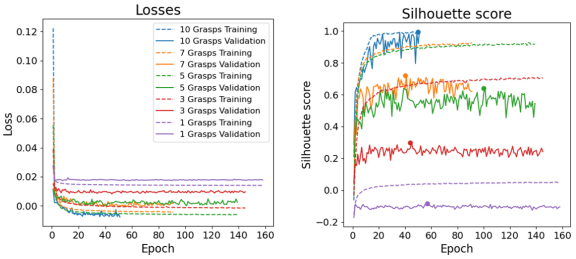

(a) (b)

Fig. 6. Learning process for the EDAMS architecture. (a) The loss function is a summation of the MSE reconstruction loss and the silhouette score loss. (b) Silhouette score relating to the geometric cluster separation in the bottleneck.

III. Data Collection

The proposed method was validated in a tactile identification task based on 7 different objects, shown in Fig. 5. They were chosen by considering daily-use objects or shapes, similar to [15]–[18], [28]. In particular, we selected close variants of the YCB dataset [29]. The cylinder and cube are rigid, the bottle, cards and cup are semi-rigid, and the sponge is compliant. The soft hand was connected to a Franka Emika robot, controlled to move the end-effector to different grasping postures. The hand was actuated by connecting each of the 15 joints to a single negative pressure supply. This supply was provided by a compressor, regulated using an analog pressure regulator (SMC IRV20-C10). When negative pressure is applied to the joints, the fingers bend as characterised in [21]. Two solenoid valves (Yosoo1210) were used to control whether the hand was connected to the pressure source or the atmosphere. The soft tactile pads were connected to 19 pressure sensors (ADP51A11 with 1-bit in 10 of noise) via 1mm diameter tubing and wired to the Arduino through a multiplexer (74HC4051) and recorded at 10Hz.

The objects were fixed in front of the robot using a

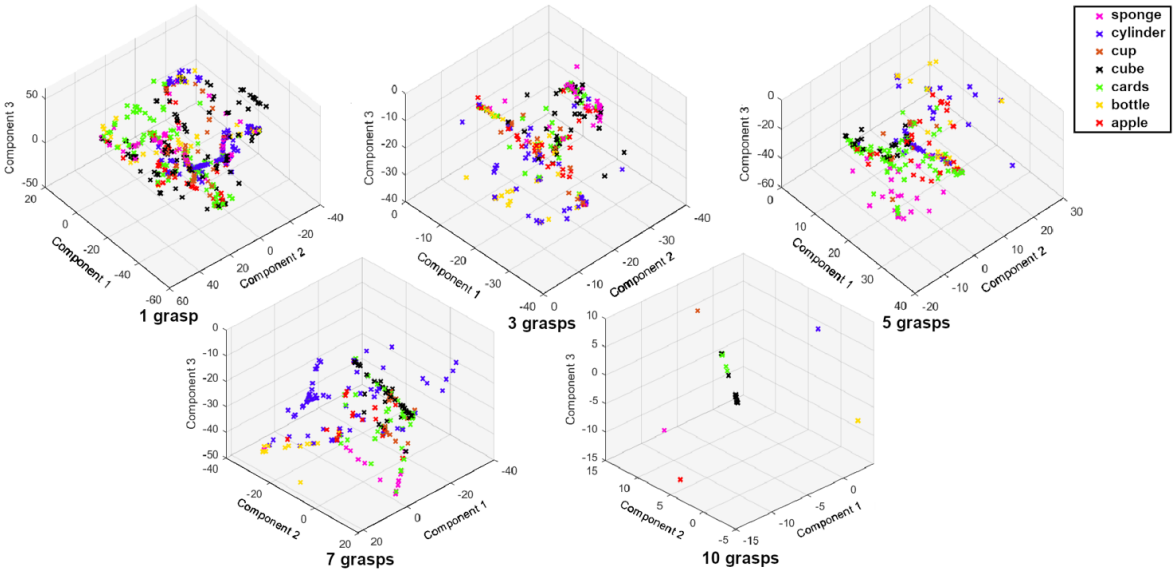

(a)

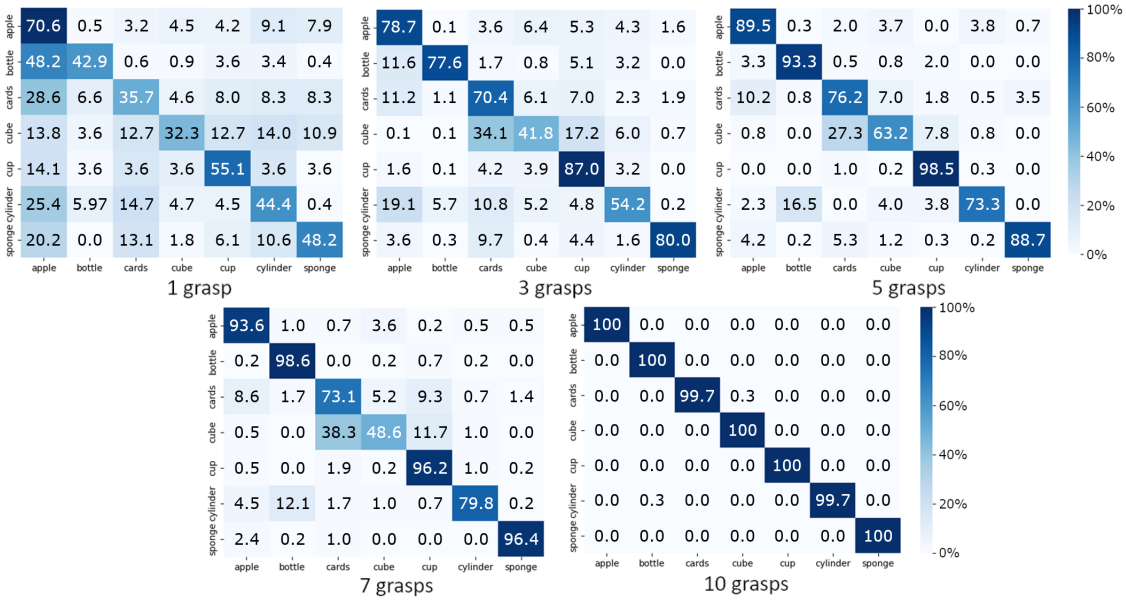

(b)

Fig. 7. Results on the test set by increasing the number of grasps (a) Object clusters from the bottleneck region in the encoder-decoder architecture. Increasing the number of grasps allows for greater separation between clusters and for the higher numbers of grasps, the datapoints are stacked in the same position. (b) Confusion matrices for the object classification. The classifier used for each number of grasps is detailed in Table I. The true values are on the y-axis and the predicted values are on the x-axis.

stand to establish a repeatable stationary position. The data sample $\hat{X}_p \in \Re^{10\times 19}$ was collected by grasping in 10 different postures. The grasp poses were manually chosen to approach each object from all directions and to cover its entire shape. Fig. 3 shows two of the 10 grasps for the cup. The procedure to collect each $\hat{X}_p$ consisted of the following steps:

1) Approach the object from an initial remote position.
2) Once the hand is in contact with the object, control the solenoid valves to reduce the pressure to -50kPa,

thus closing the hand around the object.
3) Hold the hand held in stationary contact with the object for 30 seconds. The final sensor reading from the steady state is then collected.
4) The pressure is released and the hand is removed back to a remote position.
5) Repeat the above procedure for the 10 different grasping postures.

This procedure was repeated 30 times for each of the 7 objects, therefore $P = 210$. To ensure variation between grasping postures, we added random noise (up to 10mm) to the x, y and z directions of the grasping posture. The sensor data from each sensor were normalised by the maximum value recorded across all tests for that specific sensor.

The dataset was split 80%-10%-10% for the purposes of training, validation and testing respectively and then augmented as described in Section II. It must be noted that the data splitting was performed before the data augmentation to ensure no grasps at validation/test time were observed at training time.

A video showing the data collection procedure is provided as supplementary material.

IV. Results and Discussions

The EDAMS model was trained with the datasets described in the previous Section. We used the validation dataset containing all 10 grasps to tune the model's hyper-parameters, and empirically set $\gamma = 0.015$. We then fixate those hyper-parameters and re-train the network from scratch for each dataset of different grasps. Fig. 6 shows the training process for the model with the training and validation losses, along with the values of L_s.

After training, the model can map any high-dimensional sensor matrix X_i into its corresponding embedding u_i. The classification process takes less than a second for each set of grasps. For $R < 10$ grasps, a random selection of the 10 recorded grasps were chosen without replacement to ensure the same grasp pose was not repeated in a sample. Fig. 7(a) shows the clusters resulted from mapping the test set into its latent space representation, across the different number of grasps considered. In order to determine the maximum classification capability for each number of grasps, we compared simple classifiers to perform object recognition in the projected u space: linear support vector machine (SVM), decision tree (DT), random forest (RF), and k-Nearest-Neighbours (k-NN.) For the classifiers, from Python's *sci-kit learn*, we used *GridSearchCV* over common ranges of each of their hyper-parameters and used a *StratifiedKFolds* cross-validator for the final model selection with 4 folds. We report the best performing models for each number of grasps in Table I.

As shown in Table I, by increasing the number of grasps, we observe an increase in L_s, suggesting an increased ability for the trained embedded model to appropriately encode the information belonging to each object class, and achieve higher object class separation. In turn, that allows even simple classifiers to achieve increasingly more accurate object classification, doubling the performance from 47% to 99.9%. A more detailed view showing the separation of clusters in the low dimensional space is shown in Fig. 7(a).

N grasps	L_s	Acc %	Classifier	Parameters
10	0.995	99.9	*Linear SVM*	C = 0.001
7	0.581	87.6	*k-NN*	k=9, weighted
5	0.547	83.2	*Linear SVM*	C = 0.01
3	0.275	70.0	*Linear SVM*	C = 0.1
1	0.014	47.0	*Decision tree*	Depth = 11

TABLE I. Silhouette score and mean classification accuracy computed on the test sets. For each number of grasps we reported the models and corresponding hyper-parameters that best performed on the validation sets.

Fig. 7(b) shows the confusion matrices for each number of grasps: the cube was most commonly misclassified as the deck of cards. The misclassification is likely due to local geometric similarities between the objects, considering the geometric profiles of the largest side of the cards compared with each of the cube's sides. The cause of the misclassification can also be traced back to the embedding. In Fig. 7(a), in fact, the representation in 3D u space of both the cube and the cards is overlapping across all number of grasps, only achieving some degree of separation at 10 grasps. We further observe how single grasps are indeed largely unreliable (Table I). In Fig. 7(b) we observe that beyond the misclassification between the cube and deck of cards, under the sensory system of a single grasp, other objects show a high degree of misclassification. This is for example the case for the bottle, misclassified as an apple $\approx 48\%$ of the times, and the cylinder, misclassified as an apple $\approx 25\%$ of the times. These objects, in fact, present similar local curvature information, leading to perceptual ambiguities hindering accurate tactile-based object recognition, and supporting our initial hypothesis. Finally, we observe how, although the deck of cards and the sponge are similar in geometry, the identification is capable of reliably distinguishing the two apart, suggesting success in this framework for discriminating between object stiffness.

V. Conclusion

This paper presents a framework to perform tactile object classification with a soft robotic hand and distributed tactile sensing by combining information from multiple grasps. We implemented a data pre-processing and encoder-decoder learning architecture to allow for accurate embedding and identification of objects without

reliance on the grasp pose sequence. Notably, we use a weighted silhouette score-based loss to find a low-dimensional encoding of the sensor data promoting the geometric separation of the objects. We applied machine learning classifiers to the encoded data in order to classify the objects and we showed the importance of multi-grasp sensory perception for object discrimination.

Future work will look to incorporate a Bayesian framework to instruct the hand where to grasp to confirm prior beliefs in the classification of a grasped object. This will reduce the number of grasps that are required to achieve a high classification accuracy, without restricting the ability to discern objects from any pose.

REFERENCES

[1] B. Shih, D. Shah, J. Li, T. G. Thuruthel, Y.-L. Park, F. Iida, Z. Bao, R. Kramer-Bottiglio, and M. T. Tolley, "Electronic skins and machine learning for intelligent soft robots," *Science Robotics*, vol. 5, no. 41, apr 2020.

[2] H. Wang, M. Totaro, and L. Beccai, "Toward Perceptive Soft Robots: Progress and Challenges," sep 2018.

[3] S. Luo, J. Bimbo, R. Dahiya, and H. Liu, "Robotic tactile perception of object properties: A review," *Mechatronics*, vol. 48, no. August, pp. 54–67, 2017.

[4] J. Huang and A. Rosendo, "Variable Stiffness Object Recognition with a CNN-Bayes Classifier on a Soft Gripper," *Soft Robotics*, vol. 00, no. 00, pp. 1–12, mar 2022.

[5] L. Scimeca, P. Maiolino, and F. Iida, "Soft morphological processing of tactile stimuli for autonomous category formation," in *2018 IEEE International Conference on Soft Robotics (RoboSoft)*. IEEE, 2018, pp. 356–361.

[6] L. Scimeca, J. Hughes, P. Maiolino, L. He, T. Nanayakkara, and F. Iida, "Action augmentation of tactile perception for soft-body palpation," *Soft robotics*, vol. 9, no. 2, pp. 280–292, 2022.

[7] C. Jiao, B. Lian, Z. Wang, Y. Song, and T. Sun, "Visual–tactile object recognition of a soft gripper based on faster Region-based Convolutional Neural Network and machining learning algorithm," *International Journal of Advanced Robotic Systems*, vol. 17, no. 5, pp. 1–13, 2020.

[8] H. Liu, Y. Yu, F. Sun, and J. Gu, "Visual–tactile fusion for object recognition," *IEEE Transactions on Automation Science and Engineering*, vol. 14, no. 2, pp. 996–1008, 2017.

[9] C. Piazza, G. Grioli, M. G. Catalano, and A. Bicchi, "A Century of Robotic Hands," *Robotics, and Autonomous Systems Annu. Rev. Control Robot. Auton. Syst. 2019*, vol. 22, pp. 1–32, 2019.

[10] Z. Kappassov, J. A. Corrales, and V. Perdereau, "Tactile sensing in dexterous robot hands - Review," *Robotics and Autonomous Systems*, vol. 74, pp. 195–220, 2015.

[11] J. Hughes, U. Culha, F. Giardina, F. Guenther, A. Rosendo, and F. Iida, "Soft manipulators and grippers: A review," p. 1, nov 2016.

[12] S. Abondance, C. B. Teeple, and R. J. Wood, "A Dexterous Soft Robotic Hand for Delicate In-Hand Manipulation," *IEEE Robotics and Automation Letters*, vol. 5, no. 4, pp. 5502–5509, oct 2020.

[13] J. Zhou, Y. Chen, D. C. F. Li, Y. Gao, Y. Li, S. S. Cheng, F. Chen, and Y. Liu, "50 Benchmarks for Anthropomorphic Hand Function-based Dexterity Classification and Kinematics-based Hand Design," in *2020 IEEE/RSJ International Conference on Intelligent Robots and Systems (IROS)*. IEEE, oct 2020, pp. 9159–9165.

[14] Y. Yan, C. Cheng, M. Guan, J. Zhang, and Y. Wang, "Texture Identification and Object Recognition Using a Soft Robotic Hand Innervated Bio-Inspired Proprioception," *Machines*, vol. 10, no. 3, p. 173, feb 2022.

[15] L. Chin, J. Lipton, M. C. Yuen, R. Kramer-Bottiglio, and D. Rus, "Automated recycling separation enabled by soft robotic material classification," *RoboSoft 2019 - 2019 IEEE International Conference on Soft Robotics*, pp. 102–107, 2019.

[16] B. S. Homberg, R. K. Katzschmann, M. R. Dogar, and D. Rus, "Robust proprioceptive grasping with a soft robot hand," *Autonomous Robots*, vol. 43, no. 3, pp. 681–696, 2019.

[17] P. M. Khin, J. H. Low, M. H. Ang, and C.-h. Yeow, "In-Hand Object Recognition for Sensorized Soft Hand," in *International Conference on Intelligent Autonomous Systems*, ser. Lecture Notes in Networks and Systems, vol. 412. Springer International Publishing, 2022, pp. 351–364.

[18] T. J. Pannen, S. Puhlmann, and O. Brock, "A Low-Cost, Easy-to-Manufacture, Flexible, Multi-Taxel Tactile Sensor and its Application to In-Hand Object Recognition," in *2022 International Conference on Robotics and Automation (ICRA)*, no. 390523135. IEEE, may 2022, pp. 10 939–10 944.

[19] C. Tawk, H. Zhou, E. Sariyildiz, M. In Het Panhuis, G. Spinks, and G. Alici, "Design, Modeling and Control of a 3D Printed Monolithic Soft Robotic Finger with Embedded Pneumatic Sensing Chambers," *IEEE/ASME Transactions on Mechatronics*, vol. 4435, no. c, pp. 1–1, jul 2020.

[20] M. Polic, I. Krajacic, N. Lepora, and M. Orsag, "Convolutional Autoencoder for Feature Extraction in Tactile Sensing," *IEEE Robotics and Automation Letters*, vol. 4, no. 4, pp. 3671–3678, oct 2019.

[21] O. Shorthose, A. Albini, L. He, and P. Maiolino, "Design of a 3D-Printed Soft Robotic Hand With Integrated Distributed Tactile Sensing," *IEEE Robotics and Automation Letters*, vol. 7, no. 2, pp. 3945–3952, apr 2022.

[22] T. Feix, J. Romero, H. B. Schmiedmayer, A. M. Dollar, and D. Kragic, "The GRASP Taxonomy of Human Grasp Types," *IEEE Transactions on Human-Machine Systems*, vol. 46, no. 1, pp. 66–77, 2016.

[23] A. Kapandji, "Cotation clinique de l'opposition et de la contre-opposition du pouce," *Annales de Chirurgie de la Main*, vol. 5, no. 1, pp. 67–73, jan 1986.

[24] A. Buryanov and V. Kotiuk, "Proportions of Hand Segments," *International Journal of Morphology*, vol. 28, no. 3, pp. 755–758, 2010.

[25] P. J. Rousseeuw, "Silhouettes: A graphical aid to the interpretation and validation of cluster analysis," *Journal of Computational and Applied Mathematics*, vol. 20, no. C, pp. 53–65, nov 1987.

[26] M. Shutaywi and N. N. Kachouie, "Silhouette Analysis for Performance Evaluation in Machine Learning with Applications to Clustering," *Entropy*, vol. 23, no. 6, p. 759, jun 2021.

[27] D. P. Kingma and J. Ba, "Adam: A Method for Stochastic Optimization," *3rd International Conference on Learning Representations, ICLR 2015 - Conference Track Proceedings*, pp. 1–15, dec 2014.

[28] R. Zuo, Z. Zhou, B. Ying, and X. Liu, "A soft robotic gripper with anti-freezing ionic hydrogel-based sensors for learning-based object recognition," in *2021 IEEE International Conference on Robotics and Automation (ICRA)*, 2021, pp. 12 164–12 169.

[29] B. Calli, A. Walsman, A. Singh, S. Srinivasa, P. Abbeel, and A. M. Dollar, "Benchmarking in Manipulation Research: Using the Yale-CMU-Berkeley Object and Model Set," *IEEE Robotics & Automation Magazine*, vol. 22, no. 3, pp. 36–52, sep 2015.

4.4 Supporting Information

Object characteristics As stated in the paper, the objects were chosen to be close comparisons to objects found in the YCB dataset [183]. However, in addition to the geometries that are provided, the stiffness of each object varies too. To give additional detail on those without a full physical characterisation:

1. The *apple* is a plastic replica with a foam core to allow for longevity of experimental trials without having to replace the specimen. The foam core provides a comparable level of stiffness to a standard ripe apple. A bolt is glued into place for the connection to the rigid stand.

2. The *bottle* is a standard 500ml soft drink bottle that was emptied. The empty bottle has lower stiffness when grasped compared to a full bottle. A plate was attached to the base of the bottle in order to attach it to the rigid stand.

3. The *cards* are a simple deck of cards with a hole in the base to attach to the rigid stand. The casing is made of thin cardboard and the pack was identified whilst full of cards.

4. The *cube* is a hollow FDM 3D printed geometric shape. Therefore, in comparison with the strength of the hand, it can be viewed as incompressible. A through-hole is added to the bottom to affix a bolt to the rigid stand.

5. The *cup* is an empty takeaway 340ml coffee cup with a cardboard sleeve and disposable plastic lid. A through-hole is added to the bottom to affix a bolt to the rigid stand.

6. The *cylinder* is a rigid plastic tube which was assumed to be of infinite length and therefore the ends were not explored by the hand. It that had a baseplate rigidly attached to be bolted to the rigid stand.

7. The *sponge* is a standard kitchen sponge for washing dishes with a scouring face. The stiffness is considerably lower than the other objects. A cavity was hollowed out to glue in a bolt for attachment to the rigid stand.

Data collection procedure The procedure of taking grasps is detailed within the paper and involves approaching the objects from positions that were pseudo-randomly chosen to cover the entire surface area of the object that wasn't in contact with the rigid stand. The hand was connected to a Panda Arm to allow for a suitable range of motion and the set of positions, together with the geometric noise that was added enabled the hand to contact the objects from all angles. Fig. 4.1 shows the procedure for the *apple* object.

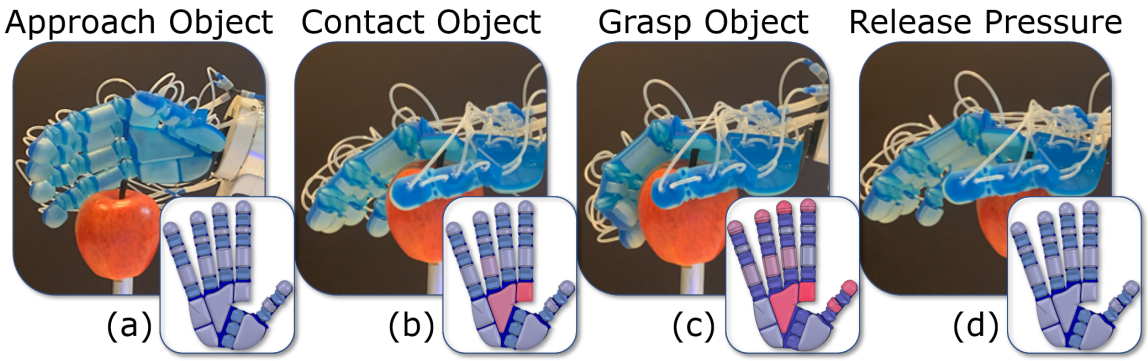

Figure 4.1: The process of approaching the object from a new position, contacting it, and grasping, before releasing it and moving to a new position. The sensor response throughout is shown in the inlays and the steady state value (c) is processed by the EDAMS network.

Dataset collection and overfitting A factor that limits the application of machine learning to tactile identification is the time required to collect datasets. This is especially prevalent with soft hands where the actuation methodologies are generally slower than traditional robots [88]. The effect of this is that the scale of a dataset that is used in visual object identification is not necessarily feasible for tactile identification. Small training datasets can easily lead to overfitting in a trained network or poor generalisability [184]. Therefore, when designing

networks and training them, it is even more important to implement measures that prevent overfitting such as dropout layers, batch normalisation, and not overcomplicating the network with depth or number of nodes [185, 186]. Furthermore, modulating the data with noise and other perturbations can help to increase the robustness of the network against overfitting [187].

For the EDAMS network, dropout layers, batch normalisation and modulating the data with normally distributed noise were tested. The work found that:

1. Whilst dropout layers reduced overfitting, they also reduced the overall accuracy of the network at all number of input grasps.

2. Batch normalisation both reduced overfitting and sped up the training time of the network whilst maintaining performance in the accuracy.

3. Modulating the data with noise slightly reduced the training accuracy of the model ($< 5\%$ accuracy loss) but improved the generalisability of the network considerably with higher accuracy in the testing data.

As a result of these findings, batch normalisation was implemented at each layer and added noise in the form:

$$X \sim \mathcal{N}(0, \sigma^2) \tag{4.1}$$

Here, σ is directly proportional to the original recorded sensor value with a scaling factor of 0.15. Empirically, this was found to reduce the overfitting of the network whilst closely retaining the accuracy of the model.

Latent space dimensionality In EDAMS, the data is encoded to 3 dimensions in the latent space. This size was empirically determined through comparison of the classifier performance and the processing time taken to learn the ML classifiers. Reducing the dimensionality to

fewer than 3 dimensions resulted in a significant loss of classification accuracy where the training process was unable to achieve geometric separation. Increasing the dimensionality to 4 or greater did not provide accuracy improvements and slowed the processing considerably such that training and classification was prohibitively slow. Additionally, in some instances, overfitting was observed. Finally, 3 dimensions allows for easy visualisation as shown in Fig. 7a of the contributed paper.

4.5 Limitations and Future Work

Dataset size As indicated in Sec. 4.4, the size of the dataset can cause problems in the quality of the results produced by neural networks applied to tactile object identification. Ideally, more data would be taken to mitigate this further than the solutions proposed. However, further data collection is limited by the reliability of the materials in long-term deployment. Empirically, small perforations were observed in the joints after ~ 500 cycles of finger-object contact. Due to the careful design of the finger, and use of vacuum actuation, data acquisition could continue for a further ~ 100 cycles before the perforations affected the hand's closure and data acquisition. To address this, two solutions are proposed:

First, the reliability of the finger joints is to be enhanced. As shown in Sec. IV B of the contributed paper in Chap. 3, an unloaded finger demonstrated repeatable output for over 1000 cycles. To improve the reliability of the loaded finger, inspiration can be taken from the solution proposed in Sec. 3.5, introducing variable stiffness to increase the overall force output of the finger. By using the original joint solely for positioning and employing variable stiffness for force enhancement, the force through the original joint can be reduced, extending its longevity.

Secondly, an automated failure detection system can be implemented to minimise human intervention, which slows down the data acquisition process. Leak detection, commonly

used in fluidic systems, can be utilised for this purpose. In this regard, a feedback system could be set up that monitors the actuation pressure. If the pressure drops below that required for complete closure of the finger, the user could be notified to fix or replace the finger. This would mitigate the need for human monitoring, allowing for longer periods of data acquisition and therefore larger datasets over time.

Future work should seek to include more objects in the dataset to demonstrate further the performance of the system and isolate any shortcomings of the method. However, for the number of objects successfully identified, which suitably demonstrate the performance of the system with regard to adaptability in grasping and accuracy of identification, the dataset was found to be sufficiently large with the factors included in the previous section. However, as the hand explores more objects, the proposed enhancements will become essential to facilitate the acquisition of larger datasets and achieve improved identification performance.

Grasp number dependency Secondly, whilst the EDAMS architecture allows for the identification of objects using a range of grasp numbers, for each one, a different network had to be trained to achieve the highest classification accuracy. This requires the user to pre-select how many grasps they require before applying the network to the task. Additionally, only $\{1,3,5,7,10\}$ grasps could be input to the network. This is a significant limitation on the flexibility of the network and it is not possible to input more than 10 grasps which may be required for higher accuracy classification. In order to progress towards the human-like identification methodology of taking subsequent grasps until sufficient confidence is achieved, an incremental model is required that can process tactile data from any number of grasps. Indeed, future work seeks to be able to use the information gained from the previous grasps to inform and influence future prediction outputs. The work presented in the following chapter facilitates this and leverages upon sequentially inputting grasps to allow for open-ended data collection and classification.

Statement of Authorship for joint/multi-authored papers for PGR thesis
To appear at the end of each thesis chapter submitted as an article/paper.

The statement shall describe the candidate's and co-authors' independent research contributions in the thesis publications. For each publication there should exist a complete statement that is to be filled out and signed by the candidate and supervisor **(only required where there isn't already a statement of contribution within the paper itself).**

Title of Paper	EDAMS: An Encoder-Decoder Architecture for Multi-grasp Soft Sensing Object Recognition
Publication Status	☒Published ☐ Accepted for Publication ☐ Submitted for Publication ☐ Unpublished and unsubmitted work written in a manuscript style
Publication Details	Shorthose, O., Albini, A., Scimeca, L., He, L., & Maiolino, P. (2023). EDAMS: An Encoder-Decoder Architecture for Multi-grasp Soft Sensing Object Recognition. *2023 IEEE International Conference on Soft Robotics (RoboSoft)*, 1–7.

Student Confirmation

Student name:	Oliver Shorthose		
Contribution to the paper:	I developed the idea for applying the hand to object identification with Alessandro Albini and Professor Maiolino I undertook the data acquisition with Alessandro Albini I developed the Encoder-Decoder architecture with Luca Scimeca I led the write-up with support from the other authors		
Signature: 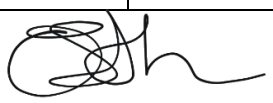		Date	19th July 2023

Supervisor Confirmation

By signing the Statement of Authorship, you are certifying that the candidate made a substantial contribution to the publication, and that the description described above is accurate.

Supervisor name and title:	Professor Maiolino		
Supervisor comments:	I confirm that the student made a substantial contribution to this publication and the contribution of the other authors is as described above		
Signature: 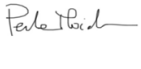		Date	19/07/23

5

Bayesian Framework for Open-Ended Object Identification

The previous chapter demonstrated a successful method of integrating information gained from multiple grasps to inform higher accuracy object identification. The motivation was based upon the haptic approach that humans take to identify objects, whereby multiple touches and grasps from around the entire surface of an object are used to build up a representation of the object. However, the great difference is the ability to continue taking grasps until the user is sufficiently confident in the classification output. This works both to allow infinite grasps if the system is unable to classify the object, and to stop taking grasps early if it converges to a solution quickly, saving valuable data collection time. This chapter develops upon the success of EDAMS and takes greater inspiration from the biological, human methodology to formulate an open-ended identification process. Additionally, a 2D

embedding is implemented within the model to allow for 2D convolutions, in an analogy to highly successful visual identification.

5.1 Recurrent Neural Networks

RNNs were first postulated in 1982 by J.J. Hopfield [188] and are most commonly used for tasks involving sequentially input data such as speech recognition or video classification [66]. The key feature that enables RNNs is the ability to retain information from previous network passes and establish dependencies between sequential inputs, applying the same processes to each input. This allows for temporal frame and data tracking for inputs that are intrinsically linked, such as object tracking within videos [189]. Recently, they have also been proposed for object recognition in an image, where the recurrence allows for detection of 'context' in the scene [190].

In contrast to CNNs and other FFNNs that process a single input to produce an output, RNNs consider a sequence of inputs that influence the final output [191]. In this final work, the objective is to establish a Bayesian framework where the classification output from the previous grasp (the *SoftMax* output) can influence the subsequent grasp's output. Therefore, the decision was made to implement an RNN structure, since it can sequentially process multiple grasps and implement the 'context' of previous grasps to affect subsequent classification.

To validate the effects of the recursive layers in this network, the work looks at a measure of the *attention* that is being paid by the output to both the recursive layers and the new grasp data being input. This allows for understanding over whether the network output is being influenced more by one or the other data inputs. It was achieved by analysing the *salience*, which is detailed in the **Saliency Computation** section of the paper.

5.2 Feature Extraction from a 2D Embedding

Convolutional layers are used ubiquitously for feature extraction across many applications, from image classification to computer vision and segmentation [66, 192]. They demonstrate extraordinary power and are generally simple to apply to a given problem. Whilst CNNs are most commonly used in visual object identification, as presented in Sec. 4.2, they have also been used for tactile object identification due to the analogous spatial relationships that can be extracted [64, 176]. In Sec. 4.3, a 1x19 convolutional layer is used first to extract features from between tactile sensor data values and then a 10x1 layer is used to extract features from between the grasps for a particular exploration sequence. In this follow-up work, the approach is changed to consider the inter-grasp relationships through the recursions of the network and, to extract the spatial relationships within the grasp data; the data is first embedded into a 2D space using a fully-connected layer before being passed through a 2D convolutional layer.

5.3 Contributed Paper

The contributed paper in this chapter has been submitted to Science Advances and is currently under review. It details the new approach to processing multi-grasp tactile data, taking inspiration from the human approach of using compliance in the grasp to conform naturally to objects' geometry and increase the sensor contact. The tactile response is shaped accordingly. Subsequent grasps are taken until sufficient confidence is attained in the output prediction. The predictions from previous grasps are concatenated to influence the subsequent predictions in a Bayesian framework called ROSE-Net. This facilitates an open-ended identification process with no theoretical limit to the number of grasps that can be considered in the classification process. The paper also postulates how using a multi-grasp procedure mitigates low-resolution sensing and the network can be modified to facilitate fault tolerance. The

2D embedding and recursive layer are analysed and an online identification framework is formulated to allow for continued data collection until a sufficient classification belief is achieved. Additionally, a transfer learning scheme is implemented to allow for efficient retraining on additional data.

Bio-inspired Tactile Object Identification Leveraging Deep-Learning and Soft Body Compliance

Oliver Shorthose[1†], Luca Scimeca[2,3,†], Alessandro Albini[1], Perla Maiolino[*,1,4]

[1]Oxford Robotics Institute, University of Oxford, Oxford, OX2 6NN, UK
[2]Harvard University, Cambridge, 02138, MA, USA
[3]Dana Farber, Boston, 02215, MA, USA
[4]University of Genoa, Genoa, Liguria, Italy

[†]Denotes co-first author.
[*]To whom correspondence should be addressed; email: perla@robots.ox.ac.uk

Tactile object identification is a fundamental human skill, underlying several core aspects of human intelligence. Humans display a range of remarkable haptic skills, enabled by the synergistic interactions of the somatosensory system with higher-level cognitive processes. In contrast, robotics' haptic sensing solutions have historically lacked the ability to achieve human-level perceptive capabilities, lacking in both the sensory system and its cognitive digital counterpart. In this work, we leverage the success of the fields of Soft Robotics and Deep Learning to show how a soft robotic hand equipped with low-resolution tactile sensing can be used to accurately identify a diverse set of objects. We let human cognitive studies inform our solution, including the ability to integrate multi-grasp information without reliance on the sequence of tactile interactions, or the generally unknown object pose. The proposed study exploits the

synergy between the adaptability of the soft hand and the multi-grasp identification strategy. In particular, we developed ROSE-Net, a neural network that leverages multiple grasps to enable accurate pose-invariant object recognition. We show that multi-grasp haptic discrimination solutions are desirable, and can lead to a significant increase in performance (up to 20% observed). The versatility and adaptability of this approach are also tested in two scenarios: one, a learning transfer scenario, where we observe ROSE-Net's ability to generalise to a diverse set of experiments with minimal retraining; two, in a fault tolerance scenario, where performance is retained over the loss of up to 15% of the sensing units. Finally, we test our framework in an online discrimination task, where this approach is shown to naturally require additional grasps only for hard-to-classify objects.

Introduction

Object discrimination, the ability to differentiate and recognise different objects, plays a crucial role in human intelligence. This cognitive ability enables us to perceive, categorise, and understand the world around us, forming the basis for higher-level cognitive processes such as perception, learning, memory, reasoning, problem-solving, and adaptive behaviour (*1, 2*). Indeed, this ability is not limited to visual discrimination but rather extends to other sensory modalities, such as haptics (*3*). The sense of touch allows us to interact dynamically with our environment, distinguish objects by their unique physical properties, and provide a far more comprehensive perceptual repertoire (*4, 5*).

Human tactile object identification is a complex process, whereby facilitated by our own cognitive abilities, we exploit our somatosensory system to successfully discriminate between objects. In particular, the softness and compliance of the human hand allows for ease of adap-

tation to a wide and diverse set of objects' shapes and surfaces, achieving safe and effective grasping and manipulation (*6*). The hand's morphology and articulation determine the scope of possible object interactions and exploration strategies. These factors influence the mode and dynamics of surface contacts and the number of subsequent actions required to gather tactile evidence (*7*). Through sensory-motor coordinated action, then, humans strategically regulate the contact with the objects to trigger the receptors uniquely for each object under scrutiny (*8*). A variety of high-density mechanoreceptors in the skin aid these explorations, and allow us to discriminate across fine tactile features (*9*). Here, the body's morphology can act as a computational resource, shaping the patterns observed in the sensory response, and ultimately simplifying the subsequent inference process (*10, 11*).

Although the importance of tactile object recognition has been widely recognised by the robotics research community (*12, 13*), solutions have been limited in their application. Historically, the majority of approaches have been based on rigid-bodied end-effectors, featuring embedded sensors often capable of capturing dense information at the contact location. Aided by the use of machine learning techniques, this has fueled an abundance of solutions for accurate tactile object classification both from a single (usually for simple or small objects) (*14–16*), or multiple (often for larger or more complex objects) (*17–20*) tactile object interactions. However, the rigidity of both the end-effector and the sensing system classically introduce the need for complex control schemes to grasp objects of different geometries, sizes and stiffness (*13,21,22*).

The paradigm of *embodied intelligence* has since garnered increased attention, taking inspiration from how biological organisms utilise the morphology of their bodies to simplify otherwise complex tasks (*23–25*). Through the design and careful selection of materials, robotic grippers and hands can make use of passive compliance and synergies to acquire the ability to naturally conform to the geometry of different objects without the need for complex control schemes (*26–29*). These advantages have since fuelled a plethora of studies on the use of

soft hands for object recognition. For example, proprioceptive and exteroceptive solutions have been proposed to distinguish successfully between different surface profiles and objects even with simple open loop grasp controls (*30–33*).

While the application of embodied intelligence can simplify the required control, the current methods of fabrication have notoriously made it difficult to integrate tactile sensors whilst retaining compliance and the high spatial resolution required to capture complex object features. As a consequence, tactile sensors with low spatial resolution usually limit the recognition task to a low number of objects with simple geometric features (*34, 35*). Recent work featuring the integration of flexible skin made from piezoresistive fabric showed promise in the integration of high spatial density sensors into soft end-effectors, but also notably reduced the compliance of the actuation (*36*). Other approaches have instead focused on multimodal sensing solutions (*37–40*) to address the problem of low spatial resolution. In particular, (*37–39*) combined force or tactile sensors with flex sensors, while (*40*) explored a vision-augmented solution.

Although these systems have shown to be applicable to recognize objects with complex shapes and to be robust to different orientations (similarly to the case of rigid grippers embedding high-resolution tactile sensors), they require either additional sensor integration on the robot (thus affecting its compliance), or make use of external sensing units, such as cameras, which may be unfeasible in unstructured environments. To minimise the impact of sensor integration on the compliance of the soft sensing unit, work in (*41*) and (*42*) have instead explored the integration of soft pneumatic sensors, showcasing improved robot hand adaptability, passive compliance and versatility in grasping tasks. This, however, comes at the expense of a low spatial resolution, being a limiting factor when attempting the recognition of complex objects.

In this article, we formulate, simplify and solve a multi-grasp identification scenario where effective object recognition is enabled by the synergistic interaction of several aspects. For one, the softness of the robot hand, provides adaptation capabilities and directly influences the

sensor response. Second, exploration via multiple grasps, allows for the incremental integration of information about different features of the same objects. We hypothesise that this aspect is crucial to overcome the problem posed by the low sensor resolution, and is complementary to morphological adaptation.

We exploit the synergy between the adaptability of the soft hand and the multi-grasp identification strategy to achieve effective and accurate object recognition of complex objects with low-resolution tactile sensors. We achieve this with simpler control than rigid robot hands, and even ensure the solution is tolerant to sensor faults. We validate our approach using a pneumatically actuated soft hand equipped with distributed low-resolution pneumatic tactile sensors, whose morphology was aimed at achieving compliance of the palm, with similar kinematics of the human hand (*42*). We propose a Recurrent cOnvolutional Spatial Embedding Network (*ROSE-Net*), a novel deep-learning architecture (Fig. 1), enabling multi-grasp tactile object recognition. We design ROSE-Net's architecture to embody several core aspects of our exploration, including the ability to integrate tactile information incrementally, with no theoretical limit on the number of interactions with the objects, or their order, and the arrangement of its architecture to allow for spatially meaningful information structure to arise from the experiments. We also ensure the system is functional without any explicit knowledge of the relative pose of the object to the sensing system. Furthermore, we directly compare our work with the method presented in (*43*) overcoming its limitations on the fixed and predetermined number of grasps required to recognize the objects, its classification performance and fault tolerance capabilities.

In summary, we show that the proposed framework can:

- Meaningfully use multi-grasp tactile information to achieve accurate object classification with low-resolution sensors. Results presented in Section **Accurate Multi-Grasp Discrimination** and compared with (*43*);

- Internally facilitate the structuring of tactile information arising from the object interactions, in Section **Emergence of Information Structure**.
- Integrate multi-grasp information incrementally, thus relying both on prior knowledge from past interactions, and novel evidence from new grasp, in Section **Incremental Integration of Tactile Information**
- Adapt to changing environments and achieve fast adaptation with minimal re-training in Section **Adaptability and Transfer Learning**
- Perform confidence-based sparse tactile explorations, where additional grasps are performed on an object until a satisfactory level of discriminative certainty is reached, in Section **Sparse Incremental Interactions**.
- Showcase sensor-fault robustness capabilities, in Section **Robustness and Fault Tolerance**.

Results

Inspired by the field of embodied intelligence, we aspire to achieve a framework whereby the soft sensory system and the object-classifying processes harmoniously interact to shape and interpret the sensory stimuli arising from object contacts. In this regard, we devised a tactile object discrimination scenario comparative to the work in (*43*). Seven objects with varied dimensions, geometries, and stiffness were selected (detail provided in Supp. Fig. S2). A soft vacuum-actuated hand with 19 distributed pneumatic tactile sensing units was used to grasp the objects from 10 different orientations (*42*). For each grasp, the tactile sensor readings are proportional to the variation in pressure sensed by the distributed pneumatic sensors in the hand (Fig. 1).

In general, we formulate a Bayesian-like framework whereby the belief distribution over the candidate classes, which determines the object class prediction, depends on both a prior class belief distribution, and new object tactile evidence. We consider an initial uniform prior, and update the running posterior incrementally as new tactile evidence is gathered. We approximate this belief distribution with ROSE-Net, a recurrent convolutional neural network designed to appropriately integrate data from consecutive grasps into a meaningful belief distribution across all objects. Further implementation details can be found in the *Bayesian Belief Updates* and *Network Design* methods sections.

Fig. 1c depicts ROSE-Net's architecture. The model has been designed with several key elements. First, the incoming tactile evidence is processed by a fully connected (FC) layer and reshaped into a 2-dimensional matrix of hidden units; these are further processed by two convolutional blocks. A detailed explanation of the architecture and inference process can be found in the Methods Section. ROSE-Net can be sequentially queried, combining the tactile evidence in input with its running inference (prior) to make a prediction, and thus it presents no theoretical limitations on the number of individual grasps to be processed. We discuss architectural inductive biases due to fading memory in the Discussion and Conclusion.

Accurate Multi-Grasp Discrimination

The ability to integrate information from several object contacts is a fundamental skill in tactile object discrimination. Given the non-symmetric nature of many objects, as well as the limited reach and conformity of the sensory system, several partial contacts are in fact often necessary for accurate object discrimination. We first wish to test the ability of our framework to perform accurate multi-grasp object discrimination.

To do this, grasp experiments were performed with objects pertaining to the categories of {Apple, Bottle, Cards (pack), Cube, Cup, Cylinder, Sponge} (Fig. S2). The objects were

chosen to comply with the YCB dataset (*44*), with slight variations to introduce additional diversity in object geometries and stiffness. Specifically, the sponge and cards were chosen to test the discrimination performance between similarly shaped objects with different stiffness.

To provide a repeatable testing procedure, the objects were affixed to a rigid metal support and approached from 10 different orientations ensuring maximum surface coverage. The setup is shown in Fig. 1b. For each grasp, $10mm$ of equally distributed positional variation in the x, y, and z directions was introduced to ensure robust invariance in object identification network performance with respect to relative pose. A static reading of the pressure for each of the 19 pneumatic sensors on the hand was recorded after 30 seconds of closing the hand around the object. Each set of 10 object grasps was repeated $T = 30$ times for each of the 7 objects, constituting a total of 2100 dataset entries of sequential data. For training, any number from 1 to 10 grasps, as well as grasp order, were randomly sampled, significantly increasing the possible observable combinations. This, in turn, induced grasp order invariance by the model.

To train ROSE-Net, a 60% train, 20% validation, and 20% test ratio was used for the grasp data. The model was trained with *CrossEntropyLoss* on the output of the final processed grasp entry in a sequence of R grasps, and the training dynamics were controlled by a vanilla *Adam* optimiser, with a learning rate of $1e^{-4}$ (*45*). Early stopping was implemented to halt training when there was no improvement in the validation loss for over 30 epochs.

Fig. 2 reports the classification confusion matrices when the network performs inference by using one, two and three consecutive grasps. First, we observe a monotonic increase in classification accuracy with an increasing number of consecutive grasps per object. This increasing accuracy indicates its ability to integrate multi-grasp information, highlighting the significance of multi-grasp prediction for precise soft object classification. From Fig. 2 we also observe single-grasp uncertainties across several objects explicable by both *curvature* and *dimension* geometric profiles. On classification errors induced by similar curvature profiles, we observe

# grasps	**Acc (%)**	**Acc** (*43*) **(%)**
1	**88.75**	47.07
2	98.33	-
3	**99.27**	69.96
4	99.38	-
5	**100.0**	83.24
6	99.90	-
7	**100.0**	87.64
8	99.79	-
9	100.0	-
10	**100.0**	99.95

Table 1: Mean classification accuracy across all objects while increasing the number of grasps. The values in bold indicate the higher accuracy between this work and the previously presented work.

single-grasp recognition on the 'apple' mistaken for the 'bottle' 5% of the times, the 'bottle' confused as the 'cylinder' 5% of the times (or vice-versa 4.2%), and the 'cards' mistaken as the cube 7.5% of the times. On misclassifications of dimensionally similar objects, we observe the 'apple' mistaken for a 'cube' 7.5% of the time (and vice-verse 5.8%), and, like before, the 'bottle' vs the 'cylinder' and the 'cards' vs the 'cube' with likewise similar dimensional profiles. As the number of grasps increases, the majority of the confusion is overcome through the integration of multi-grasp additional object information. Interestingly, we observe an almost complete disappearance of dimensionally-induced sample misclassification, while some curvature-induced confusions still remain (Fig. 2).

We compare the performance of *ROSE-Net* against our previous model, *EDAMS* (*43*), showcasing several shortcomings. First, EDAMS successfully demonstrated multi-grasp object identification capabilities but the integration of tactile evidence was not incremental, and the number of grasps had to be pre-determined. Second, the model would only be able to process the pre-determined number of grasps and needed re-training for any new application requiring additional tactile evidence. Finally, EDAMS performance was limited when few grasp tactile

information was available.

Table 1 reports the classification accuracy by the number of grasps used for inference. As before, as the number of grasps increases, so does the accuracy of the classifier - from 88.75% at 1 grasp to 100% at 5 grasps and beyond. Observing the performance of ROSE-Net, we infer how the data collection process is intrinsically noisy, reflecting real-world grasp settings. Occasionally, the inclusion of additional, noisy, evidence may induce slight fluctuations in performance, which can be mitigated by collecting additional evidence. Comparing the two models, we observe higher classification accuracies for all numbers of grasps. Most significantly, ROSE-Net is capable of outperforming *EDAMS* by over 40% accuracy with single grasp object classification and almost 30% after 3 grasps. In general, the collection of additional tactile evidence is a time costly process which is greatly reduced by requiring less exploration. This is achieved by optimised integration of multi-grasp predictions for accurate classification after relatively fewer hand-object interactions. Finally, ROSE-Net can be trained once and tested on any number of grasps, as opposed to *EDAMS*, which suffers from costly retraining in each instance and can only be deployed on 1, 3, 5, 7 or 10 grasps.

Emergence of Information Structure

One of the focal design elements in ROSE-Net is the spatial layout of the hidden units prior to the recurrent blocks in the architecture (Fig. 1c). Making an analogy to pixel adjacency in images, the spatial adjacency of tactile elements in a sensor presents meaningful information that can be extremely relevant for accurate classification. Enabled by the sensory rich nature of the contact dynamics arising from the object grasps, we hypothesise that the convolutional inductive bias of the forward blocks, together with the 2D arrangement of the hidden units after the first layer, can naturally lead to a meaningful 2D spatial embedding of the tactile features in the input. We test this hypothesis by observing ROSE-Net's 2-dimensional embedding layer

as a grey-scale image. To compute a measure of information content we employ the notion of entropy and refer the reader to the details of this computation in the *Spatially Meaningful 2D Embedding* Section.

Fig. 3a shows the average entropy level across the validation data while training ROSE-Net, where lower values of entropy are associated with higher information content (*46*). We observe a largely monotonic drop in entropy over epochs, showcasing an increase in 2-dimensional information contained within the spatial embedding units.

The model is qualitatively tested before and after training, to visualise the activation patterns that maximise the belief distribution skew towards a particular object. To achieve this, we loosely follow the gradient-based optimisation process in (*47*), and optimise a 2D embedding layer input which maximally activates the network's output with respect to each class in turn. The optimisation is performed both at the beginning and at the end of the ROSE-Net training routine.

Fig. 3b reports the embedding layer activation patterns that maximise the prediction for each class, both before (top row) and after (bottom row) training. Corroborating the results in Fig. 3a, we observe random and sharp gradients for each of the patterns representing the objects before training (where the entropy of the embedded layer is highest). After training, distinguished patterns of activation across objects are visible. More importantly, the smooth edges in the bottom half of the images in Fig. 3b suggest a high degree of spatial correlation between a pixel and its neighbours, as induced by the inductive bias in the convolutional blocks. Quantitatively, this is shown further in the low entropy levels in Fig. 3a for the corresponding epoch.

Incremental Integration of Tactile Information

As multiple object contacts are often necessary to form a more comprehensive understanding of an object's physical characteristics, the exact number of grasps is usually known and depends

on several factors, including the similarities of the objects under scrutiny, their local surface features, and the order of the contact locations (*41, 42*). We devise our framework to mimic human tactile identification and execute multiple grasps incrementally until a satisfactory level of discriminative certainty is reached (*5*). To achieve this, we design ROSE-Net recursively, concatenating the output of the previous inferred classification beliefs with the output of the convolutions to manifest the Bayesian inference process described. We also ensure minimal cross-dependencies by only combining the embedding with the recurrent information after it has been processed by the convolutional blocks.

Given ROSE-Net's design then, the classification belief of our model for each grasp relies on the combination of two factors: first, the new grasp tactile evidence; and second, the prior beliefs, uniformly initialised and then recursively aggregated via iteratively performing predictions on the previous grasp tactile data. We analyse the amount by which ROSE-Net, on average, relies on each of the inputs while making predictions. We investigate a measure of *attention* by the pre-trained ROSE-Net model on either the new tactile data, or the prior belief, during prediction. We perform this analysis by computing a saliency map of the inputs with respect to the output, following the work in (*48*). For additional implementation details, we refer the reader to the *Spatially Meaningful 2D Embedding* Section.

Fig. 4 shows the normalised Expected saliency of the network outputs with respect to (a) the new grasp being input, and (b) the recurrent input, across sequential grasps. In line with our Bayesian expectations, for the first grasps, the network relies more often on the new evidence for its classification (Fig. 4). As the number of processed grasps increases and the network belief becomes more salient, the network indicates a tendency to rely increasingly on its prior beliefs when several grasps have been processed. Moreover, we observe a plateau in the increase of the importance of the prior after 4 to 5 grasps, suggesting the ability for new evidence to be integrated even after a steady belief state is reached.

Adaptability and Transfer Learning

Humans have the ability to learn quickly and adapt their discriminative capabilities to new and unknown tactile discrimination tasks. We investigate a similar scenario whereby the previously learned solutions by our framework are adapted and tested in a novel discriminative scenario, where a new control strategy is used to grasp the objects. To achieve this, we perform additional grasps whereby each object is grasped from 10 new, random, previously unseen poses. A new hand was printed to ensure the model can generalise against specimen variation. Each pose was repeated 10 times with the same positional noise that was added in the initial data acquisition, split and pre-processed similarly to the first batch of grasps experiments.

We fine-tune the pre-trained ROSE-Net model with the new set of data while avoiding catastrophic forgetting by randomly combining an equally abundant subset from the previous set of experiments for both training and validation batches. Fig. 5 reports the validation loss and accuracy dynamics during fine-tuning, and compares them to the same when fully re-training ROSE-Net on the same data. In the figure, we observe that fine-tuning our pre-trained ROSE-Net allows for fast retraining and performance convergence, reaching top discrimination performance within 75 fine-tuning epochs, as opposed to over 350 epochs for retraining. The results suggest ROSE-Net can extract generalisable features for grasp prediction with limited data availability and training, only requiring small adjustments for domain adaptation. Table 2 shows the final grasp-specific accuracy of the fine-tuned model on the new set of data, as compared to the initial results. The results show comparable performance to our initial results, with increasing accuracy over additional grasps. The fast convergence and final results indicate the potency of fine-tuning ROSE-Net for domain transfer within variations in both end-effector and grasp strategy.

# grasps	Original Model Acc (%)	Fine-tuned Model Acc. (%)
1	**91.41**	88.75
2	97.66	**98.33**
3	98.26	**99.27**
4	**100.0**	99.38
5-10	**100.0**	**100.0**

Table 2: Mean classification accuracy across all objects while increasing the number of grasps for the model fine-tuning. The data from the newly acquired grasps was randomly combined with the originally acquired data.

Sparse Incremental Interactions

When instantaneous differentiation amongst objects is not possible, tactile manipulation and discrimination can often be a costly process, involving several physical interactions with the object under scrutiny. The complexity of the tactile discrimination task and the ensuing interactions depend on several factors, including the similarity of the objects under scrutiny, the complexity of their features (size, shape, texture etc.) and several other factors besides. Ideally, interactions should be sparse, and further object inspections should be executed only when strictly necessary.

In robotics, tactile information is likewise a costly process, both in terms of data acquisition time as well as end-effector stress (*49, 50*). By taking advantage of the Bayesian belief framework proposed, we investigate the ability of our model to motivate further experimental interactions between the robot and the objects to classify. Here, the robot can halt the process of gathering additional tactile evidence on a particular object when the classification belief for a class candidate reaches a desired confidence threshold. We analyse this process with our fine-tuned model and the newly acquired grasp data (*Transfer Learning* Section). We monitor the maximum belief and halt data acquisition when ROSE-Net attributes over 99% of its output prediction to any one particular object.

Fig. 6a shows the average belief in each of the objects as the number of grasps increases.

The number of bars indicates the greatest number of grasps required to reach the 99% belief threshold. As the figure shows, this number varies across objects, where hard-to-classify objects would require additional grasps for accurate prediction. The robot, for example, can classify the deck of cards reliably after just one grasp, whereas the cup requires at most 5 grasps. Fig. 6b shows ROSE-Net's belief progression while classifying the cup across 5 grasps. In the figure, we observe how the model can re-adjust an erroneous classification by integrating multi-grasp information, and finally correct its belief state towards the class under scrutiny. For completeness, a selection of belief sequences for each object is provided in Supplementary Section B.

Robustness and Fault Tolerance

From temporary tissue damage to cognitive impairment, several occurrences can negatively impact humans' ability to perceive and process information from all the mechanoreceptors in our hands. however, when under impediments, even up to digit amputation, humans mostly still retain the ability to adapt and resume discriminative performance in tactile discrimination tasks (*51*).

We investigate the ability of a robot to perform reliably within a fault-tolerant scenario, where we enforce random sensor drops fault at test time. To achieve this, we re-train ROSE-Net on the original data, incorporating a simulation of sensor failure by randomly zeroing a subset of sensors between 0 and N_d during training. We perform a hyper-parameter search at train time, assessing values of N_d that would induce fault tolerance without affecting the model performance. Supplementary Fig. S4 shows the hyper-parameter search results. We pick the saddle point at $N_d = 3$ offering the best ratio between performance retention and the number of dropped sensors.

We analysed the fault tolerance in two ways: first, we allocated a set number of sensors to be randomly zeroed at test time, and examined the effect on each object's classification accuracy;

secondly, we specifically zeroed each sensor in turn to examine the significance of each sensor in the model.

Fig. 7a shows the results of zeroing different numbers of sensors on the classification accuracy of each object by ROSE-Net. We compared the fault-tolerant ROSE-Net model (continuous line) with the original trained version (dotted line). Each line represents the accuracy of the models as a random increasing number of sensors (from 0 to 9) are zeroed out. Performance beyond 9 blocked sensors was found to be trivially poor and the original model had poor performance across all numbers of drops. From the results, we observe that the fault-tolerant ROSE-Net model is capable of performing accurate object discrimination (accuracy greater than 80%) when up to 3 sensors are dropped. Fault-tolerant object classification also depended on the object features. Objects with relatively 'simple' shape profiles, such as the 'cylinder', the 'sponge' and the 'apple', could be reliably classified with increased sensor faults, while more complex objects, like the 'cup', showed skewed performance drops. The fault-tolerant ROSE-Net outperforms the original trained model across all sensor faults larger than one, while achieving comparable performance, and at times under-performing, when no sensor faults are induced. These results indicate how the sensor drop re-training may function as a regularizer for the model. Finally, Fig. 7b shows the effect of blocking individual sensors. As can be seen, blocking the sensors in the ring finger and at the base of the index finger have the greatest effect on classification. From this, we can infer that they are triggered the most in grasping each object, which can be used to inform future sensor design choices.

Generally, we observe that the model shows robustness against faulty sensors with a maximum of 8.0% accuracy drop between full coverage and any single blocked sensor. These results showcase the ability of ROSE-Net to be able to be robust against reduced sensor numbers. However, high-resolution sensing remains of paramount importance for top performance, and significantly so for objects with complex geometries.

Discussion

Tactile object identification in real-world settings is a complex task which requires highly adaptive and accurate solutions. Humans display an impressive array of synergistic factors, which all contribute to the extraordinary ability to perform accurate object recognition in various settings. Amongst these, the intrinsic compliance of the joints and skin of the hand, as well as the cognitive capability of integrating multiple distinct partial views of an object are predominant.

In this work, we investigate the ability of a robotic system to display several of these capabilities, and propose a framework exploiting a soft robotic hand to achieve highly accurate tactile object identification by compositionally integrating multi-grasp tactile information. We perform the experiments on an anthropomorphic hand with soft pneumatic actuation and distributed sensing, which facilitates the multi-grasp object identification task by significantly simplifying the control scheme. This is akin to human haptic identification, where the explicit control schemes for grasping and manipulation are simplified and complemented by softness and synergies, allowing for greater adaptation to the object being examined (*6*).

The framework proposed leverages an ad-hoc Recurrent Convolutional Neural Network-based architecture, ROSE-Net, designed to approximate a Bayesian framework whereby a robot can iteratively improve its running belief distribution over object identities by additional tactile evidence. This is showcased on a tactile object identification task of seven objects with varying geometries, sizes and stiffness.

Comparison with previous work has shown that ROSE-Net boasts excellent single-shot, as well as multi-grasp, inference performance, bypassing similar models, such as *EDAMS*, on a comparable tactile object identification task. ROSE-Net achieves this by encoding the tactile information on a 2-dimensional embedding, which is later integrated, via model recurrence, with the running inference on the object under scrutiny. We show that the 2-dimensional embedding

is indeed capable of retaining 2D information, as suggested by the decreased 2D entropy during model training. On the other hand, the impact of the recursive nature of the model was studied by comparing the average saliency magnitude of the model with respect to both its tactile inputs and recurrent layer. The input saliency is known to correlate with the areas in the input space that the model is attending to more closely while making a prediction. We observe the salience of the recursive layer increasing over the first four grasps and thereon reaching a plateau. The increase is a strong indication of the ability of ROSE-Net to give more weight to the prior beliefs after several observations, while the plateau is desirable to be able to question the current beliefs when additional evidence deviates largely from prior beliefs over consecutive new observations. A limitation of the current framework, however, also lies with the architectural inductive recursive bias. In fact, recurrent neural networks are known to suffer from fading memory, due to their limited mnemonic ability over longer sequences of output. In this context, ROSE-Net's prior, although compositionally built on previous tactile information, is likely to be predominantly affected by the last several object grasps, while mostly not retaining information from longer sequences.

In real-world settings, it is oftentimes the case that the task objective or sensor output range varies, ultimately leading to a dramatic domain shift over time. For example, material hysteresis can cause shifts in sensor value ranges, leading to significant differences in sensor outputs over time. Similarly, a change in the interaction regime by the robot with the object (e.g. directional force, orientation, dynamic interaction) can produce a diverse range of tactile information that is often hard to replicate and generalise over. For machine learning solutions to the object identification problem, pre-trained models face the dire consequences of this shift, causing large drops in performance. By training regime design, we have developed our framework to be able to perform accurate object identification despite the order of tactile information observed at input. More importantly, the ability to adapt to a shifting distribution is an important topic in

the active learning community. Re-training a model is an expensive process, which initiates with time-consuming and costly data-gathering procedures, as well as compute-power and compute-time requirements. Transfer learning is a desirable technique aimed at re-adjusting the internal weights of a working pre-trained model to re-align the model with the distributional shift in the data. To achieve appropriate fine-tuning, the model needs to be able to encode generalisable data processing procedures, which can be re-adjusted successfully for the shifted distribution with minimal retraining. We perform additional experiments with both sensor specimen variation and unseen tactile grasp procedures in mind, and observe the ability of ROSE-Net to adapt to distributional shifts induced by the variations. We observe that our model is capable of resuming ideal object identification performance with little additional training, avoiding the need for expensive re-training procedures.

Finally, for deployable solutions, tolerance to distributional shifts induced by the loss of sensing units is of paramount importance. With fault tolerance in mind, we show how a simple shift in the training regime of ROSE-Net can induce the model to maintain its performance when up to 20% of the hand's sensors are inactive. In line with previous work, we observe a significant drop in performance when the number of sensing units falls beneath tolerable levels. Interestingly, we observe these levels to vary by the object, whereby objects with more complex geometrical features generally necessitate higher sensor resolution for accurate discrimination.

Materials and Methods

Hand Design: The soft robotic hand is an improved version of the work in (*42*), with the relevant changes detailed in (*43*). Fifteen vacuum-actuated W-joints are integrated monolithically into the hand to achieve similar DOFs to humans. The hand is designed to combine human-like dexterity with the adaptability afforded by softness in the joints. This adaptability is paramount to being able to conform to diverse geometries without an explicit, complex control scheme.

The joints were underactuated together using a single internal actuation pressure to simplify the control and exploit the compliance of the design. A compressor and analogue pressure (SMC IRV20-C10) regulator provided a negative pressure source at -75kPa, connected to each joint. Two solenoid valves (Yosoo1210) were used to control whether to open or close the hand. The joints' behaviour is characterised in (*42*).

To achieve distributed tactile sensing, 19 soft pneumatic tactile pads were arranged around the fingers and palm. The sensors' soft design further increased the conformity of the hand to the surface profile in contact with the objects. 19 pressure sensors (ADP51A1) were connected to the soft tactile pads via $1mm$ internal diameter tubing to ensure the electronics were separate from the main body of the hand.

Through the use of multi-material 3D printing, the fingers and palm can easily be reproduced to a high degree of repeatability.

Learning Framework: In order to emulate the human ability to integrate multiple object contacts incrementally, we formulate a multi-grasp Bayesian classification framework whereby a model can use incoming grasp evidence to update and additively improve its classification beliefs. We also aim to reformulate the object recognition task proposed in (*43*), while augmenting the framework to improve on its shortcomings. First, we wish to train a single inference model for any number of grasps in input. This allows the robot to collect data until a satisfactory classification belief threshold has been reached. Secondly, we wish to remove any theoretical upper limits on the number of grasps used, thus enabling focused data collection, as informed by increasingly more accurate classification.

Bayesian Belief Updates: Let $x^{(i)}$ be the tactile data generated from the ith grasp of an unknown object. In short, we wish to formulate a predictive scenario where

$$\Gamma^{(i)} = \begin{cases} U_H(0,1) & i = 0 \\ P(C \mid x^{(i)}, \Gamma^{(i-1)}) & i > 0 \end{cases} \tag{1}$$

where $\Gamma^{(i)}$ is the belief distribution over object classes at the ith grasp and C is the object class. Initially, the beliefs are drawn from an H-dimensional uniform distribution over all classes. As grasp evidence is collected, however, the inferred distribution is computed conditionally on the current grasp data $x^{(i)}$ and a prior, which in this case corresponds to the running inferred class distribution, $\Gamma^{(i-1)}$. At any grasp, we can thus retrieve the most likely predicted class by

$$\hat{c}^{(i)} = \ argmax\, \Gamma^{(i)} \tag{2}$$

Here, we wish to approximate this inference process by a DNN architecture. We do so by designing ROSE-Net, a Recurrent cOnvolutional Spatial Embedding Network.

Network Design: Recurrent neural networks have been widely used in several tasks, including speech synthesis & recognition, translation, image recognition, and last but not least object identification (*52, 53*). For this application, we build an ad-hoc output-to-input recurrent architecture, ROSE-Net, which, by the nature of its recursive design, can fit the sequential inference process described in Eq. 1. The RCNN ROSE-Net architecture is shown in Fig. 1c.

The model presents a few key elements:

1. The incoming tactile evidence is processed by an FC layer and reshaped into an 8x8 2-dimensional matrix of hidden units; these are further processed by two blocks of convolutional layers with batch normalisation and ReLU activation layers. Analogous to vision, the adjacency of tactile elements (akin to pixel adjacency) presents spatially pertinent features which may be relevant for accurate classification. Without the need for sensor

spatial calibration, we wish to design a model capable of learning spatially meaningful embeddings via end-to-end training. We hypothesise that the 2D spatial arrangement and the subsequent convolutional layers push the network towards embedding 2D solutions that present recurring 2D spatial patterns which are recognisable by sliding convolutions. We test this hypothesis in the *Spatially meaningful 2D embedding* Section.

2. We concatenate the network output on the previous inferred classification beliefs with the output of the convolution, to manifest the Bayesian inference process described in Eq.1.

3. We ensure the network is modular, with minimal cross-dependencies. For example, we ensure the convolutional embedding learns to embed spatial evidence based only on the new evidence and is otherwise uninhibited by historical beliefs. The final FC feed-forward layers, instead, join the historical beliefs and the new information to generate new beliefs.

Thus, we train the network to fit the recurrent inference process:

$$P(C \mid x^{(i)}, \Gamma^{(i-1)}) = \begin{cases} G(x^{(i)}, U_H(0,1)) & i = 1 \\ G(x^{(i)}, P(C \mid x^{(i-1)}, \Gamma^{(i-2)})) & i > 1 \end{cases} \tag{3}$$

where G is the approximate conditional inference process computed by ROSE-Net.

Spatially meaningful 2D embedding

2D Entropy Computation: For a general array of values x, we can compute the entropy as

$$H(x) = -\sum_{jk} p(x_{jk}) \log(x_{jk}) \tag{4}$$

where $p(x_{jk})$ is the probability of value x_{jk} in position j, k. For a 2D array, we seek a measure proportional to the complexity contained in a given 2D neighbourhood. We compute this as the

expectation of the entropy for a 2D array neighbourhood, thus:

$$E[H(x)] = -\frac{1}{N}\sum_{n}\sum_{jk} p(\arctan(o_{jk}))\log p(\arctan(o_{jk})) \tag{5}$$

where N is the number of n neighbourhoods in the array, and (o_{jk}) is the jk^{th} element in the 2D embedding layer. We use the $\arctan$ to bound the possible array values to [-1, 1]. We define the neighbourhood by a structuring element. To compare the information content appropriately with the network's downstream components, we use a square 3 by 3 filter element, akin to the dimension of the convolutional filters in the downstream convolutional blocks.

2D Embedding Layer Optimisation: Let $G(x^{(i)}, \Gamma^{(i-1)})$ be the function computed by ROSE-Net, estimating a belief distribution from both history and the tactile information in $x^{(i)}$. We can define a function $G'(o^{(i)}, \Gamma^{(i-1)})$ by discarding the first FC layer in ROSE-Net. G' computes a belief distribution directly from the 2-dimensional embedding layer. We can randomly generate an 8x8 vector o' and compute $\Delta o = \frac{\partial CE(G'(o',\Gamma^{(i-1)}),c)}{\partial o'}$, where CE is the Cross-Entropy Loss between the output and an object class c of choice. we can use Δo to perturb the values in o' into an array that evaluates to the object class of choice c. We use Stochastic Gradient Descent (SGD) with a learning rate of $1e-5$ on a batch of 1000 randomly generated 8x8 arrays, to find an optimised 2-dimensional embed layer for each of the object classes. This method has been successful in generating preferred visual input in several DNNs (*47*).

Saliency Computation: We follow the saliency computation devised in (*48*), corresponding to the simple computation of $inputs * gradients$, and shown to be successful in identifying the input pixels attended to by DNNs when making predictions. For ROSE-Net, we can compute the expected saliency for the grasp $x^{(i)}$ as $Saliency(x^{(i)}) = x^{(i)}\frac{\partial G(x^{(i)},\Gamma^{(i-1)})}{\partial x^{(i)}})$ and the saliency

for the belief prior as $Saliency(\Gamma^{(i-1)}) = \Gamma^{(i-1)} \frac{\partial G(x^{(i)}, \Gamma^{(i-1)})}{\partial \Gamma^{(i-1)}}$. We compute these measures for each object and each number of grasps, and average the saliency values over the test data.

References

1. S. J. Lederman, R. L. Klatzky, Haptic perception: A tutorial, *Attention, Perception & Psychophysics* **71**, (2009).

2. A. Montagu, The skin, touch, and human development, *Clinics in Dermatology* **2**, (1984).

3. C. Wallraven, H. H. Bülthoff, S. Waterkamp, L. van Dam, N. Gaißert, The eyes grasp, the hands see: Metric category knowledge transfers between vision and touch, *Psychonomic Bulletin & Review* **21**, (2014).

4. R. Pfeifer, J. Bongard, *How the body shapes the way we think: A new view of intelligence.* (Boston Review, Cambridge, MA, US, 2007).

5. R. L. Klatzky, S. J. Lederman, V. A. Metzger, Identifying objects by touch: An "expert system", *Perception & Psychophysics* **37**, (1985).

6. P. H. Thakur, A. J. Bastian, S. S. Hsiao, Multidigit Movement Synergies of the Human Hand in an Unconstrained Haptic Exploration Task, *The Journal of Neuroscience* **28**, (2008).

7. S. J. Lederman, R. L. Klatzky, Hand movements: A window into haptic object recognition, *Cognitive Psychology* **19**, (1987).

8. R. S. Johansson, J. R. Flanagan, Coding and use of tactile signals from the fingertips in object manipulation tasks, *Nature Reviews Neuroscience* **10**, (2009).

9. A. B. Vallbo, R. S. Johansson, Properties of cutaneous mechanoreceptors in the human hand related to touch sensation., *Human neurobiology* **3**, (1984).

10. R. Pfeifer, C. Scheier, Sensory—motor coordination: The metaphor and beyond, *Robotics and Autonomous Systems* **20**, (1997).

11. L. Scimeca, P. Maiolino, E. Bray, F. Iida, Structuring of tactile sensory information for category formation in robotics palpation, *Autonomous Robots* **44**, (2020).

12. L. Seminara, *et al.*, Active haptic perception in robots: a review, *Frontiers in neurorobotics* **13**, (2019).

13. Z. Kappassov, J. A. Corrales, V. Perdereau, Tactile sensing in dexterous robot hands - Review, *Robotics and Autonomous Systems* **74**, (2015).

14. H. Liu, X. Song, T. Nanayakkara, L. D. Seneviratne, K. Althoefer, A computationally fast algorithm for local contact shape and pose classification using a tactile array sensor, *2012 IEEE International Conference on Robotics and Automation* (2012), pp. 1410–1415.

15. S. Luo, W. Mou, K. Althoefer, H. Liu, Novel tactile-sift descriptor for object shape recognition, *IEEE Sensors Journal* **15**, (2015).

16. S. Luo, J. Bimbo, R. Dahiya, H. Liu, Robotic tactile perception of object properties: A review, *Mechatronics* **48**, (2017).

17. Z. Pezzementi, E. Plaku, C. Reyda, G. D. Hager, Tactile-object recognition from appearance information, *IEEE Transactions on Robotics* **27**, (2011).

18. A. Schneider, *et al.*, Object identification with tactile sensors using bag-of-features, *2009 IEEE/RSJ International Conference on Intelligent Robots and Systems* (2009), pp. 243–248.

19. A. Schmitz, *et al.*, Tactile object recognition using deep learning and dropout, *2014 IEEE-RAS International Conference on Humanoid Robots* (2014), pp. 1044–1050.

20. H. Liu, *et al.*, Tactile image based contact shape recognition using neural network, *IEEE International Conference on Multisensor Fusion and Integration for Intelligent Systems* pp. 138–143 (2012).

21. P. Rothemund, *et al.*, Shaping the future of robotics through materials innovation, *Nature Materials* **20**, (2021).

22. C. Piazza, G. Grioli, M. G. Catalano, A. Bicchi, A Century of Robotic Hands, *Robotics, and Autonomous Systems Annu. Rev. Control Robot. Auton. Syst. 2019* **22**, (2019).

23. C. Laschi, Embodied Intelligence in soft robotics: joys and sorrows, *IOP Conference Series: Materials Science and Engineering* **1261**, (2022).

24. L. Scimeca, P. Maiolino, F. Iida, Soft morphological processing of tactile stimuli for autonomous category formation, *2018 IEEE International Conference on Soft Robotics (RoboSoft)* (IEEE, 2018), pp. 356–361.

25. A. Cangelosi, J. Bongard, M. H. Fischer, S. Nolfi, *Springer Handbook of Computational Intelligence* (Springer Berlin Heidelberg, Berlin, Heidelberg, 2015), pp. 697–714.

26. J. Hughes, *et al.*, Soft manipulators and grippers: A review (2016).

27. S. Abondance, C. B. Teeple, R. J. Wood, A Dexterous Soft Robotic Hand for Delicate In-Hand Manipulation, *IEEE Robotics and Automation Letters* **5**, (2020).

28. J. Zhou, *et al.*, 50 Benchmarks for Anthropomorphic Hand Function-based Dexterity Classification and Kinematics-based Hand Design, *2020 IEEE/RSJ International Conference on Intelligent Robots and Systems (IROS)* (IEEE, 2020), pp. 9159–9165.

29. L. Scimeca, J. Hughes, P. Maiolino, F. Iida, Model-free soft-structure reconstruction for proprioception using tactile arrays, *IEEE Robotics and Automation Letters* **4**, (2019).

30. T. Watanabe, K. Yamazaki, Y. Yokokohji, Survey of robotic manipulation studies intending practical applications in real environments -object recognition, soft robot hand, and challenge program and benchmarking-, *Advanced Robotics* **31**, (2017).

31. Y. Yan, C. Cheng, M. Guan, J. Zhang, Y. Wang, Texture Identification and Object Recognition Using a Soft Robotic Hand Innervated Bio-Inspired Proprioception, *Machines* **10**, (2022).

32. L. Chin, J. Lipton, M. C. Yuen, R. Kramer-Bottiglio, D. Rus, Automated recycling separation enabled by soft robotic material classification, *RoboSoft 2019 - 2019 IEEE International Conference on Soft Robotics* pp. 102–107 (2019).

33. B. S. Homberg, R. K. Katzschmann, M. R. Dogar, D. Rus, Robust proprioceptive grasping with a soft robot hand, *Autonomous Robots* **43**, (2019).

34. J. Huang, A. Rosendo, Variable Stiffness Object Recognition with a CNN-Bayes Classifier on a Soft Gripper, *Soft Robotics* **00**, (2022).

35. J. Cao, J. Huang, A. Rosendo, Variable stiffness object recognition with bayesian convolutional neural network on a soft gripper, *2022 IEEE/RSJ International Conference on Intelligent Robots and Systems (IROS)* (2022), pp. 9431–9436.

36. T. J. Pannen, S. Puhlmann, O. Brock, A Low-Cost, Easy-to-Manufacture, Flexible, Multi-Taxel Tactile Sensor and its Application to In-Hand Object Recognition, *2022 International Conference on Robotics and Automation (ICRA)* (IEEE, 2022), pp. 10939–10944.

37. P. M. Khin, J. H. Low, M. H. Ang, C. H. Yeow, Development and Grasp Stability Estimation of Sensorized Soft Robotic Hand, *Frontiers in Robotics and AI* **8** (2021).

38. T. G. Thuruthel, B. Shih, C. Laschi, M. T. Tolley, Soft robot perception using embedded soft sensors and recurrent neural networks, *Science Robotics* **4** (2019).

39. Z. Zhou, *et al.*, A sensory soft robotic gripper capable of learning-based object recognition and force-controlled grasping, *IEEE Transactions on Automation Science and Engineering* pp. 1–11 (2022).

40. C. Jiao, B. Lian, Z. Wang, Y. Song, T. Sun, Visual–tactile object recognition of a soft gripper based on faster Region-based Convolutional Neural Network and machining learning algorithm, *International Journal of Advanced Robotic Systems* **17**, (2020).

41. L. He, Q. Lu, S.-A. Abad, N. Rojas, T. Nanayakkara, Soft fingertips with tactile sensing and active deformation for robust grasping of delicate objects, *IEEE Robotics and Automation Letters* **5**, (2020).

42. O. Shorthose, A. Albini, L. He, P. Maiolino, Design of a 3D-Printed Soft Robotic Hand With Integrated Distributed Tactile Sensing, *IEEE Robotics and Automation Letters* **7**, (2022).

43. O. Shorthose, A. Albini, L. Scimeca, L. He, P. Maiolino, Edams: An encoder-decoder architecture for multi-grasp soft sensing object recognition, *2023 IEEE International Conference on Soft Robotics (RoboSoft)* (IEEE, 2023).

44. B. Calli, *et al.*, Benchmarking in Manipulation Research: Using the Yale-CMU-Berkeley Object and Model Set, *IEEE Robotics & Automation Magazine* **22**, (2015).

45. D. P. Kingma, J. Ba, Adam: A Method for Stochastic Optimization, *3rd International Conference on Learning Representations, ICLR 2015 - Conference Track Proceedings* pp. 1–15 (2014).

46. Y. Wu, *et al.*, Local shannon entropy measure with statistical tests for image randomness, *Information Sciences* **222**, (2013).

47. M. D. Zeiler, R. Fergus, Visualizing and understanding convolutional networks, *Computer Vision–ECCV 2014: 13th European Conference, Zurich, Switzerland, September 6-12, 2014, Proceedings, Part I 13* (Springer, 2014), pp. 818–833.

48. A. Shrikumar, P. Greenside, A. Shcherbina, A. Kundaje, Not just a black box: Learning important features through propagating activation differences, *arXiv preprint arXiv:1605.01713* (2016).

49. P. Polygerinos, *et al.*, Soft robotics: Review of fluid-driven intrinsically soft devices; manufacturing, sensing, control, and applications in human-robot interaction, *Adv. Eng. Mat* **19**, (2017).

50. C. Laschi, J. Rossiter, F. Iida, M. Cianchetti, L. Margheri, *Soft Robotics: Trends, Applications and Challenges* (Springer Cham, 2017).

51. F. Vega-Bermudez, K. O. Johnson, Spatial acuity after digit amputation, *Brain* **125**, (2002).

52. Y. Yu, X. Si, C. Hu, J. Zhang, A Review of Recurrent Neural Networks: LSTM Cells and Network Architectures, *Neural Computation* **31**, (2019).

53. Ming Liang, Xiaolin Hu, Recurrent convolutional neural network for object recognition, *2015 IEEE Conference on Computer Vision and Pattern Recognition (CVPR)* (IEEE, 2015), pp. 3367–3375.

Acknowledgments

We gratefully acknowledge support by EPSRC Programme Grant 'From Sensing to Collaboration' (EP/V000748/1)

Author Contributions Oliver Shorthose and Luca Scimeca contributed equally to this work. Oliver Shorthose's contributions included the creation and implementation of the robotic hand utilised for the experiments, the ideation and implementation of the robot experiments, the generation of several figures and the co-writing of the manuscript. Luca Scimeca's contributions included the ideation and implementation of the Bayesian Framework proposed in the manuscript, the conception, implementation and training of ROSE-Net, the conception and implementation of several figures, the writing of the manuscript, and co-supervision of the project. Alessandro Albini co-supervised the project, contributed to the conception and implementation of the robot experiments, and contributed to the writing of the manuscript. Perla Maiolino was the principal project supervisor, contributing to the conception of the project, supervision of the experiments, and manuscript writing.

Figures and tables

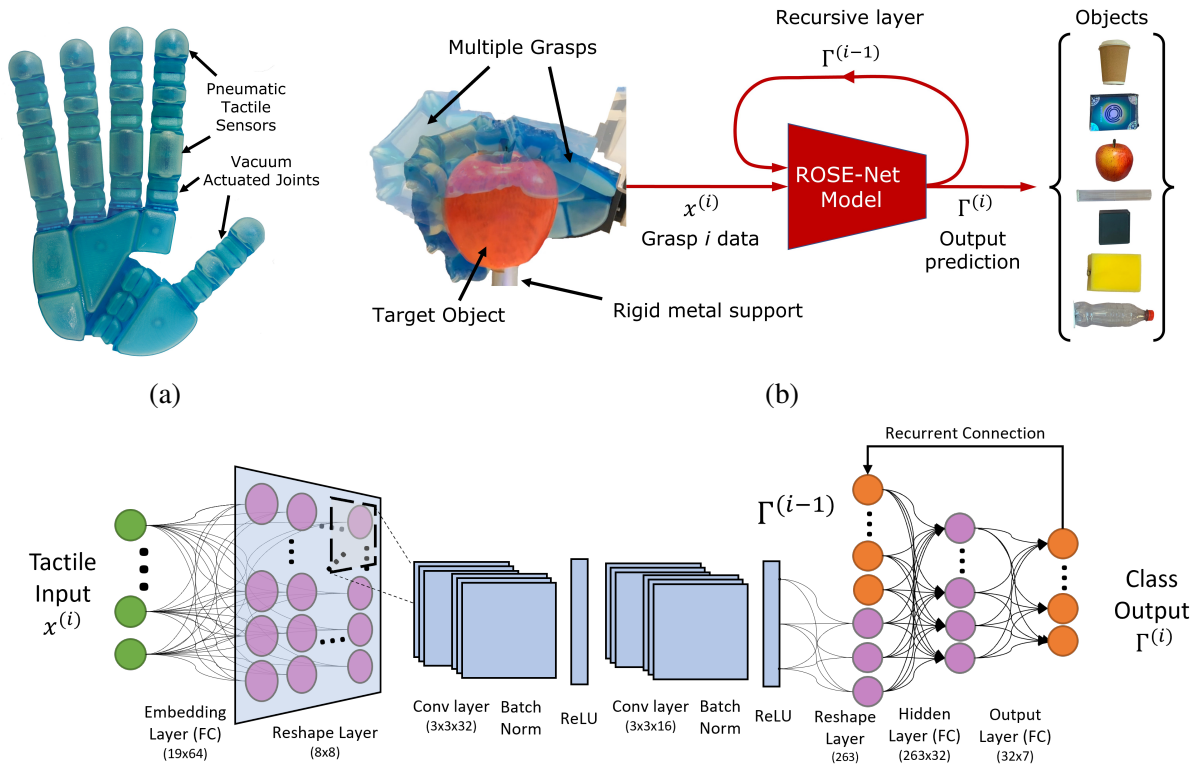

Figure 1: (a) The multi-material hand, modified from (*42*). It can be monolithically 3D-printed and contains 15 actuating chambers and 19 pneumatic tactile sensors. (c) Data acquisition experimental setup and overview of the model, leading to the classification of the objects based on tactile grasp data and prior belief distributions. (d) ROSE-Net network architecture.

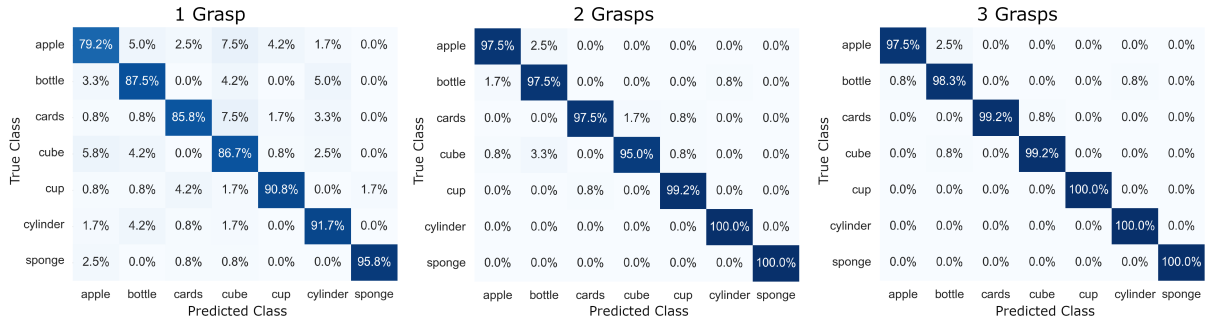

Figure 2: Confusion matrices for 1-3 grasps. The matrices for all grasps can be found in Supplementary Figure S5.

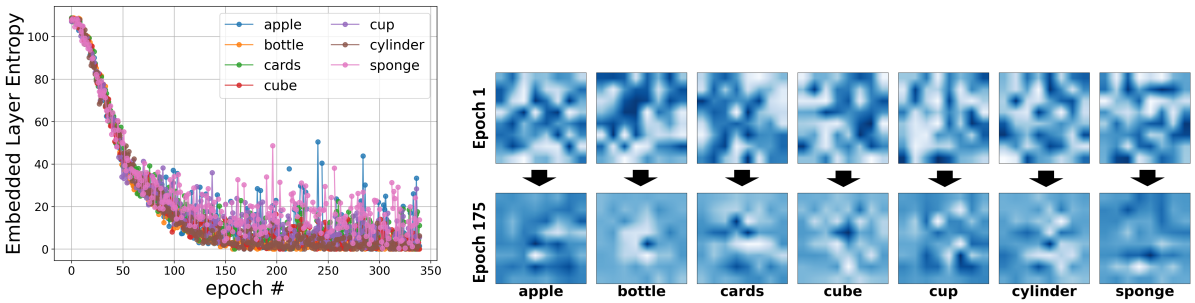

(a) (b)

Figure 3: (a) Entropy of the 2D embed layer during ROSE-Net training. (b) Excited 2D spatial embeddings for the network at first (top row) and last training epoch (bottom row).

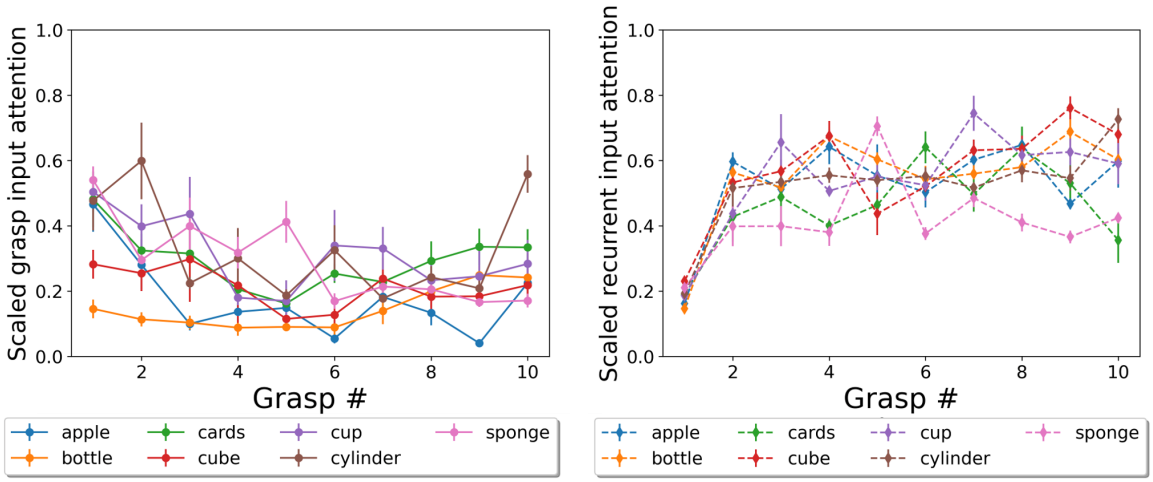

(a) (b)

Figure 4: (a) scaled cumulative saliency of the input image when performing predictions over 10 consequent grasps. (b) scaled cumulative saliency of the recurrent input when performing predictions over 10 consequent grasps.

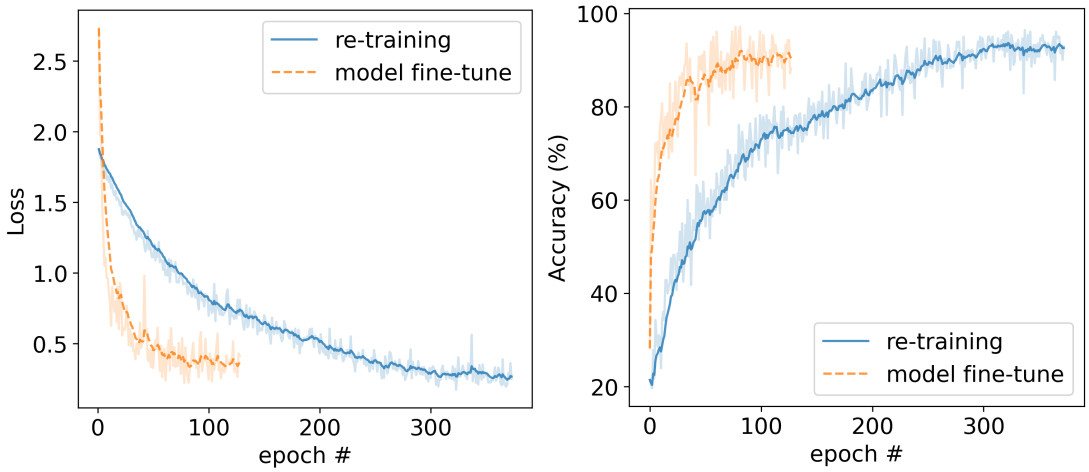

(a) (b)

Figure 5: (a) Validation loss and (b) validation accuracy of ROSE-Net when re-trained from random weights, or fine-tuned after transfer learning.

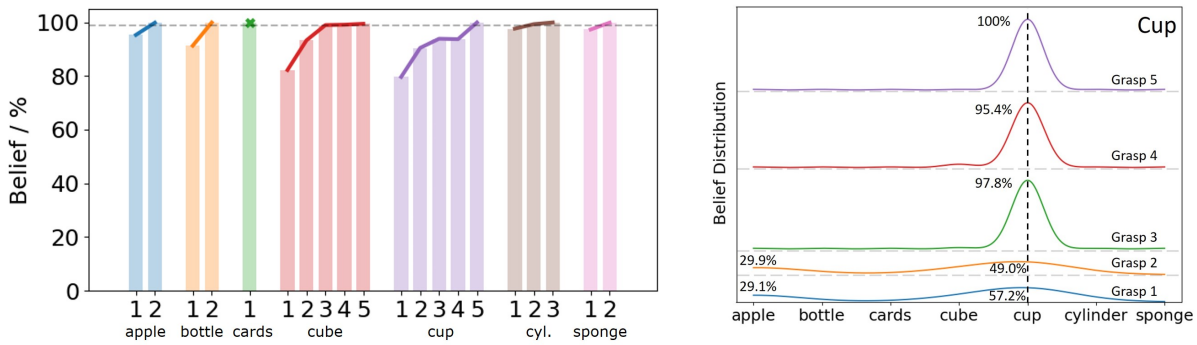

(a) (b)

Figure 6: (a) Average belief at each number of grasps for the objects. No further grasps were taken once the 99% threshold was reached. The belief was taken as the output of the *Softmax* operator. (b) Example progression of the belief distribution when classifying the cup across 5 grasps exemplifying the benefit of multi-grasp classification.

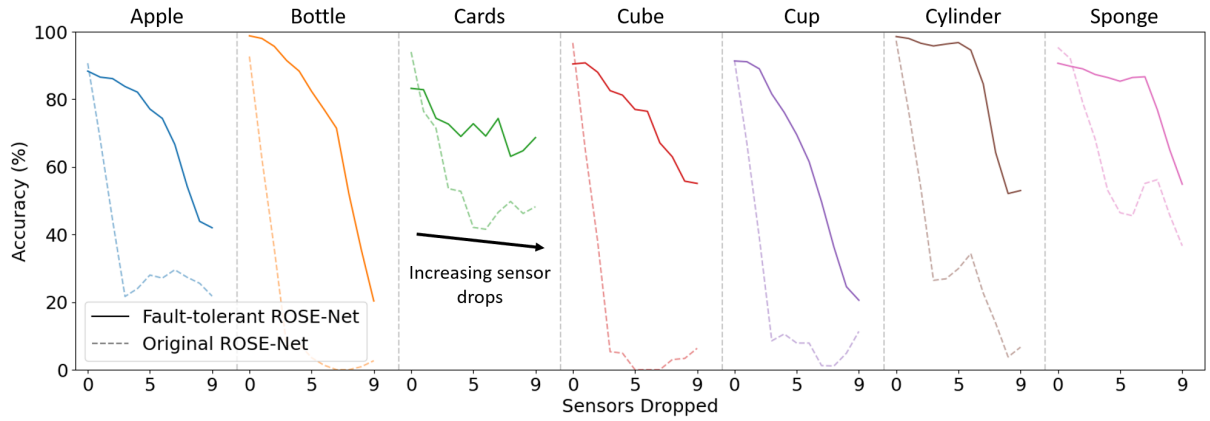

(a)

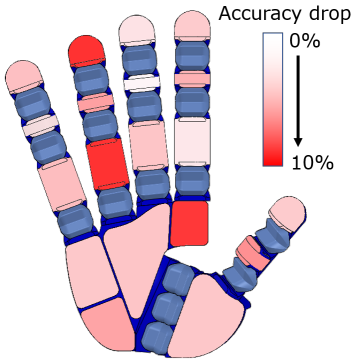

(b)

Figure 7: (a) Effect of blocking up to 9 sensors on the classification of each object. (b) Accuracy drop caused by blocking each specific sensor.

Supplementary materials

Supplementary Methods

Supplementary Results

Video M1

Supplementary Methods

Data Structure Formation

The array $\hat{X}$ is formed of the individual grasps taken from different poses on the object in question. The array has a width of M, the number of sensors, which is 19 for this particular soft robotic hand. The array height is R and ROSE-Net is designed such that R has no limit and may increase until the belief in the classification is sufficiently high.

The order of the grasps is permuted during the learning process to prevent any reliance in the model on the grasp sequence.

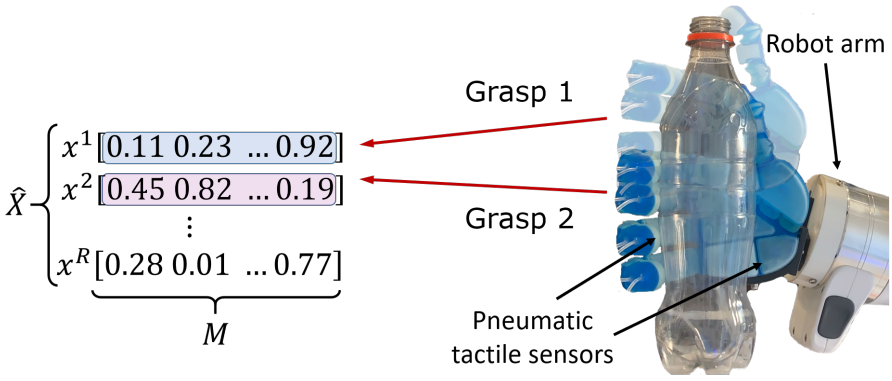

Figure 1: Structure of the sample array $\hat{X}$.

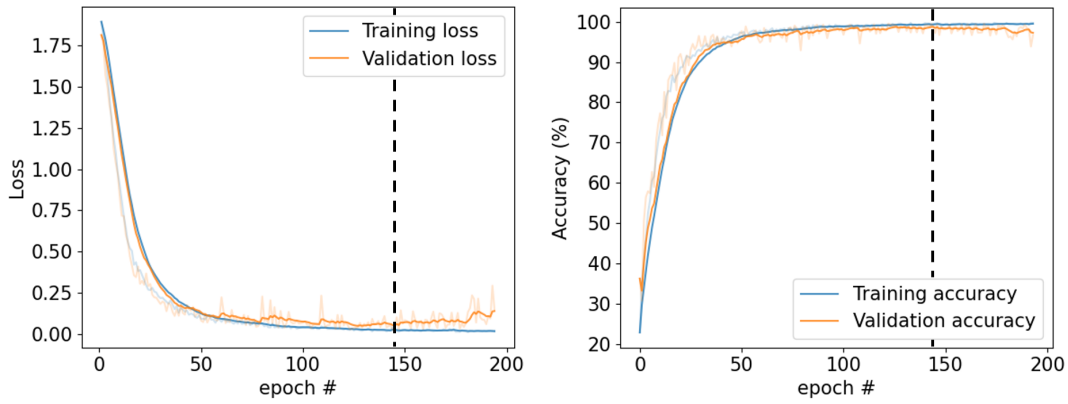

(a) (b)

Figure 2: (a) Training and validation losses for the model learning (b) Classification accuracy for the model. The dashed line indicates the epoch with the lowest validation loss.

Object Selection

The objects were chosen as small variants upon the YCB object set *(36)*.A variety of shapes, sizes and stiffness were selected to validate both the conformability of the soft hand and the ability to discriminate across a range of parameters. The results in the *Accurate Multi-Grasp Prediction* Section present mild confusion between objects based on curvature and dimension but that diminishes as the number of grasps increases. Fig. 3 shows each object with its respective dimensions. The apple was approximated to be spherical. To investigate the discrimination performance between objects with different stiffness, the sponge was also included in this set.

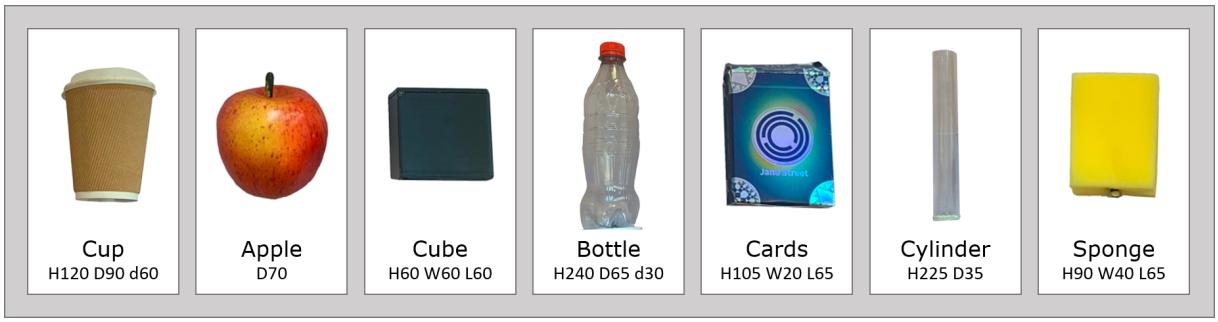

Figure 3: Objects used for the identification with corresponding dimensions in millimetres. H, height; D, largest diameter; d, smallest diameter; W, width; L, length.

Supplementary Results

Sensor Fault Training

We trained the model to be resilient to fault tolerance. To achieve this, we selectively retrain the model to randomly mask out up to N_d sensors, where with higher values of N_d we have on average a higher number of simulated sensor faults. We perform a grid search to find a viable value for N_d. Fig. 4 shows the average accuracy and loss for each number of simulated faulty sensors during the hyper-parameter search in training. From the figure, we observe a significant drop in performance by all objects after the loss of more than 3 sensors. We thus choose $N_d = 3$ for the purpose of our experiments.

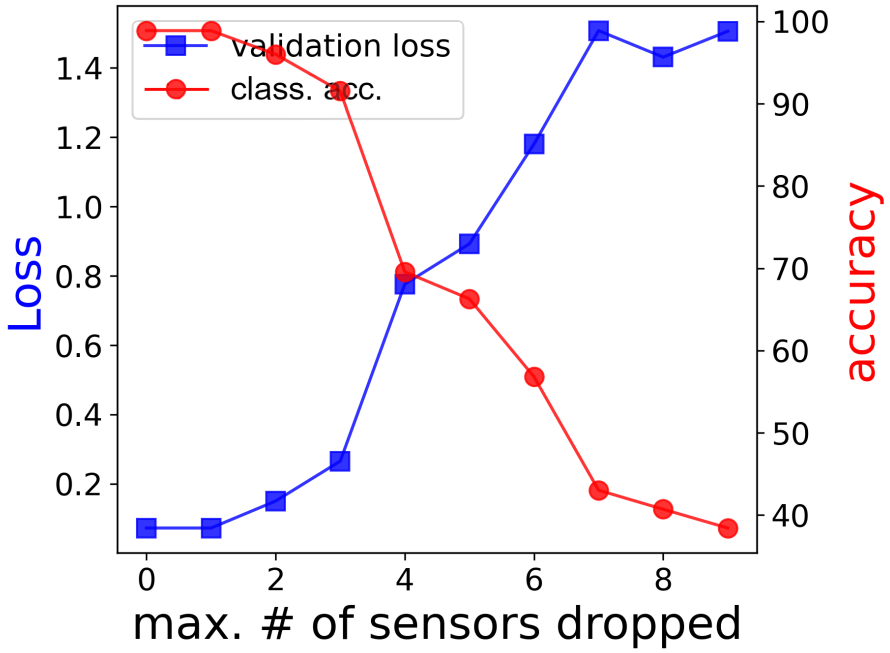

Figure 4: Hyper-parameter search to train ROSE-net for robustness to sensor faults. As increasing sensors are dropped out, the validation set classification accuracy drops whilst the loss increases.

Confusion Matrices

Confusion matrices are useful in classification analysis to portray which objects have been misclassified as each other. In Fig.2, we showed the confusion matrices for the first three grasps but here in Fig. 5 we provide the complete results for up to 10 grasps. 100% accuracy was achieved for the first time after 5 grasps, and beyond that, there is reliably $> 99\%$ accuracy.

Belief Distributions

The belief distributions are taken as the *SoftMax* output from the ROSE-Net. The distribution is fed back into the model to provide our Bayesian framework.

In the online learning scenario depicted in the *Belief-driven Data Collection and Object Classification* Section, we halt the acquisition of additional grasp data once the belief of ROSE-Net with respect to any of the object is greater than 99%. Fig. 6 shows a set of example progressions of the belief distribution as more grasps are taken. Each subfigure relates to one grasping sequence. We observe a progression variation between objects and see how the initial belief uncertainty can often be ruled out with subsequent grasps. The cube and cup are prime examples of this, where there is initial confusion with the apple but after 3 grasps, the correct classification emerges.

The final subfigure, 'Cylinder Indecision' is included to demonstrate why a high belief threshold is essential for this framework. Initially, in this grasp sequence, the belief reaches 96% for the wrong object, but we continue to take grasps until the 99% threshold is reached, which, in this instance, only occurs once the correct object has been identified.

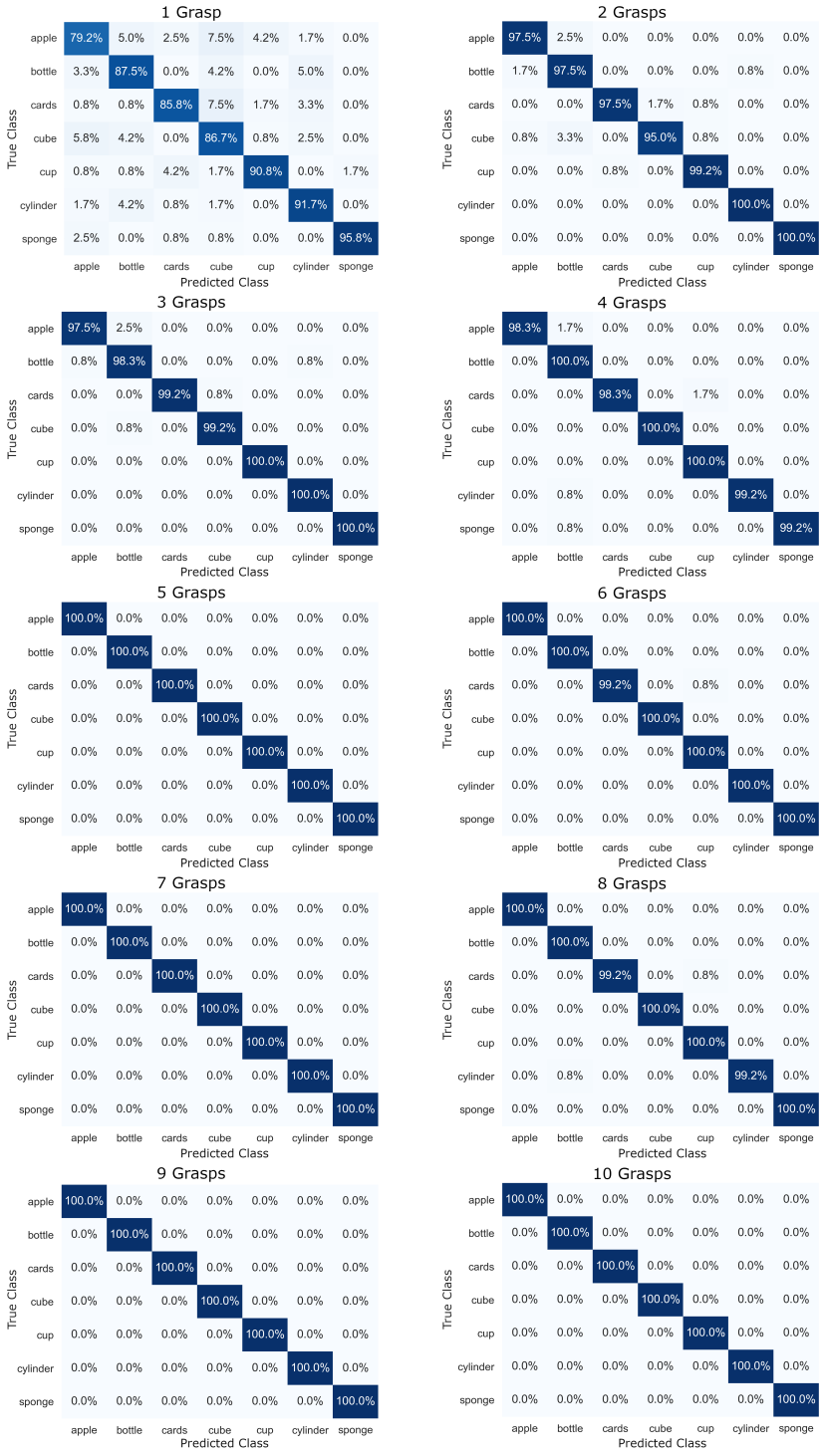

Figure 5: Confusion matrices for each number of grasp. The darker shading represents higher classification accuracy.

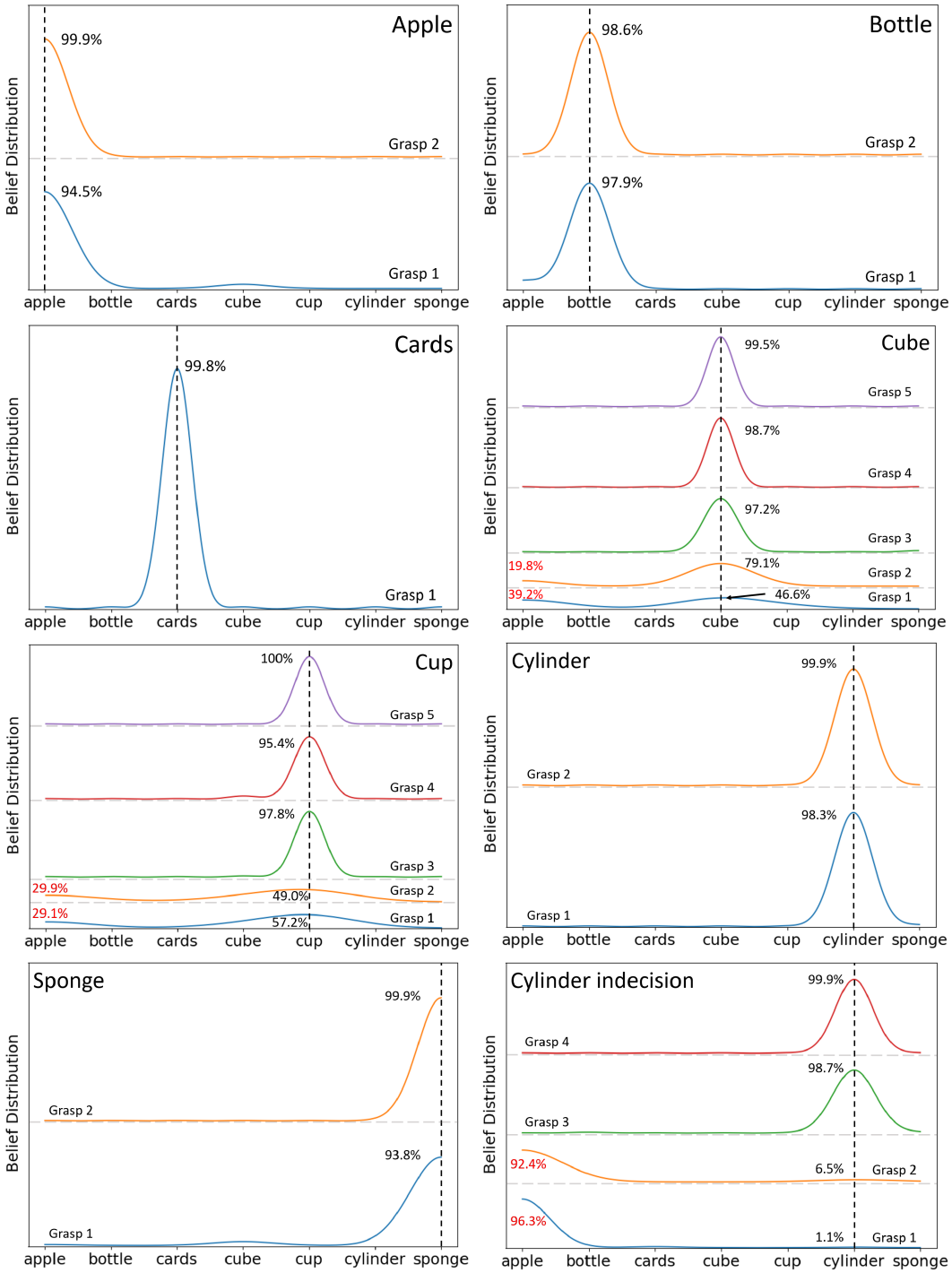

Figure 6: Selection of belief progressions for each object demonstrating: single grasp identification, indecision, and the benefit of multiple grasps to increase confidence. The black dotted line indicates the target object.

5.4 Limitations and Future Work

Bayesian Hand Guidance For the data acquisition process in the previous two chapters, the hand was guided to pre-set positions that were specifically chosen for each object to cover the entire surface area. Noise was then added to those positions to increase the robustness of the system to positional variation. From this, it can reliably be said that the dataset contains data from any pose that may be required in a grasping scenario but, when classifying that data, the pose geometry that has been used is not recorded. As a result, it is impossible to track the information gain or entropy reduction from each particular pose.

The effect of this is that grasps may be taken from regions with little distinguishing information rather than poses that distinguish strongly between objects from similar classes. For example, to distinguish between the cards and the cube, one set of faces is geometrically very similar, whereas others differ far more. If the system was to target the more easily differentiable faces, it would likely achieve a higher classification accuracy at a low number of grasps.

By extension, a framework could be set up whereby the expected information gain is calculated from each pose and, based on that, subsequent poses are targeted that are expected to provide the most information. The framework could either be based on 1-vs-all differentiation, to maximise the information gained for the predicted object against all others, or 1-vs-1, where the maximum difference between the current predicted object and the closest neighbour is targeted. Either of these would allow for a more efficient data collection process and would likely lead to a higher classification accuracy at a lower number of grasps.

Belief Volatility In some classification sequences, there is volatility in the belief output of the network as multiple grasps are taken. For example in Fig. 5.1, the network alternates from 92.4% belief in the classification of the apple to 98.7% belief in the cylinder. Whilst this example has eventually resulted in the correct classification, such volatility can lead to unpredictable or unreliable belief distribution sequences and subsequently worse performance. A potential solution to this would be to investigate using an LSTM or GRU structure to control how much of the previous memory is propagated through to the future passes. Alternatively, a bespoke solution could be formulated that weights the previous memory based on the detected volatility, or allows for initial volatility whilst there is uncertainty over the object, to begin with, but favours stabilisation over time.

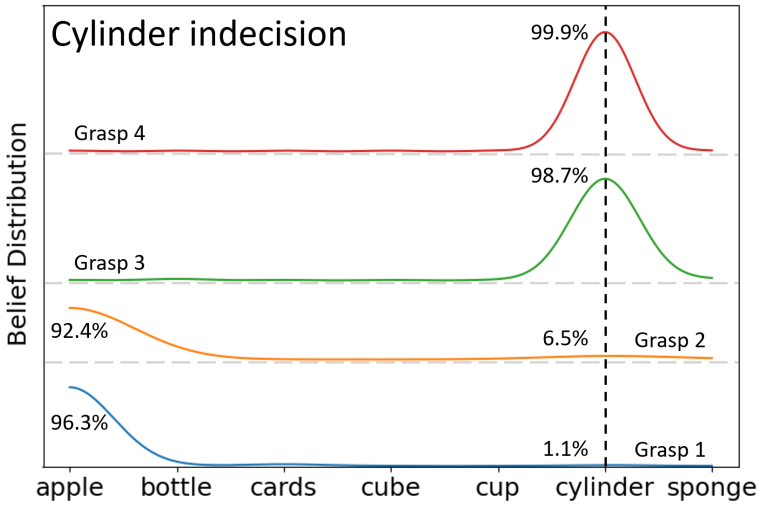

Figure 5.1: Indecision in the process of identifying a cylinder. After 1 and 2 grasps, the network classified it as an apple before converging to the correct classification afterwards.

Statement of Authorship for joint/multi-authored papers for PGR thesis

To appear at the end of each thesis chapter submitted as an article/paper.

The statement shall describe the candidate's and co-authors' independent research contributions in the thesis publications. For each publication there should exist a complete statement that is to be filled out and signed by the candidate and supervisor **(only required where there isn't already a statement of contribution within the paper itself).**

Title of Paper	Bio-inspired Tactile Object Identification Leveraging Deep-Learning and Soft Body Compliance
Publication Status	☐Published ☐ Accepted for Publication ☒ Submitted for Publication ☐ Unpublished and unsubmitted work written in a manuscript style
Publication Details	Shorthose, O., Albini, A., Scimeca, L., & Maiolino, P. (2023). Bio-inspired Tactile Object Identification Leveraging Deep-Learning and Soft Body Compliance. Submitted to *Science Advances*

Student Confirmation

Student name:	Oliver Shorthose		
Contribution to the paper:	I developed the idea for applying the hand to object identification with Alessandro Albini and Professor Maiolino I undertook the data acquisition with Alessandro Albini I contributed to the design and implementation of the ROSE-Net architecture I co-wrote the manuscript, primarily with Luca Scimeca		
Signature: 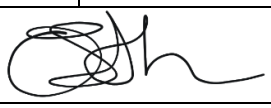		Date	19th July 2023

Supervisor Confirmation

By signing the Statement of Authorship, you are certifying that the candidate made a substantial contribution to the publication, and that the description described above is accurate.

Supervisor name and title:	Prof. Perla Maiolino		
Supervisor comments:	I confirm that the student made a substantial contribution to this publication and the contribution of the other authors is as described above		
Signature: 		Date	19/07/23

6

Conclusion

Whilst the capabilities of robots have increased remarkably in recent decades, there are still many tasks that humans undertake that robots have yet to achieve. Typically, this is because traditional robotic designs approach these tasks with complex control schemes, aiming to centrally and explicitly compute an agent's body dynamics. Soft Robotics seeks to simplify the approach towards these tasks by distributing the required computation throughout and into the agent's morphology to allow for more intuitive interactions with the environment. This use of morphological computation represents a paradigm shift in the approach to robotic design to take greater inspiration from the natural world around and to implement softness in actuation and sensing. Through this paradigm shift, roboticists are able to design agents that naturally conform to the world around them for greater adaptability in contact and shape the information that is acquired through that contact.

This thesis approaches the overall task of using Soft Robotic principles to formulate, simplify and achieve a multi-grasp object identification task. The task was broken down into two questions to be answered: Chapters 2 and 3 answer the first question of how softness can be implemented into the actuation and sensing of a robotic hand to facilitate highly adaptive grasping, allowing us to grasp a wide range of objects without requiring explicit dexterous control; chapters 4 and 5 answer the second question of how the morphological computation of that hand can be exploited to simplify a multi-grasp object identification task, whilst implementing bespoke neural networks to process data across those multiple grasps.

Chap. 2 considers the actuation and fabrication methodologies that have facilitated the rapid increase in Soft Robotics research and would be used in the subsequent hand design. Pneumatic actuation was applied to the design of a 3D-printed bi-directional actuator that features parallel symmetrical chambers. Multimaterial 3D printing was used to enable rapid and repeatable fabrication of samples, incorporating multiple material behaviours within a single body. The pneumatic actuation in the parallel chambers is used to enable variable stiffness and multiple control modes for the deployment into different scenarios depending on the desired application.

The concepts and designs explored in Chap. 2 were then applied to the design of a soft robotic hand in Chap. 3. Taking inspiration from the kinematics and DOFs of the human hand, the chapter details the design that combines the dexterity of a high number of DOFs with the adaptability provided by vacuum-actuated soft joints which was validated by the Feix taxonomy and Kapandji thumb opposition tasks. Additionally, distributed tactile sensing was used to provide contact feedback across the entire surface of the hand.

Chap. 4 leverages on the softness and adaptability of the hand to formulate a pose-invariant multi-grasp object recognition task. The compliance of the hand allowed us to grasp each object with a simple open-loop control scheme whilst conforming naturally to the respective geometries. The distributed sensing was used to acquire tactile data from

each grasp to be processed by the EDAMS model, which extracted patterns both within the grasps and between grasps. The classification accuracy increased in accordance with the number of grasps being considered, validating taking inspiration from the human approach of taking multiple contacts to identify unsighted objects.

The success of the object identification posed in Chap. 4 was extended in Chap. 5. The previously acquired data was applied to a novel architecture that targeted the strategy employed by humans to grasp and identify objects. The novel architecture allowed for open-ended data collection and processing until a satisfactory classification belief was achieved. The 2D embedding and recursive layer facilitated high accuracy classification after just a few grasps in comparison with the EDAMS architecture.

Each chapter within this thesis closes by highlighting future work either for improvement of the hand's design, or the performance of the object identification. Notably, these include: increasing the output grasping force; improving the reliability of the materials used whilst retaining the ease and repeatability of fabrication; increasing the dataset size, augmenting the dataset and exploring more objects; implementing a Bayesian framework for choosing the next grasp pose based on predicted information gain; and reducing the volatility in the belief distribution of ROSE-Net. However, whilst these potential directions have been identified, the hand designed in this thesis has shown strong performance in the overall scope of this work, which was to formulate, simplify and achieve a multi-grasp object identification task.

References

[1] Rolf Pfeifer, Fumiya Iida, and Gabriel Gomez. “Designing Intelligent Robots - On the Implications of Embodiment”. In: *Journal of the Robotics Society of Japan* 24.7 (2006), pp. 783–790. DOI: 10.7210/jrsj.24.783.

[2] Rolf Pfeifer and Josh Bongard. *How the body shapes the way we think: A new view of intelligence.* Cambridge, MA, US: Boston Review, 2007, pp. xxiv, 394–xxiv, 394.

[3] Rolf Pfeifer and Christian Scheier. “Sensory—motor coordination: The metaphor and beyond”. In: *Robotics and Autonomous Systems* 20.2-4 (June 1997), pp. 157–178. DOI: 10.1016/S0921-8890(97)80707-5.

[4] A. B. Vallbo and R. S. Johansson. “Properties of cutaneous mechanoreceptors in the human hand related to touch sensation.” In: *Human neurobiology* 3.1 (1984), pp. 3–14.

[5] Roland S. Johansson and J. Randall Flanagan. “Coding and use of tactile signals from the fingertips in object manipulation tasks”. In: *Nature Reviews Neuroscience* 10.5 (May 2009), pp. 345–359. DOI: 10.1038/nrn2621.

[6] Thomas Feix, Ian M. Bullock, and Aaron M. Dollar. “Analysis of Human Grasping Behavior: Object Characteristics and Grasp Type”. In: *IEEE Transactions on Haptics* 7.3 (2014), pp. 311–323. DOI: 10.1109/TOH.2014.2326871.

[7] Thomas Feix, Ian M. Bullock, and Aaron M. Dollar. “Analysis of Human Grasping Behavior: Correlating Tasks, Objects and Grasps”. In: *IEEE Transactions on Haptics* 7.4 (Oct. 2014), pp. 430–441. DOI: 10.1109/TOH.2014.2326867.

[8] T.E. Milner and D.W. Franklin. “Characterization of multijoint finger stiffness: dependence on finger posture and force direction”. In: *IEEE Transactions on Biomedical Engineering* 45.11 (1998), pp. 1363–1375. DOI: 10.1109/10.725333.

[9] Lynette A Jones and Susan J Lederman. *Human hand function*. Oxford university press, 2006.

[10] Pramodsingh H. Thakur, Amy J. Bastian, and Steven S. Hsiao. “Multidigit Movement Synergies of the Human Hand in an Unconstrained Haptic Exploration Task”. In: *The Journal of Neuroscience* 28.6 (Feb. 2008), pp. 1271–1281. DOI: 10.1523/JNEUROSCI.4512-07.2008.

[11] Néstor J. Jarque-Bou et al. “Kinematic synergies of hand grasps: a comprehensive study on a large publicly available dataset”. In: *Journal of NeuroEngineering and Rehabilitation* 16.1 (Dec. 2019), p. 63. DOI: 10.1186/s12984-019-0536-6.

[12] Rolf Pfeifer, Max Lungarella, and Fumiya Iida. “Self-Organization, Embodiment, and Biologically Inspired Robotics”. In: *Science* 318.5853 (Nov. 2007), pp. 1088–1093. DOI: 10.1126/science.1145803.

[13] S. J. Lederman and R. L. Klatzky. “Haptic perception: A tutorial”. In: *Attention, Perception & Psychophysics* 71.7 (Oct. 2009), pp. 1439–1459. DOI: 10.3758/APP.71.7.1439.

[14] Roberta L. Klatzky, Susan J. Lederman, and Victoria A. Metzger. “Identifying objects by touch: An “expert system””. In: *Perception & Psychophysics* 37.4 (July 1985), pp. 299–302. DOI: 10.3758/BF03211351.

[15] Susan J. Lederman and Roberta L. Klatzky. “Hand movements: A window into haptic object recognition”. In: *Cognitive Psychology* 19.3 (July 1987), pp. 342–368. DOI: 10.1016/0010-0285(87)90008-9.

[16] Roland S Johansson and Kelly J. Cole. “Sensory-motor coordination during grasping and manipulative actions”. In: *Current Opinion in Neurobiology* 2.6 (Dec. 1992), pp. 815–823. DOI: 10.1016/0959-4388(92)90139-C.

[17] Mohamad Bdiwi, Marko Pfeifer, and Andreas Sterzing. “A new strategy for ensuring human safety during various levels of interaction with industrial robots”. In: *CIRP Annals* 66.1 (2017), pp. 453–456. DOI: 10.1016/j.cirp.2017.04.009.

[18] M Bonilla et al. “Grasping with Soft Hands”. In: *IEEE-RAS International Conference on Humanoid Robots*. IEEE, 2014, pp. 581–587. DOI: 10.1109/HUMANOIDS.2014.7041421.

[19] Erika Nathalia Gama Melo, Oscar Fernando Avilés Sánchez, and Darío Amaya Hurtado. “Anthropomorphic robotic hands: a review”. In: *ingeniería y desarrollo* 32.2 (June 2014), pp. 279–313. DOI: 10.14482/inde.32.2.4715.

[20] Qaid Mohammed Marwan, Shing Chyi Chua, and Lee Chung Kwek. “Comprehensive Review on Reaching and Grasping of Objects in Robotics”. In: *Robotica* 39.10 (Oct. 2021), pp. 1849–1882. DOI: 10.1017/S0263574721000023.

[21] Chao Wang et al. “Feature Sensing and Robotic Grasping of Objects with Uncertain Information: A Review”. In: *Sensors* 20.13 (July 2020), p. 3707. DOI: 10.3390/s20133707.

[22] Ryuta Ozawa and Kenji Tahara. “Grasp and dexterous manipulation of multi-fingered robotic hands: a review from a control view point”. In: *Advanced Robotics* 31.19-20 (Oct. 2017), pp. 1030–1050. DOI: 10.1080/01691864.2017.1365011.

[23] Zhanat Kappassov, Juan Antonio Corrales, and Véronique Perdereau. “Tactile sensing in dexterous robot hands - Review”. In: *Robotics and Autonomous Systems* 74 (2015), pp. 195–220. DOI: 10.1016/j.robot.2015.07.015.

[24] Shan Luo et al. “Robotic tactile perception of object properties: A review”. In: *Mechatronics* 48.August (2017), pp. 54–67. DOI: 10.1016/j.mechatronics.2017.11.002. eprint: 1711.03810.

[25] Ebrahim Mattar. “A survey of bio-inspired robotics hands implementation: New directions in dexterous manipulation”. In: *Robotics and Autonomous Systems* 61.5 (May 2013), pp. 517–544. DOI: 10.1016/j.robot.2012.12.005.

[26] Huaping Liu et al. “Recent progress on tactile object recognition”. In: *International Journal of Advanced Robotic Systems* 14.4 (July 2017). DOI: 10.1177/1729881417717056.

[27] C Piazza et al. “A Century of Robotic Hands”. In: *Robotics, and Autonomous Systems Annu. Rev. Control Robot. Auton. Syst. 2019* 22 (2019), pp. 1–32. DOI: 10.1146/annurev-control-060117.

[28] Matej Hoffmann and Rolf Pfeifer. “The implications of embodiment for behavior and cognition: animal and robotic case studies”. In: (Feb. 2012), pp. 31–58. arXiv: 1202.0440.

[29] Sangbae Kim, Cecilia Laschi, and Barry Trimmer. “Soft robotics: a bioinspired evolution in robotics”. In: *Trends in Biotechnology* 31.5 (May 2013), pp. 287–294. DOI: 10.1016/j.tibtech.2013.03.002.

[30] Falk Tauber et al. “Perspective for soft robotics: the field’s past and future”. In: *Bioinspiration & Biomimetics* 18.3 (May 2023). DOI: 10.1088/1748-3190/acbb48.

[31] Josie Hughes et al. “Online Morphological Adaptation for Tactile Sensing Augmentation”. In: *Frontiers in Robotics and AI* 8 (July 2021), pp. 1–13. DOI: 10.3389/frobt.2021.665030.

[32] Kieran Gilday, Josie Hughes, and Fumiya Iida. “Sensing, Actuating, and Interacting Through Passive Body Dynamics: A Framework for Soft Robotic Hand Design”. In: *Soft Robotics* 00.00 (June 2022), pp. 1–15. DOI: 10.1089/soro.2021.0077.

[33] Angelo Cangelosi et al. “Embodied Intelligence”. In: *Springer Handbook of Computational Intelligence*. Berlin, Heidelberg: Springer Berlin Heidelberg, 2015, pp. 697–714. DOI: 10.1007/978-3-662-43505-2_37.

[34] Cecilia Laschi. “Embodied Intelligence in soft robotics: joys and sorrows”. In: *IOP Conference Series: Materials Science and Engineering* 1261.1 (Oct. 2022), p. 012002. DOI: 10.1088/1757-899X/1261/1/012002.

[35] Matteo Cianchetti et al. “Biomedical applications of soft robotics”. In: *Nature Reviews Materials* 3.6 (May 2018), pp. 143–153. DOI: 10.1038/s41578-018-0022-y.

[36] Haider Abidi and Matteo Cianchetti. “On Intrinsic Safety of Soft Robots”. In: *Frontiers in Robotics and AI* 4.2 (Feb. 2017), pp. 1–6. DOI: 10.3389/frobt.2017.00005.

[37] Josie Hughes et al. *Soft manipulators and grippers: A review*. Nov. 2016. DOI: 10.3389/frobt.2016.00069.

[38] Jun Shintake et al. *Soft Robotic Grippers*. July 2018. DOI: 10.1002/adma.201707035.

[39] Tetsuyou Watanabe, Kimitoshi Yamazaki, and Yasuyoshi Yokokohji. “Survey of robotic manipulation studies intending practical applications in real environments -object recognition, soft robot hand, and challenge program and benchmarking-”. In: *Advanced Robotics* 31.19-20 (Oct. 2017), pp. 1114–1132. DOI: 10.1080/01691864.2017.1365010.

[40] Clark B Teeple et al. “Multi-segment soft robotic fingers enable robust precision grasping”. In: *The International Journal of Robotics Research* 39.14 (Dec. 2020), pp. 1647–1667. DOI: 10.1177/0278364920910465.

[41] Hongbo Wang, Massimo Totaro, and Lucia Beccai. “Toward Perceptive Soft Robots: Progress and Challenges”. In: *Advanced Science* 5.9 (Sept. 2018), p. 1800541. DOI: 10.1002/advs.201800541.

[42] P. M. Khin et al. “Development and Grasp Stability Estimation of Sensorized Soft Robotic Hand”. In: *Frontiers in Robotics and AI* 8 (Mar. 2021). DOI: 10.3389/frobt.2021.619390.

[43] Gereon Buscher et al. “Augmenting curved robot surfaces with soft tactile skin”. In: *IEEE International Conference on Intelligent Robots and Systems* 2015-Decem (2015), pp. 1514–1519. DOI: 10.1109/IROS.2015.7353568.

[44] Juan M. Gandarias, Jesús M. Gómez-de-Gabriel, and Alfonso J. García-Cerezo. “Enhancing Perception with Tactile Object Recognition in Adaptive Grippers for Human–Robot Interaction”. In: *Sensors* 18.3 (2018). DOI: 10.3390/s18030692.

[45] Phone May Khin et al. “In-Hand Object Recognition for Sensorized Soft Hand”. In: *International Conference on Intelligent Autonomous Systems*. Vol. 412. Springer International Publishing, 2022, pp. 351–364. DOI: 10.1007/978-3-030-95892-3.

[46] Tetsushi Nonaka et al. “Soft robotic tactile perception of softer objects based on learning of spatiotemporal pressure patterns”. In: *2023 IEEE International Conference on Soft Robotics (RoboSoft)*. IEEE, Apr. 2023, pp. 1–7. DOI: 10.1109/RoboSoft55895.2023.10121950.

[47] Marsela Polic et al. “Convolutional Autoencoder for Feature Extraction in Tactile Sensing”. In: *IEEE Robotics and Automation Letters* 4.4 (Oct. 2019), pp. 3671–3678. DOI: 10.1109/LRA.2019.2927950.

[48] Luca Scimeca, Perla Maiolino, and Fumiya Iida. “Soft morphological processing of tactile stimuli for autonomous category formation”. In: *2018 IEEE International Conference on Soft Robotics (RoboSoft)*. IEEE, Apr. 2018, pp. 356–361. DOI: 10.1109/ROBOSOFT.2018.8404945.

[49] Alexander Schneider et al. “Object identification with tactile sensors using bag-of-features”. In: *2009 IEEE/RSJ International Conference on Intelligent Robots and Systems*. 2009, pp. 243–248. DOI: 10.1109/IROS.2009.5354648.

[50] Tessa J. Pannen, Steffen Puhlmann, and Oliver Brock. “A Low-Cost, Easy to Manufacture, Flexible, Multi-Taxel Tactile Sensor and its Application to In-Hand Object Recognition”. In: *2022 International Conference on Robotics and Automation (ICRA)*. IEEE, May 2022, pp. 10939–10944. DOI: 10.1109/ICRA46639.2022.9811761.

[51] Alexander Schmitz et al. “Tactile object recognition using deep learning and dropout”. In: *2014 IEEE-RAS International Conference on Humanoid Robots*. Vol. 2015-Feb. IEEE, Nov. 2014, pp. 1044–1050. DOI: 10.1109/HUMANOIDS.2014.7041493.

[52] Narendra Gariya and Pushpendra Kumar. “A review on soft materials utilized for the manufacturing of soft robots”. In: *Materials Today: Proceedings* 46 (2021), pp. 11177–11181. DOI: 10.1016/j.matpr.2021.02.380.

[53] Philipp Rothemund et al. “Shaping the future of robotics through materials innovation”. In: *Nature Materials* 20.12 (Dec. 2021), pp. 1582–1587. DOI: 10.1038/s41563-021-01158-1.

[54] Shadab Zaidi et al. “Actuation Technologies for Soft Robot Grippers and Manipulators: A Review”. In: *Current Robotics Reports* 2.3 (Sept. 2021), pp. 355–369. DOI: 10.1007/s43154-021-00054-5.

[55] Jahan Zeb Gul et al. “3D printing for soft robotics – a review”. In: *Science and Technology of Advanced Materials* 19.1 (Dec. 2018), pp. 243–262. DOI: 10.1080/14686996.2018.1431862.

[56] Gabriel Dammer et al. “Design and shape optimization of PolyJet bellows actuators”. In: *2018 IEEE International Conference on Soft Robotics (RoboSoft)*. IEEE, Apr. 2018, pp. 282–287. DOI: 10.1109/ROBOSOFT.2018.8404933.

[57] Alessandro Carfì et al. “Hand-Object Interaction: From Human Demonstrations to Robot Manipulation”. In: *Frontiers in Robotics and AI* 8.October (Oct. 2021), pp. 1–7. DOI: 10.3389/frobt.2021.714023.

[58] M. J. Barakat, J. Field, and J. Taylor. “The range of movement of the thumb”. In: *Hand* 8.2 (2013), pp. 179–182. DOI: 10.1007/s11552-013-9492-y.

[59] James N. Ingram et al. “The statistics of natural hand movements”. In: *Experimental Brain Research* 188.2 (June 2008), pp. 223–236. DOI: 10.1007/s00221-008-1355-3.

[60] A. Kapandji. “Clinical opposition and reposition test of the thumb”. In: *Annales de Chirurgie de la Main* 5.1 (1986), pp. 67–73. DOI: 10.1016/S0753-9053(86)80053-9.

[61] Giuseppe Cotugno, Kaspar Althoefer, and Thrishantha Nanayakkara. “The Role of the Thumb: Study of Finger Motion in Grasping and Reachability Space in Human and Robotic Hands”. In: *IEEE Transactions on Systems, Man, and Cybernetics: Systems* 47.7 (July 2017), pp. 1061–1070. DOI: 10.1109/TSMC.2016.2531679.

[62] Subramanian Sundaram et al. “Learning the signatures of the human grasp using a scalable tactile glove”. In: *Nature* 569.7758 (May 2019), pp. 698–702. DOI: 10.1038/s41586-019-1234-z.

[63] Benjamin Shih et al. “Electronic skins and machine learning for intelligent soft robots”. In: *Science Robotics* 5.41 (Apr. 2020). DOI: 10.1126/scirobotics.aaz9239.

[64] Jingyi Huang and Andre Rosendo. “Variable Stiffness Object Recognition with a CNN-Bayes Classifier on a Soft Gripper”. In: *Soft Robotics* 00.00 (Mar. 2022), pp. 1–12. DOI: 10.1089/soro.2021.0105.

[65] Qiang Bai et al. “Object Detection Recognition and Robot Grasping Based on Machine Learning: A Survey”. In: *IEEE Access* 8 (2020), pp. 181855–181879. DOI: 10.1109/ACCESS.2020.3028740.

[66] Farhad Mortezapour Shiri et al. “A Comprehensive Overview and Comparative Analysis on Deep Learning Models: CNN, RNN, LSTM, GRU”. In: (May 2023). arXiv: 2305.17473.

[67] Tadeo Corradi, Peter Hall, and Pejman Iravani. “Bayesian tactile object recognition: Learning and recognising objects using a new inexpensive tactile sensor”. In: *2015 IEEE International Conference on Robotics and Automation (ICRA)*. 2015-june. IEEE, May 2015, pp. 3909–3914. DOI: 10.1109/ICRA.2015.7139744.

[68] Francisco Pastor et al. “Bayesian and Neural Inference on LSTM-Based Object Recognition From Tactile and Kinesthetic Information”. In: *IEEE Robotics and Automation Letters* 6.1 (Jan. 2021), pp. 231–238. DOI: 10.1109/LRA.2020.3038377.

[69] Yu Han Liu. "Feature Extraction and Image Recognition with Convolutional Neural Networks". In: *Journal of Physics: Conference Series* 1087.6 (2018). DOI: 10.1088/1742-6596/1087/6/062032.

[70] Courtney J. Spoerer, Patrick McClure, and Nikolaus Kriegeskorte. "Recurrent convolutional neural networks: A better model of biological object recognition". In: *Frontiers in Psychology* 8.9 (2017), pp. 1–14. DOI: 10.3389/fpsyg.2017.01551.

[71] Matthew D Zeiler and Rob Fergus. "Visualizing and understanding convolutional networks". In: *Computer Vision–ECCV 2014: 13th European Conference, Zurich, Switzerland, September 6-12, 2014, Proceedings, Part I 13*. Springer. 2014, pp. 818–833.

[72] Nazek El-Atab et al. "Soft Actuators for Soft Robotic Applications: A Review". In: *Advanced Intelligent Systems* 2.10 (Oct. 2020), p. 2000128. DOI: 10.1002/aisy.202000128.

[73] Ang Chen et al. "Soft robotics: Definition and research issues". In: *2017 24th International Conference on Mechatronics and Machine Vision in Practice (M2VIP)*. 2017, pp. 366–370. DOI: 10.1109/M2VIP.2017.8267170.

[74] Nikolas Kastor et al. "A Definition of Soft Materials for Use in the Design of Robots". In: *Soft Robotics* 4.3 (Sept. 2017), pp. 181–182. DOI: 10.1089/soro.2017.29012.nka.

[75] Liyu Wang and Fumiya Iida. "Deformation in Soft-Matter Robotics: A Categorization and Quantitative Characterization". In: *IEEE Robotics & Automation Magazine* 22.3 (2015), pp. 125–139. DOI: 10.1109/MRA.2015.2448277.

[76] Nafiseh Ebrahimi et al. “Magnetic Actuation Methods in Bio/Soft Robotics”. In: *Advanced Functional Materials* 31.11 (Mar. 2021), p. 2005137. DOI: 10.1002/adfm.202005137.

[77] Tiantian Xu et al. “Magnetic actuation based motion control for microrobots: An overview”. In: *Micromachines* 6.9 (2015), pp. 1346–1364. DOI: 10.3390/mi6091346.

[78] Yoonho Kim and Xuanhe Zhao. “Magnetic Soft Materials and Robots”. In: *Chemical Reviews* 122.5 (Mar. 2022), pp. 5317–5364. DOI: 10.1021/acs.chemrev.1c00481.

[79] Feifei Chen et al. “Topology Optimized Design, Fabrication, and Characterization of a Soft Cable-Driven Gripper”. In: *IEEE Robotics and Automation Letters* 3.3 (2018), pp. 2463–2470. DOI: 10.1109/LRA.2018.2800115.

[80] N. Vasudha and K. Uma Rao. “Shape memory alloy properties, modelling aspects and potential applications - a review”. In: *Journal of Physics: Conference Series* 1706.1 (Dec. 2020). DOI: 10.1088/1742-6596/1706/1/012190.

[81] Asaf Dana, Shahaf Vollach, and Doron Shilo. “Use the Force: Review of High-Rate Actuation of Shape Memory Alloys”. In: *Actuators* 10.7 (June 2021), p. 140. DOI: 10.3390/act10070140.

[82] Nasim Sabahi et al. “A Review on Additive Manufacturing of Shape-Memory Materials for Biomedical Applications”. In: *ADVANCED MANUFACTURING FOR BIOMATERIALS AND BIOLOGICAL MATERIALS* 72.3 (Mar. 2020), pp. 1229–1253. DOI: 10.1007/s11837-020-04013-x.

[83] Jaronie Mohd Jani et al. “A review of shape memory alloy research, applications and opportunities”. In: *Materials & Design (1980-2015)* 56 (2014), pp. 1078–1113. DOI: 10.1016/j.matdes.2013.11.084.

[84] Paolo Ariano et al. “Polymeric Materials as Artificial Muscles: An Overview”. In: *Journal of Applied Biomaterials & Functional Materials* 13.1 (Jan. 2015), pp. 1–9. DOI: 10.5301/jabfm.5000184.

[85] Guoying Gu et al. “Editorial: Soft Robotics Based on Electroactive Polymers”. In: *Frontiers in Robotics and AI* 8.6 (Apr. 2021), pp. 822–827. DOI: 10.3389/frobt.2021.676406.

[86] Iain A. Anderson et al. “Multi-functional dielectric elastomer artificial muscles for soft and smart machines”. In: *Journal of Applied Physics* 112.4 (Aug. 2012), p. 041101. DOI: 10.1063/1.4740023.

[87] Yoseph Bar-Cohen. “Electroactive Polymers as Artificial Muscles: Capabilities, Potentials and Challenges”. In: *Robotics 2000*. Vol. 299. Reston, VA: American Society of Civil Engineers, Feb. 2000, pp. 188–196. DOI: 10.1061/40476(299)24.

[88] Bobak Mosadegh et al. “Pneumatic Networks for Soft Robotics that Actuate Rapidly”. In: *Advanced Functional Materials* 24.15 (Apr. 2014), pp. 2163–2170. DOI: 10.1002/adfm.201303288.

[89] Andrew D. Marchese, Robert K. Katzschmann, and Daniela Rus. “A recipe for soft fluidic elastomer robots”. In: *Soft Robotics* 2.1 (Mar. 2015), pp. 7–25. DOI: 10.1089/soro.2014.0022.

[90] Amir Pagoli et al. “Review of soft fluidic actuators: classification and materials modeling analysis”. In: *Smart Materials and Structures* 31.1 (Jan. 2022), p. 013001. DOI: 10.1088/1361-665X/ac383a.

[91] Panagiotis Polygerinos et al. “Soft Robotics: Review of Fluid-Driven Intrinsically Soft Devices; Manufacturing, Sensing, Control, and Applications in Human-Robot

Interaction". In: *Advanced Engineering Materials* 19.12 (2017), p. 1700016. DOI: 10.1002/adem.201700016.

[92] James Walker et al. "Soft Robotics: A Review of Recent Developments of Pneumatic Soft Actuators". In: *Actuators* 9.1 (Jan. 2020), p. 3. DOI: 10.3390/act9010003.

[93] Haili Li et al. "High-force soft pneumatic actuators based on novel casting method for robotic applications". In: *Sensors and Actuators A: Physical* 306 (May 2020), p. 111957. DOI: 10.1016/j.sna.2020.111957.

[94] R. Adam Bilodeau, Edward L. White, and Rebecca K. Kramer. "Monolithic fabrication of sensors and actuators in a soft robotic gripper". In: *2015 IEEE/RSJ International Conference on Intelligent Robots and Systems (IROS)*. Vol. 2015-Decem. IEEE, Sept. 2015, pp. 2324–2329. DOI: 10.1109/IROS.2015.7353690.

[95] Chil-Chyuan Kuo and Yi-Ruei Chen. "Rapid optical inspection of bubbles in the silicone rubber". In: *Optik* 124.13 (July 2013), pp. 1480–1485. DOI: 10.1016/j.ijleo.2012.04.010.

[96] Osman Dogan Yirmibesoglu et al. "Direct 3D printing of silicone elastomer soft robots and their performance comparison with molded counterparts". In: *2018 IEEE International Conference on Soft Robotics, RoboSoft 2018*. Institute of Electrical and Electronics Engineers Inc., July 2018, pp. 295–302. DOI: 10.1109/ROBOSOFT.2018.8404935.

[97] Scott Crump. *APPARATUS AND METHOD FOR CREATING THREE- DIMENSIONAL OBJECTS*. 1992.

[98] Xin Wang et al. "3D printing of polymer matrix composites: A review and prospective". In: *Composites Part B: Engineering* 110 (2017), pp. 442–458. DOI: 10.1016/j.compositesb.2016.11.034.

[99] Ela Sachyani Keneth et al. “3D Printing Materials for Soft Robotics”. In: *Advanced Materials* 33.19 (May 2021), p. 2003387. DOI: 10.1002/adma.202003387.

[100] Benjamin Ang Wee Keong and Raye Yeow Chen Hua. “A Novel Fold-Based Design Approach toward Printable Soft Robotics Using Flexible 3D Printing Materials”. In: *Advanced Materials Technologies* 3.2 (Feb. 2018), p. 1700172. DOI: 10.1002/admt.201700172.

[101] Hong Kai Yap, Hui Yong Ng, and Chen Hua Yeow. “High-Force Soft Printable Pneumatics for Soft Robotic Applications”. In: *Soft Robotics* 3.3 (Sept. 2016), pp. 144–158. DOI: 10.1089/soro.2016.0030.

[102] Kumaresan Rajan et al. *Fused deposition modeling: process, materials, parameters, properties, and applications*. Vol. 120. 3-4. Springer London, 2022, pp. 1531–1570. DOI: 10.1007/s00170-022-08860-7.

[103] Fred Fischer. “FDM and Polyjet 3D Printing”. In: *Stratasys* (2014), p. 7. URL: https://designs.pixweaver.com/file_uploads/FDM%20and%20Polyjet.pdf.

[104] Antonia Georgopoulou et al. “A Sensorized Soft Pneumatic Actuator Fabricated with Extrusion-Based Additive Manufacturing”. In: *Actuators* 10.5 (May 2021), p. 102. DOI: 10.3390/act10050102.

[105] Bryan N. Peele et al. “3D printing antagonistic systems of artificial muscle using projection stereolithography”. In: *Bioinspiration and Biomimetics* 10.5 (Sept. 2015), p. 055003. DOI: 10.1088/1748-3190/10/5/055003.

[106] Parth Patpatiya et al. “A review on polyjet 3D printing of polymers and multi-material structures”. In: *Proceedings of the Institution of Mechanical Engineers, Part C: Journal of Mechanical Engineering Science* 236.14 (July 2022), pp. 7899–7926. DOI: 10.1177/09544062221079506.

[107] Jochen Mueller et al. “Mechanical Properties of Interfaces in Inkjet 3D Printed Single- and Multi-Material Parts”. In: *3D Printing and Additive Manufacturing* 4.4 (Dec. 2017), pp. 193–199. DOI: 10.1089/3dp.2017.0038.

[108] Aitor Cazón, Paz Morer, and Luis Matey. “PolyJet technology for product prototyping: Tensile strength and surface roughness properties”. In: *Proceedings of the Institution of Mechanical Engineers, Part B: Journal of Engineering Manufacture* 228.12 (Dec. 2014), pp. 1664–1675. DOI: 10.1177/0954405413518515.

[109] Stratasys Ltd. “Digital Materials - Polyjet technology material specifications”. In: (2013), pp. 1–5. URL: https://www.stratasys.com/-/media/files/material-spec-sheets/mss_pj_digitalmaterialsdatasheet_0617a.pdf.

[110] Stratasys Ltd. “Agilus 30 - Poly jet material specifications”. In: (2021), p. 1. URL: https://www.stratasys.com/globalassets/materials/materials-catalog/polyjet-materials/agilus30/mds_pj_agilus30_0121b.pdf.

[111] Stratasys Ltd. “VeroWhitePlus - Polyjet technology material specifications”. In: (2015), p. 1. URL: https://www.stratasys.com/siteassets/sdm/materials/resins/vero/polyjet_verowhiteplus_material_specifications.pdf.

[112] A. Kesy and J. Kotlinski. “Mechanical properties of parts produced by using polymer jetting technology”. In: *Archives of Civil and Mechanical Engineering* 10.3 (Jan. 2010), pp. 37–50. DOI: 10.1016/S1644-9665(12)60135-6.

[113] Fady F. Abayazid and Mazdak Ghajari. “Material characterisation of additively manufactured elastomers at different strain rates and build orientations”. In: *Additive Manufacturing* 33 (May 2020). DOI: 10.1016/j.addma.2020.101160.

[114] Lindsey Bass, Nicholas Alexander Meisel, and Christopher B. Williams. “Exploring variability of orientation and aging effects in material properties of multi-material

jetting parts". In: *Rapid Prototyping Journal* 22.5 (Aug. 2016), pp. 826–834. DOI: 10.1108/RPJ-11-2015-0169.

[115] P. Gay et al. "Analysis of Factors Influencing the Mechanical Properties of Flat PolyJet Manufactured Parts". In: *Procedia Engineering* 132 (2015), pp. 70–77. DOI: 10.1016/j.proeng.2015.12.481.

[116] Thomas S. Lumpe, Jochen Mueller, and Kristina Shea. "Tensile properties of multi-material interfaces in 3D printed parts". In: *Materials & Design* 162 (Jan. 2019), pp. 1–9. DOI: 10.1016/j.matdes.2018.11.024.

[117] Yang Yang, Yingtian Li, and Yonghua Chen. "Principles and methods for stiffness modulation in soft robot design and development". In: *Bio-Design and Manufacturing* 1.1 (Mar. 2018), pp. 14–25. DOI: 10.1007/s42242-018-0001-6.

[118] Mariangela Manti, Vito Cacucciolo, and Matteo Cianchetti. "Stiffening in Soft Robotics: A Review of the State of the Art". In: *IEEE Robotics & Automation Magazine* 23.3 (Sept. 2016), pp. 93–106. DOI: 10.1109/MRA.2016.2582718.

[119] Heinrich Jaeger. "Soft Matter Celebrating Soft Matter's 10th Anniversary: Toward jamming by design". In: *Soft Matter* 11.12 (2015), pp. 12–27. DOI: 10.1039/c4sm01923g.

[120] Eric Brown et al. "Universal robotic gripper based on the jamming of granular material". In: *Proceedings of the National Academy of Sciences* 107.44 (Nov. 2010), pp. 18809–18814. DOI: 10.1073/pnas.1003250107.

[121] Seth G. Fitzgerald, Gary W. Delaney, and David Howard. "A Review of Jamming Actuation in Soft Robotics". In: *Actuators* 9.4 (Oct. 2020), p. 104. DOI: 10.3390/act9040104.

[122] Elliot Thompson-Bean, Oliver Steiner, and Andrew McDaid. "A soft robotic exoskeleton utilizing granular jamming". In: *2015 IEEE International Conference on Advanced Intelligent Mechatronics (AIM)*. Vol. 2015-Augus. IEEE, July 2015, pp. 165–170. DOI: 10.1109/AIM.2015.7222526.

[123] Maria Elena Giannaccini et al. "Novel Design of a Soft Lightweight Pneumatic Continuum Robot Arm with Decoupled Variable Stiffness and Positioning". In: *Soft Robotics* 5.1 (Feb. 2018), pp. 54–70. DOI: 10.1089/soro.2016.0066.

[124] S P Murali Babu et al. "Antagonistic Pneumatic Actuators with Variable Stiffness for Soft Robotic Applications". In: *2019 2nd IEEE International Conference on Soft Robotics (RoboSoft)*. IEEE, Apr. 2019, pp. 283–288. DOI: 10.1109/ROBOSOFT.2019.8722803.

[125] Yaohui Chen et al. "Pneumatic actuation-based bidirectional modules with variable stiffness and closed-loop position control". In: *2021 IEEE International Conference on Robotics and Automation (ICRA)*. Vol. 2021-May. Icra. IEEE, May 2021, pp. 6797–6803. DOI: 10.1109/ICRA48506.2021.9561576.

[126] Oliver Shorthose et al. "Design of a Multimaterial 3D-Printed Soft Actuator with Bidirectional Variable Stiffness". In: *Annual Conference Toward Autonomous Robotics Systems*. Vol. 13054 LNAI. Springer, 2021, pp. 238–248. DOI: 10.1007/978-3-030-89177-0_25.

[127] Jianshu Zhou et al. "A Soft-Robotic Approach to Anthropomorphic Robotic Hand Dexterity". In: *IEEE Access* 7 (2019), pp. 101483–101495. DOI: 10.1109/ACCESS.2019.2929690.

[128] Thomas Feix et al. "The GRASP Taxonomy of Human Grasp Types". In: *IEEE Transactions on Human-Machine Systems* 46.1 (2016), pp. 66–77. DOI: 10.1109/THMS.2015.2470657.

[129] Antonio Bicchi. “Hands for dexterous manipulation and robust grasping: a difficult road toward simplicity”. In: *IEEE Transactions on Robotics and Automation* 16.6 (2000), pp. 652–662. DOI: 10.1109/70.897777.

[130] Vincent Mendez et al. “Current Solutions and Future Trends for Robotic Prosthetic Hands”. In: *Annual Review of Control, Robotics, and Autonomous Systems* 4.1 (May 2021), pp. 595–627. DOI: 10.1146/annurev-control-071020-104336.

[131] Tsuneo Yoshikawa. “Multifingered robot hands: Control for grasping and manipulation”. In: *Annual Reviews in Control* 34.2 (Dec. 2010), pp. 199–208. DOI: 10.1016/j.arcontrol.2010.09.001.

[132] Visakha K. Nanayakkara et al. “The Role of Morphology of the Thumb in Anthropomorphic Grasping: A Review”. In: *Frontiers in Mechanical Engineering* 3.June (June 2017). DOI: 10.3389/fmech.2017.00005.

[133] Nikolaus Correll et al. “Analysis and observations from the first amazon picking challenge”. In: *IEEE Transactions on Automation Science and Engineering* 15.1 (2016), pp. 172–188.

[134] Gill Pratt and Justin Manzo. “The DARPA Robotics Challenge [Competitions]”. In: *IEEE Robotics & Automation Magazine* 20.2 (2013), pp. 10–12. DOI: 10.1109/MRA.2013.2255424.

[135] Yu Sun et al. “Robotic Grasping and Manipulation Competition: Task Pool”. In: *Robotic Grasping and Manipulation*. Ed. by Yu Sun and Joe Falco. Cham: Springer International Publishing, 2018, pp. 1–18. DOI: 10.1007/978-3-319-94568-2_1.

[136] Jianshu Zhou et al. “50 Benchmarks for Anthropomorphic Hand Function-based Dexterity Classification and Kinematics-based Hand Design”. In: *2020 IEEE/RSJ*

International Conference on Intelligent Robots and Systems (IROS). IEEE, Oct. 2020, pp. 9159–9165. DOI: 10.1109/IROS45743.2020.9340982.

[137] Jan Fras and Kaspar Althoefer. "Soft Biomimetic Prosthetic Hand: Design, Manufacturing and Preliminary Examination". In: *2018 IEEE/RSJ International Conference on Intelligent Robots and Systems (IROS)*. IEEE, Oct. 2018, pp. 1–6. DOI: 10.1109/IROS.2018.8593666.

[138] Haihang Wang et al. "A Novel Soft Robotic Hand Design With Human-Inspired Soft Palm: Achieving a Great Diversity of Grasps". In: *IEEE Robotics & Automation Magazine* 28.2 (June 2021), pp. 37–49. DOI: 10.1109/MRA.2021.3065870.

[139] Guoying Gu et al. "A soft neuroprosthetic hand providing simultaneous myoelectric control and tactile feedback". In: *Nature Biomedical Engineering* (Aug. 2021). DOI: 10.1038/s41551-021-00767-0.

[140] Barry C. Stillman. "Making Sense of Proprioception". In: *Physiotherapy* 88.11 (Nov. 2002), pp. 667–676. DOI: 10.1016/S0031-9406(05)60109-5.

[141] Ludovic Righetti et al. "An autonomous manipulation system based on force control and optimization". In: *Autonomous Robots* 36.1-2 (Jan. 2014), pp. 11–30. DOI: 10.1007/s10514-013-9365-9.

[142] Wenbin Chen et al. "Fabrication and Dynamic Modeling of Bidirectional Bending Soft Actuator Integrated with Optical Waveguide Curvature Sensor". In: *Soft Robotics* 6.4 (Aug. 2019), pp. 495–506. DOI: 10.1089/soro.2018.0061.

[143] Tim Helps and Jonathan Rossiter. "Proprioceptive Flexible Fluidic Actuators Using Conductive Working Fluids". In: *Soft Robotics* 5.2 (Apr. 2018), pp. 175–189. DOI: 10.1089/soro.2017.0012.

[144] Runze Zuo et al. “A Soft Robotic Gripper with Anti-Freezing Ionic Hydrogel-Based Sensors for Learning-Based Object Recognition”. In: *2021 IEEE International Conference on Robotics and Automation (ICRA)*. Vol. 2021-May. Icra. IEEE, May 2021, pp. 12164–12169. DOI: 10.1109/ICRA48506.2021.9561287.

[145] Luca Scimeca et al. “Model-free soft-structure reconstruction for proprioception using tactile arrays”. In: *IEEE Robotics and Automation Letters* 4.3 (2019), pp. 2479–2484.

[146] Bianca S. Homberg et al. “Robust proprioceptive grasping with a soft robot hand”. In: *Autonomous Robots* 43.3 (2019), pp. 681–696. DOI: 10.1007/s10514-018-9754-1.

[147] Yadong Yan et al. “Texture Identification and Object Recognition Using a Soft Robotic Hand Innervated Bio-Inspired Proprioception”. In: *Machines* 10.3 (Feb. 2022), p. 173. DOI: 10.3390/machines10030173.

[148] Qiang Zou, Yaodong Wang, and Fengrui Yang. “An intrinsically embedded pressure-temperature dual-mode soft sensor towards soft robotics”. In: *Sensors and Actuators A: Physical* 332 (Dec. 2021), p. 113084. DOI: 10.1016/j.sna.2021.113084.

[149] Peter Roberts, Mason Zadan, and Carmel Majidi. “Soft Tactile Sensing Skins for Robotics”. In: *Current Robotics Reports* 2.3 (July 2021), pp. 343–354. DOI: 10.1007/s43154-021-00065-2.

[150] Xiandi Wang et al. “Recent Progress in Electronic Skin”. In: *Advanced Science* 2.10 (Oct. 2015), p. 1500169. DOI: 10.1002/advs.201500169.

[151] Raunaq Bhirangi et al. “All the Feels: A dexterous hand with large area sensing”. In: (Oct. 2022). arXiv: 2210.15658. URL: http://arxiv.org/abs/2210.15658.

[152] Zhen Deng et al. “Grasping Force Control of Multi-Fingered Robotic Hands through Tactile Sensing for Object Stabilization”. In: *Sensors* 20.4 (Feb. 2020), p. 1050. DOI: 10.3390/s20041050.

[153] Liang He et al. “Soft Fingertips with Tactile Sensing and Active Deformation for Robust Grasping of Delicate Objects”. In: *IEEE Robotics and Automation Letters* 5.2 (2020), pp. 2714–2721. DOI: 10.1109/LRA.2020.2972851.

[154] Charbel Tawk et al. “Design, Modeling and Control of a 3D Printed Monolithic Soft Robotic Finger with Embedded Pneumatic Sensing Chambers”. In: *IEEE/ASME Transactions on Mechatronics* 4435.c (July 2020), pp. 1–1. DOI: 10.1109/TMECH.2020.3009365.

[155] Hui Yang et al. “A novel pneumatic soft sensor for measuring contact force and curvature of a soft gripper”. In: *Sensors and Actuators A: Physical* 266 (Oct. 2017), pp. 318–327. DOI: 10.1016/j.sna.2017.09.040.

[156] Xiaolong Ma et al. “Sensor Embedded Soft Fingertip for Precise Manipulation and Softness Recognition”. In: *IEEE Robotics and Automation Letters* 6.4 (Oct. 2021), pp. 8734–8741. DOI: 10.1109/LRA.2021.3115156.

[157] Chandana Paul. “Morphological computation”. In: *Robotics and Autonomous Systems* 54.8 (Aug. 2006), pp. 619–630. DOI: 10.1016/j.robot.2006.03.003.

[158] Rolf Pfeifer and Christian Scheier. *Understanding intelligence*. MIT press, 2001.

[159] Markellos Ntagios et al. “Robotic Hands with Intrinsic Tactile Sensing via 3D Printed Soft Pressure Sensors”. In: *Advanced Intelligent Systems* 2.6 (June 2020), p. 1900080. DOI: 10.1002/aisy.201900080.

[160] Benjamin Shih et al. “Design Considerations for 3D Printed, Soft, Multimaterial Resistive Sensors for Soft Robotics”. In: *Frontiers in Robotics and AI* 6.APR (Apr. 2019), p. 30. DOI: 10.3389/frobt.2019.00030.

[161] Oliver Shorthose et al. “Design of a 3D-Printed Soft Robotic Hand With Integrated Distributed Tactile Sensing”. In: *IEEE Robotics and Automation Letters* 7.2 (Apr. 2022), pp. 3945–3952. DOI: 10.1109/LRA.2022.3149037.

[162] David Howard et al. “Shape, Size, and Fabrication Effects in 3D Printed Granular Jamming Grippers”. In: *2021 IEEE 4th International Conference on Soft Robotics (RoboSoft)*. IEEE, Apr. 2021, pp. 458–464. DOI: 10.1109/RoboSoft51838.2021.9479438.

[163] Allen Jiang et al. “A Variable Stiffness Joint by Granular Jamming”. In: *Volume 4: 36th Mechanisms and Robotics Conference, Parts A and B*. Vol. 4. PARTS A AND B. American Society of Mechanical Engineers, Aug. 2012, pp. 267–275. DOI: 10.1115/DETC2012-70670.

[164] Vincent Wall, Raphael Deimel, and Oliver Brock. “Selective stiffening of soft actuators based on jamming”. In: *2015 IEEE International Conference on Robotics and Automation (ICRA)*. Vol. 2015-June. June. IEEE, May 2015, pp. 252–257. DOI: 10.1109/ICRA.2015.7139008.

[165] Gabriel Robles-De-La-Torre. “The Importance of the Sense of Touch in Virtual and Real Environments”. In: *IEEE Multimedia* 13.3 (July 2006), pp. 24–30. DOI: 10.1109/MMUL.2006.69.

[166] R.S. Dahiya et al. “Tactile Sensing—From Humans to Humanoids”. In: *IEEE Transactions on Robotics* 26.1 (Feb. 2010), pp. 1–20. DOI: 10.1109/TRO.2009.2033627.

[167] Soledad Ballesteros and Morton A. Heller. “Haptic object identification”. In: *Human Haptic Perception: Basics and Applications*. Basel: Birkhäuser Basel, 2008, pp. 207–222. DOI: 10.1007/978-3-7643-7612-3_16.

[168] Li Liu et al. “Deep Learning for Generic Object Detection: A Survey”. In: *International Journal of Computer Vision* 128.2 (2020), pp. 261–318. DOI: 10.1007/s11263-019-01247-4. eprint: 1809.02165.

[169] Guozhen Li et al. “Skin-inspired quadruple tactile sensors integrated on a robot hand enable object recognition”. In: *Science Robotics* 5.49 (Dec. 2020), pp. 1–12. DOI: 10.1126/scirobotics.abc8134.

[170] Farshad Khadivar et al. “Online active and dynamic object shape exploration with a multi-fingered robotic hand”. In: *Robotics and Autonomous Systems* 166 (Aug. 2023), p. 104461. DOI: 10.1016/j.robot.2023.104461.

[171] Aude Billard and Danica Kragic. “Trends and challenges in robot manipulation”. In: *Science* 364.6446 (June 2019). DOI: 10.1126/science.aat8414.

[172] Lillian Chin et al. “Automated recycling separation enabled by soft robotic material classification”. In: *RoboSoft 2019 - 2019 IEEE International Conference on Soft Robotics* (2019), pp. 102–107. DOI: 10.1109/ROBOSOFT.2019.8722747.

[173] Arti Patle and Deepak Singh Chouhan. “SVM kernel functions for classification”. In: *2013 International Conference on Advances in Technology and Engineering, ICATE 2013* (2013), pp. 1–9. DOI: 10.1109/ICAdTE.2013.6524743.

[174] Nitin Bhatia and Vandana. “Survey of Nearest Neighbor Techniques”. In: 8.2 (July 2010), pp. 302–305. arXiv: 1007.0085.

[175] Stephen Notley and Malik Magdon-Ismail. "Examining the Use of Neural Networks for Feature Extraction: A Comparative Analysis using Deep Learning, Support Vector Machines, and K-Nearest Neighbor Classifiers". In: (May 2018). arXiv: 1805.02294.

[176] Satoshi Funabashi et al. "Morphology-Specific Convolutional Neural Networks for Tactile Object Recognition with a Multi-Fingered Hand". In: *2019 International Conference on Robotics and Automation (ICRA)*. Vol. 2019-May. 50185. IEEE, May 2019, pp. 57–63. DOI: 10.1109/ICRA.2019.8793901.

[177] Yuzhu Ji et al. "CNN-based encoder-decoder networks for salient object detection: A comprehensive review and recent advances". In: *Information Sciences* 546 (Feb. 2021), pp. 835–857. DOI: 10.1016/j.ins.2020.09.003.

[178] Kaiming He et al. "Deep residual learning for image recognition". In: *Proceedings of the IEEE conference on computer vision and pattern recognition*. 2016, pp. 770–778.

[179] Karen Simonyan and Andrew Zisserman. "Very Deep Convolutional Networks for Large-Scale Image Recognition". In: *3rd International Conference on Learning Representations, ICLR 2015 - Conference Track Proceedings* (Sept. 2014), pp. 1–14. arXiv: 1409.1556.

[180] Christian Szegedy et al. "Going deeper with convolutions". In: *Proceedings of the IEEE conference on computer vision and pattern recognition*. 2015, pp. 1–9.

[181] Peter J. Rousseeuw. "Silhouettes: A graphical aid to the interpretation and validation of cluster analysis". In: *Journal of Computational and Applied Mathematics* 20.C (Nov. 1987), pp. 53–65. DOI: 10.1016/0377-0427(87)90125-7.

[182] Oliver Shorthose et al. "EDAMS: An Encoder-Decoder Architecture for Multi-grasp Soft Sensing Object Recognition". In: *2023 IEEE International Conference on Soft Robotics (RoboSoft)*. IEEE. 2023.

[183] Berk Calli et al. “Benchmarking in Manipulation Research: Using the Yale-CMU-Berkeley Object and Model Set”. In: *IEEE Robotics & Automation Magazine* 22.3 (Sept. 2015), pp. 36–52. DOI: 10.1109/MRA.2015.2448951.

[184] Jason Brownlee. *Impact of Dataset Size on Deep Learning Model Skill And Performance Estimates*. Machine Learning Mastery. Jan. 2019.

[185] Hyun-il Lim. “A Study on Dropout Techniques to Reduce Overfitting in Deep Neural Networks”. In: *Advanced Multimedia and Ubiquitous Engineering*. Springer Singapore, 2021, pp. 133–139. DOI: 10.1007/978-981-15-9309-3_20.

[186] Christian Garbin, Xingquan Zhu, and Oge Marques. “Dropout vs. batch normalization: an empirical study of their impact to deep learning”. In: *Multimedia Tools and Applications* 79.19-20 (May 2020), pp. 12777–12815. DOI: 10.1007/s11042-019-08453-9.

[187] Xue Ying. “An Overview of Overfitting and its Solutions”. In: *Journal of Physics: Conference Series* 1168.2 (Feb. 2019), p. 022022. DOI: 10.1088/1742-6596/1168/2/022022.

[188] J. J. Hopfield. “Neural networks and physical systems with emergent collective computational abilities.” In: *Proceedings of the National Academy of Sciences* 79.8 (Apr. 1982), pp. 2554–2558. DOI: 10.1073/pnas.79.8.2554.

[189] Guanbin Li et al. “Flow Guided Recurrent Neural Encoder for Video Salient Object Detection”. In: *2018 IEEE/CVF Conference on Computer Vision and Pattern Recognition*. IEEE, June 2018, pp. 3243–3252. DOI: 10.1109/CVPR.2018.00342.

[190] Ming Liang and Xiaolin Hu. “Recurrent convolutional neural network for object recognition”. In: *2015 IEEE Conference on Computer Vision and Pattern Recognition (CVPR)*. IEEE, June 2015, pp. 3367–3375. DOI: 10.1109/CVPR.2015.7298958.

[191] Mahreen Zainab et al. “FPGA Based Implementations of RNN and CNN: A Brief Analysis”. In: *3rd International Conference on Innovative Computing, ICIC 2019* Icic (2019). DOI: 10.1109/ICIC48496.2019.8966676.

[192] Jiuxiang Gu et al. “Recent advances in convolutional neural networks”. In: *Pattern Recognition* 77 (May 2018), pp. 354–377. DOI: 10.1016/j.patcog.2017.10.013.

[193] “ASTM D638 - Standard test method for tensile properties of plastics 1”. In: *Open J. Compos. Mater.* 3 (2006), pp. 1–15. DOI: 10.1520/D0638-14.

[194] Vaughan Pratt. “Direct least-squares fitting of algebraic surfaces”. In: *ACM SIGGRAPH Computer Graphics* 21.4 (Aug. 1987), pp. 145–152. DOI: 10.1145/37402.37420.

[195] Nikolai Chernov. “Circle Fit (Pratt method)”. In: (2009), p. 1. URL: https://uk.mathworks.com/matlabcentral/fileexchange/22643-circle-fit-pratt-method.

[196] G. I. Bain et al. “The functional range of motion of the finger joints”. In: *Journal of Hand Surgery (European Volume)* 40.4 (May 2015), pp. 406–411. DOI: 10.1177/1753193414533754.

Appendix to Chapter 2

A.1 Material Characterisation

Material characterisation was undertaken to assess the mechanical properties of the materials used in the fabrication of the soft hand. The materials used were the digital materials provided by the Stratasys J735 printer. The materials were tested in accordance with ASTM D638-14 [193] using an Instron Universal Testing Machine. The strain rate was set at $1 mm/mm \cdot min$ and the setup is shown in Fig. A1a. The test specimen geometry is shown in Fig. A1b and the stress/strain results of the testing are shown in Figure A2. The calculated Young's modulus for each material was significantly lower than the values provided by the manufacturer [109–111] but comparable with similar work in the literature [107, 113]. The tensile stress was generally lower and the strain at break was higher than the quoted values. These values were then used to inform the simulations presented in Chap. 2.

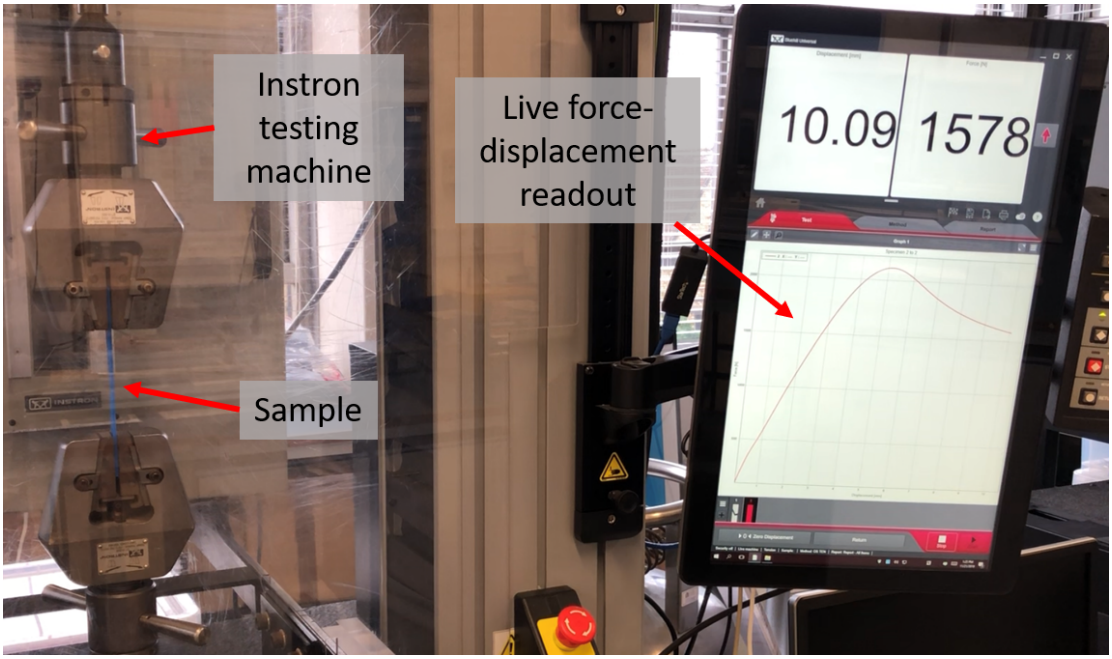

(a)

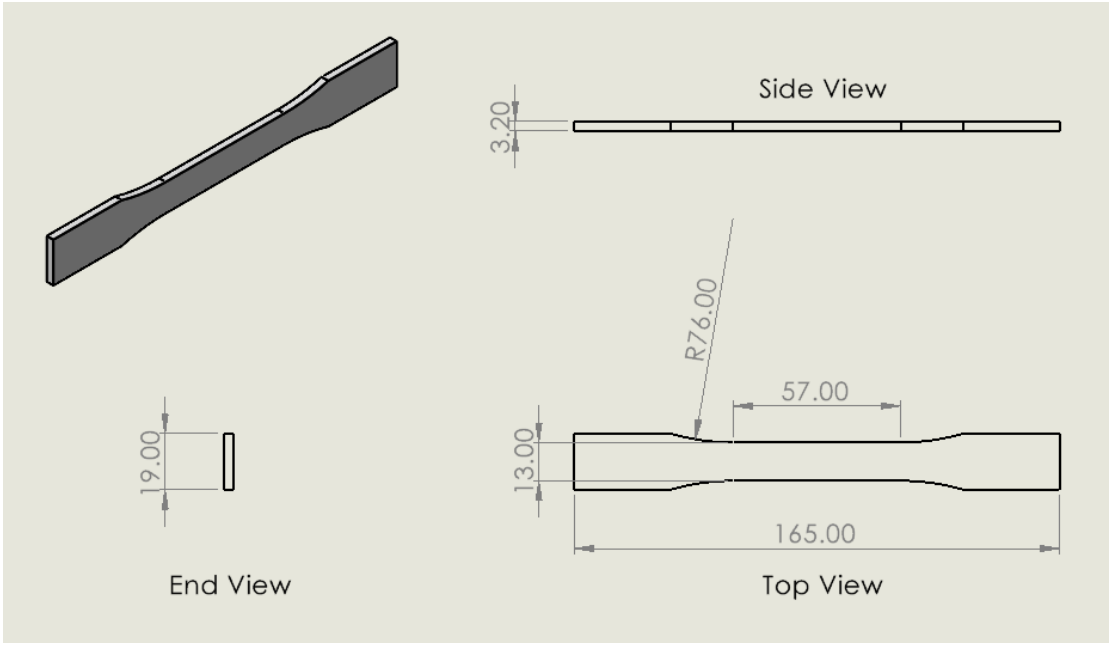

(b)

Figure A1: (a) Setup of the Instron Universal Testing Machine for tensile testing. (b) Dogbone dimensions used in material characterisation in accordance with ASTM D638-14.

In Fig. A2 and Tables. A1 & A2, ‘long’ refers to the test pieces printed longitudinally to the print head direction; ‘tran’ refers to the pieces printed transverse to the print head direction. The difference between those reflect what was presented from the literature in Sec. 2.2.2 and those printed longitudinally generally have a higher tensile strength than those printed transverse. The entries for pure Vero in Fig. A2 have been excluded because they populate a different Shore scale of hardness, but the tabulated values can be found in Table A1.

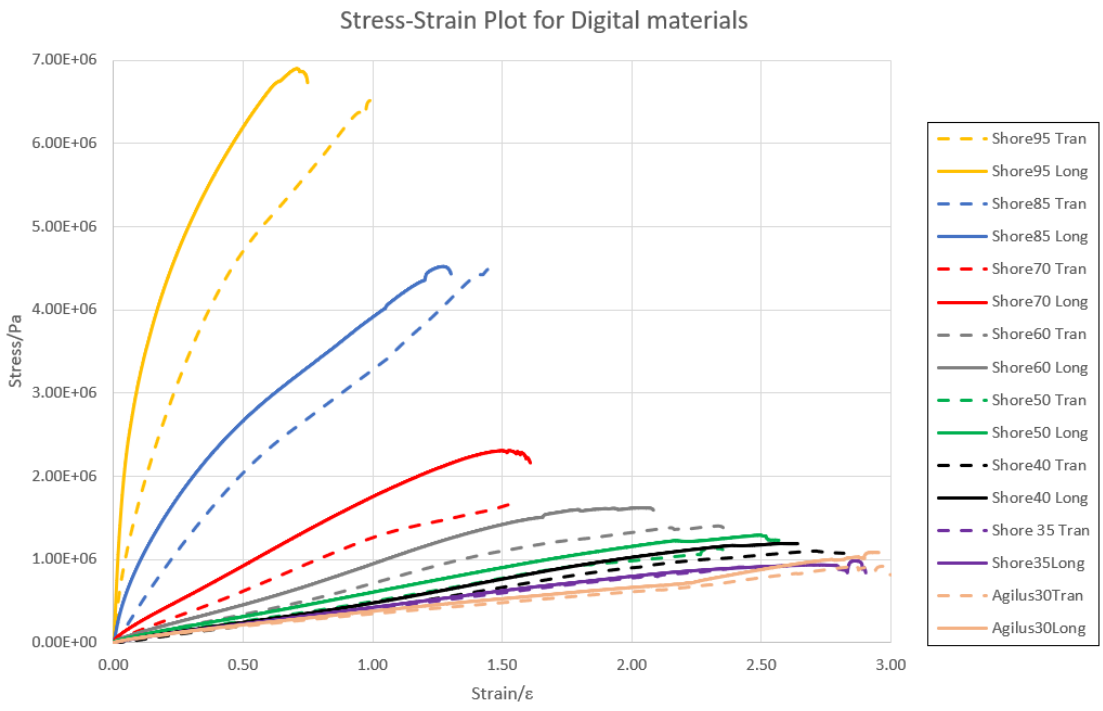

Figure A2: Results of the tensile testing of the digital materials provided by the Stratasys J735 Printer. A blend of VeroCyan and Agilus30 were used in each sample.

Material	**Orientation**	**Quoted Tensile Strength (MPa)**	**Measured Tensile Strength (MPa)**
VeroCyan	Tran	58.0	51.6
VeroCyan	Long	58.0	52.3
Shore95	Tran	12.0	6.52
Shore95	Long	12.0	6.90
Shore85	Tran	8.0	4.62
Shore85	Long	8.0	4.52
Shore70	Tran	5.0	1.70
Shore70	Long	5.0	2.31
Shore60	Tran	4.0	1.40
Shore60	Long	4.0	1.62
Shore50	Tran	3.5	1.13
Shore50	Long	3.5	1.30
Shore40	Tran	3.0	1.11
Shore40	Long	3.0	1.20
Shore35	Tran	2.9	0.95
Shore35	Long	2.9	0.99
Agilus30	Tran	2.7	1.08
Agilus30	Long	2.7	0.92

Table A1

Material	**Orientation**	**Quoted Strain at Break** (mm/mm)	**Measured Strain at Break** (mm/mm)
VeroCyan	Tran	0.2	0.85
VeroCyan	Long	0.2	0.10
Shore95	Tran	0.6	0.99
Shore95	Long	0.6	0.70
Shore85	Tran	0.8	1.44
Shore85	Long	0.8	1.27
Shore70	Tran	1.3	1.56
Shore70	Long	1.3	1.52
Shore60	Tran	1.6	2.33
Shore60	Long	1.6	2.03
Shore50	Tran	1.9	2.33
Shore50	Long	1.9	2.49
Shore40	Tran	2.0	2.70
Shore40	Long	2.0	2.56
Shore35	Tran	2.1	2.65
Shore35	Long	2.1	2.84
Agilus30	Tran	2.5	2.96
Agilus30	Long	2.5	2.93

Table A2

A.2 Identification of the Actuator Shape

As briefly discussed in [126], the actuated shape of the actuator is approximated to be circular. The shape was identified through the use of snapshots taken from a webcam. The identification process is shown in Fig. A3. First, the RGB channels are respectively isolated from the snapshot and the darkest regions were identified to provide a binary image. The 'dark' region is calibrated by selecting a threshold in the lighting conditions that isolates the markers without including the background or supports. The *AND* logical operator is applied to the three channel images to return only the darkest areas. This combined image is then filtered to fill in small holes and regions that arise from noise using the disc-shaped structuring element for the *imclose* function in MATLAB's *Image Processing Toolbox* and then *imfill* to remove any further outlying regions. The largest N regions in the image are then identified using the *bwareafilt*. The centroids of these regions are calculated and fit to a circular shape using the method proposed by Pratt [194]. By calculating the angle subtended between the first and last markers, we acquire the output angle of the actuator.

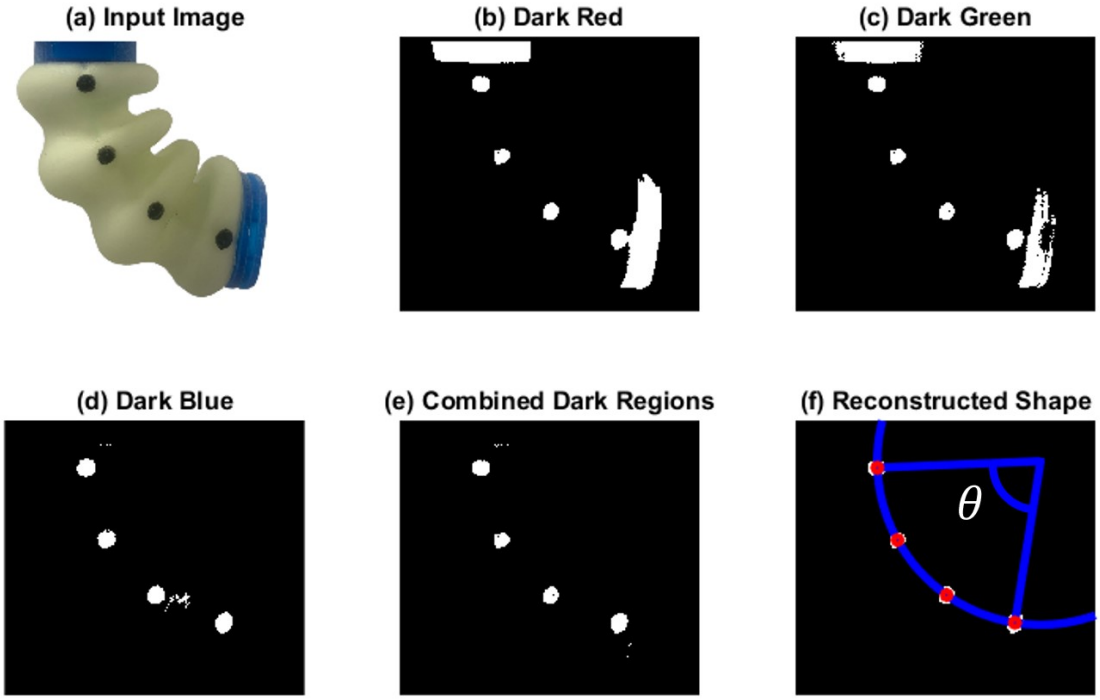

Figure A3: The process of identifying the shape of the actuator. (a) A snapshot is taken by the affixed webcam. (b-d) The darkest regions of the RGB channels are isolated and converted to binary images. (e) The binary images are combined using the logical *AND* function. (f) The combined image is filtered to remove noise and small regions then the centroids of each region are calculated and fit to a circular shape.

MATLAB Code for Shape Detection

The code for fitting a circular shape to the actuator is presented below and *CircleFitByPratt* is taken from [195]:

```
function [angle] = IdentifyByColourAndCurvature(cam)
    rgb = snapshot(camera);
    threshold = 75; %Calibrated threshold for the lighting
       conditions
```

```
% Identify the darkest patches of each colour channel
   with lower threshold for the red and green channels,
    which are generally noisier
darkRed = rgb(:,:,1)<(threshold-15);
darkGreen = rgb(:,:,2)<(threshold-15);
darkBlue = rgb(:,:,3)<threshold;

% Black spots will be the combined dark patches of each
    channel
darkSpots = darkRed & darkBlue & darkGreen;

% Fill in small holes that have appeared
se = strel('disk',3, 0);
BW = imclose(darkSpots,se);
BW = imfill(BW,'holes');

% Isolate 4 largest regions (the 4 drawn on dots)
BW = bwareafilt(BW, 4, 'largest');

% Find the boundaries of the dots and sort them by
   their y location
[B,L,N,A] = bwboundaries(BW,'noholes');
boundaryCentroids = zeros(length(B),2);
for k=1:length(B)
    boundaryCentroids(k,:) = [mean(B{k}(:,1));
```

```
                                    mean(B{k}(:,2))];
    end
    if size(boundaryCentroids) >1
        boundaryCentroids = sortrows(boundaryCentroids);
        Par = CircleFitByPratt(boundaryCentroids);
        angle = Par(4);
    else
        return
    end

    % Code to view the identified regions to produce Fig.A3
    figure;
    subplot(2,3,1); imshow(rgb)
    subplot(2,3,2); imshow(darkRed);
    subplot(2,3,3); imshow(darkGreen);
    subplot(2,3,4); imshow(darkBlue);
    subplot(2,3,5); imshow(darkSpots);
    % Plot the identified regions and the fitted circle
    subplot(2,3,6); hold on;
    plotCircle(Par,boundaryCentroids(1,:),boundaryCentroids
       (end,:));
    plot(boundaryCentroids(:,2),boundaryCentroids(:,1),'ow'
       ,'MarkerSize',6,'LineWidth',3);

end
```

```
function plotCircle(params,topDot,bottomDot)
    %extract variables from the inputs - centre and radius
       of circle
    yCentre = params(1);
    xCentre = params(2);
    r = params(3);

    %make lines from the centroid to the top and bottom
       boundaries found
    topLine = [linspace(topDot(1),yCentre);linspace(topDot
       (2),xCentre)]';
    bottomLine = [linspace(bottomDot(1),yCentre);linspace(
       bottomDot(2),xCentre)]';

    ang=0:0.01:2*pi;
    xp=r*cos(ang);
    yp=r*sin(ang);
    plot(xCentre+xp,yCentre+yp,'Color','b','LineWidth',4);
       %[0.3010 0.9 0.9]
    plot(topLine(:,2),topLine(:,1),'Color','b','LineWidth'
       ,4); %[0.3010 0.9 0.9]
    plot(bottomLine(:,2),bottomLine(:,1),'Color','b','
       LineWidth',4); %[0.3010 0.9 0.9]
end
```

Appendices to Chapter 3

B.1 Soft Hand Kinematics

In Sec. 3.1, we introduced the design of a soft hand based on human-like kinematics and soft-material-enabled adaptability. The kinematics of the hand were primarily taken from sources such as [59, 196] and provided us with the target joint ranges for each finger. We simplified this model to target at least 74° for each joint. In addition, we wanted to examine the range of motion of with active DOFs in the STT and MCP joints of the thumb to achieve the requisite poses of the Kapandji thumb opposition test and the benefits afforded to grasping through this ROM [132]. In order to simulate this motion in the context of a hand, we designed a rigid bodied kinematic model that can be seen in Fig. A4. This model was formulated in MATLAB, and allowed us to validate the proposed ROM of each of the hand's joints.

The Kapandji test requires that we can touch each fingertip and then each joint in the pinky finger. It is used in neurology to test the opposition and reposition of the mobility of the thumb in the case of nervous damage or otherwise. Within robotics, it is commonly used to provide a good indication of the dexterity of the hand. Fig. A4 shows the simulated workspace with the thumb reaching each of the fingertips under each respective configuration. Successfully contacting each requisite position allowed us to proceed with designing the joints to achieve those angles. The realised version of each of these poses is presented in the paper in Sec. 3.3.

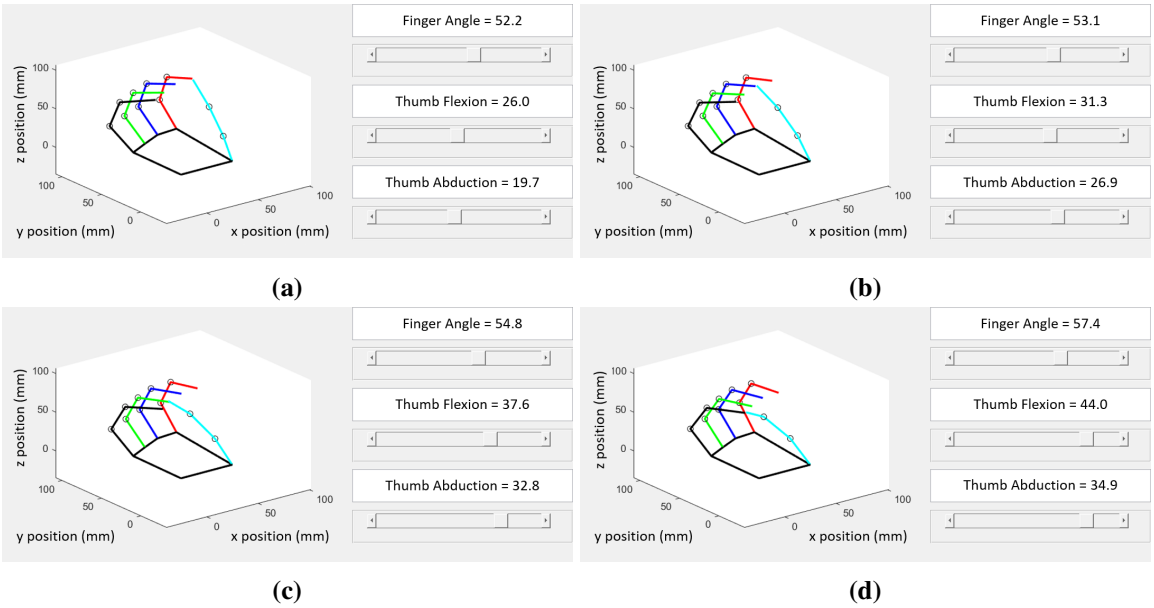

Figure A4: Kinematic foundations of the soft hand in the context of the Kapandji thumb opposition test. (a) Index finger. (b) Middle finger. (c) Ring finger. (d) Pinky finger.

MATLAB Code for Hand Kinematics

The code used to simulate and present the kinematics in MATLAB is presented below. The joint angles were taken from [59, 196]:

```
f = figure;
hboxAxes = uix.HBox('Parent',f,'Spacing',3);
axes1 = axes( 'Parent',hboxAxes, '
   ActivePositionProperty', 'outerposition' );
view(3)
%plot joint paths
%plot(J1)
hold on
xyz = gca;
xyz.YLim = [-50; 200];
```

```
xyz.XLim = [-50; 200];
xyz.ZLim = [-50; 200];
xyz.XLabel.String = 'x position (mm)';
xyz.YLabel.String = 'y position (mm)';
xyz.ZLabel.String = 'z position (mm)';

%On the right side of the panel, add a VBox that hosts
   sliders with boxes that update their angles
vboxSlide1 = uix.VBox('Parent',hboxAxes,'Spacing',10);
t1 = uicontrol('style','edit','Parent',vboxSlide1,'
   Position',[10,60,40,40]);
p1 = uipanel(vboxSlide1);
h1 = uicontrol(p1,'Style', 'slider',...
     'String', 'MCP Flexion',...
     'Min',0,'Max',87,...
     'Position', [20 20 250 20],...
     'Callback',{@su1});
set(t1,'String',strcat('Finger Angle = ','0'))
fun1 = @(~,e)set(t1,'String',strcat('Finger Angle = ',
   num2str(get(e.AffectedObject,'Value'))));
addlistener(h1,'Value','PostSet',fun1);

t2 = uicontrol('style','edit','Parent',vboxSlide1,'
   Position',[10,60,40,40]);
p2 = uipanel(vboxSlide1);
```

```
h2 = uicontrol(p2,'Style', 'slider',...
     'String', 'Thumb Flexion',...
     'Min',0,'Max',53,...
     'Position', [20 20 250 20],...
     'Callback',{@su2});
set(t2,'String',strcat('Thumb Flexion = ','0'))
fun2 = @(~,e)set(t2,'String',strcat('Thumb Flexion = ',
   num2str(get(e.AffectedObject,'Value'))));
addlistener(h2,'Value','PostSet',fun2);

t3 = uicontrol('style','edit','Parent',vboxSlide1,'
   Position',[10,60,40,40]);
p3 = uipanel(vboxSlide1);
h3 = uicontrol(p3,'Style', 'slider',...
     'String', 'Thumb Abduction',...
     'Min',0,'Max',42,...
     'Position', [20 20 250 20],...
     'Callback',{@su2});
set(t3,'String',strcat('Thumb Abduction = ','0'))
fun3 = @(~,e)set(t3,'String',strcat('Thumb Abduction =
   ',num2str(get(e.AffectedObject,'Value'))));
addlistener(h3,'Value','PostSet',fun3);

% Scale the various GUI elements to improve
   presentation
```

```
f.Position = [488 342 800 420];
set( hboxAxes, 'Widths', [-3 300]);
set( vboxSlide1, 'Heights', [ 45 45 45 45 45 45 ]);
sectionLength = 35;
theta = linspace(0,2*pi,360);
s = sin(theta);
c = cos(theta);

global jointsA
global thumb
global fingerA
global fingerB
global fingerC
global fingerD

% J1: MCP, J2: PIP, J3: DIP, J4: end of finger
% Setup the possible configurations of each joint
   position for all values of theta.
% jointsA.Jn defines where each joint will be under the
    given value of theta
jointsA = struct('J1',[],'J2',[],'J3',[],'J4',[]);
for k = 1:size(theta,2)/3
    jointsA.J1(:,k) = [0;0];
    jointsA.J2(:,k) = [ jointsA.J1(1,k) + c(k)*
       sectionLength;
```

```
                jointsA.J1(2,k) + s(k)*sectionLength];
        jointsA.J3(:,k) = [ jointsA.J2(1,k) + c(2*k)*
            sectionLength;
                jointsA.J2(2,k) + s(2*k)*sectionLength];
        jointsA.J4(:,k) = [ jointsA.J3(1,k) + c(3*k)*(
            sectionLength);
                jointsA.J3(2,k) + s(3*k)*(sectionLength)];
    end

    guidata(h1,jointsA)

    % Set the starting pose as 0degrees (index 1)
    % pos is input to index from jointsA which angle will
       be chosen for each joint
    % baseFinger is the standard curved finger oriented at
       the origin. It is then translated and rotated to
       each finger's position in the moveFinger function
    pos = 1;
    baseFinger = findLines(pos,jointsA);
    [fingerA,fingerB,fingerC,fingerD] = moveFingers(
       baseFinger);
    thumb = moveThumb(baseFinger);

    % Plot bars with circles at the joints
    plotFingers(fingerA,fingerB,fingerC,fingerD)
```

```
plotThumb(thumb)
plotPalm()

function val = su1(h1,~)
    % This is the callback function for the first
       slider. It defines how the fingers will each be
       bent, given the position of the slider
    global thumb
    global fingerA
    global fingerB
    global fingerC
    global fingerD
    val = get(h1,'Value');
    val = round(val)+1;
    jointsA = guidata(h1);

    baseFinger = findLines(val,jointsA);
    [fingerA,fingerB,fingerC,fingerD] = moveFingers(
       baseFinger);

    % Remove the old lines and re-plot
    lines = h1.Parent.Parent.Parent.Children(2).
       Children;
    delete(lines)
    plotFingers(fingerA,fingerB,fingerC,fingerD)
```

```
        plotThumb(thumb)
        plotPalm()
    end
    function val = su2(h2,h3,~)
        % This is the callback function for the second and
           third sliders. It defines how the thumb will be
           flexed and abducted, given the position of the
           sliders
        global thumb
        global fingerA
        global fingerB
        global fingerC
        global fingerD

        %check if the gui is activated or it is trying to
           read the other sliders and reach the 'Source' if
            needed
        if strcmp(h2.String,'Thumb Flexion')%isprop(h3, '
           Source')
            val = get(h2,'Value');
            jointsA = guidata(h2);
            rot = get(h3.Source.Parent.Parent.Children(1).
               Children,'Value');
            %jointsB = guidata(h3.Source.Parent.Parent.
               Children(1).Children);
```

```
        elseif strcmp(h2.String,'Thumb Abduction')
            rot = get(h2,'Value');
            %jointsB = guidata(h2);
            val = get(h3.Source.Parent.Parent.Children(3).
               Children,'Value');
            jointsA = guidata(h3.Source.Parent.Parent.
               Children(3).Children);
        end
        val = round(val)+1;
        rot = round(rot)+1;

        baseThumb = findLines(val,jointsA);
        thumb = abductThumb(baseThumb,rot);
        thumb = moveThumb(thumb);
        lines = h2.Parent.Parent.Parent.Children(2).
           Children;
        delete(lines)
        plotThumb(thumb)
        plotFingers(fingerA,fingerB,fingerC,fingerD)
        plotPalm()
    end
    function bar = findLines(pos,joints)
        %Form the links by connecting each joint and then
           form it as a single array
```

```
        bar1 = [zeros(1,100);linspace(joints.J1(1,pos),
           joints.J2(1,pos));
            linspace(joints.J1(2,pos),joints.J2(2,pos))];
        bar2 = [zeros(1,100);linspace(joints.J2(1,pos),
           joints.J3(1,pos));
            linspace(joints.J2(2,pos),joints.J3(2,pos))];
        bar3 = [zeros(1,100);linspace(joints.J3(1,pos),
           joints.J4(1,pos));
            linspace(joints.J3(2,pos),joints.J4(2,pos))];
        bar = [bar1,bar2,bar3];
    end
    function [fingerA,fingerB,fingerC,fingerD] =
       moveFingers(oldFinger)
        % Translate the fingers based on the original
           finger
        % Finger A translation
        transA = [1,62,0];
        angleA = 21/180*pi;
        fingerA = transFing(oldFinger, transA, angleA);

        % Finger B translation
        transB = [20,72,0];
        angleB = pi/18;
        fingerB = transFing(oldFinger, transB, angleB);
```

```
    % Finger C translation
    transC = [40,82,0];
    angleC = 6/180*pi;
    fingerC = transFing(oldFinger, transC, angleC);

    % Finger D translation
    transD = [60,84,0];
    angleD = 0;
    fingerD = transFing(oldFinger, transD, angleD);
end
function thumb = moveThumb(baseFinger)
    % The base of the thumb is taken at the 0y but
       translated 50x. The angle of opposition is 35deg
    transT = [50,0,0];
    angleT = -35/180*pi;
    baseThumb = baseFinger;
    thumb = [ baseThumb(1,:)*cos(angleT) - baseThumb
       (2,:)*sin(angleT) + transT(1);...
        baseThumb(2,:)*cos(angleT) +  baseThumb(1,:)*
           sin(angleT) + transT(2);...
        baseThumb(3,:) + transT(3)];
end
function thumb = abductThumb(baseFinger,rot)
    transT = [0,0,0];
    angleT = rot/360*2*pi;
```

```
        baseThumb = baseFinger;
        thumb = [ baseThumb(1,:)*cos(angleT) - baseThumb
            (3,:)*sin(angleT) + transT(1);...
             baseThumb(2,:) + transT(2);...
             baseThumb(3,:)*cos(angleT) + baseThumb(1,:)*sin
                (angleT)+ transT(3)];
    end
    function plotFingers(fingerA,fingerB,fingerC,fingerD)

        lw = 2;
        plot3(fingerA(1,:),fingerA(2,:),fingerA(3,:),'k','
            LineWidth',lw)
        for fing=1:2
             plot3(fingerA(1,fing*100),fingerA(2,fing*100),
                fingerA(3,fing*100),'ok')
        end

        plot3(fingerB(1,:),fingerB(2,:),fingerB(3,:),'g','
            LineWidth',lw)
        for fing=1:2
             plot3(fingerB(1,fing*100),fingerB(2,fing*100),
                fingerB(3,fing*100),'ok')
        end
```

```
        plot3(fingerC(1,:),fingerC(2,:),fingerC(3,:),'b','
           LineWidth',lw)
        for fing=1:2
            plot3(fingerC(1,fing*100),fingerC(2,fing*100),
               fingerC(3,fing*100),'ok')
        end

        plot3(fingerD(1,:),fingerD(2,:),fingerD(3,:),'r','
           LineWidth',lw)
        for fing=1:2
            plot3(fingerD(1,fing*100),fingerD(2,fing*100),
               fingerD(3,fing*100),'ok')
        end
    end
    function plotThumb(thumb)
        lw =2;
        plot3(thumb(1,:),thumb(2,:),thumb(3,:),'c','
           LineWidth',lw)
        for fing=1:2
            plot3(thumb(1,fing*100),thumb(2,fing*100),thumb
               (3,fing*100),'ok')
        end
    end
    function newFinger = transFing(oldFinger, trans, angle)
```

```
        % Translate and rotate the finger based on the
           original finger
        newFinger = [ oldFinger(1,:)*cos(angle) -
           oldFinger(2,:)*sin(angle) + trans(1);...
            oldFinger(2,:)*cos(angle) + oldFinger(1,:)*sin(
               angle) + trans(2);...
            oldFinger(3,:) + trans(3)];
    end
    function plotPalm()
        % The main palm area does not move with the
           position of the sliders so does not require
           callback
        global thumb
        global fingerA
        global fingerB
        global fingerC
        global fingerD

        origin = [0;0;0];
        lw = 2;
        pinkyBase = fingerA(:,1);
        ringBase = fingerB(:,1);
        middleBase = fingerC(:,1);
        indexBase = fingerD(:,1);
        thumbBase = thumb(:,1);
```

```
        palm = [origin, pinkyBase, ringBase, middleBase,
            indexBase, thumbBase, origin];
        plot3(palm(1,:),palm(2,:),palm(3,:),'-k','LineWidth
            ',lw)
        plot([pinkyBase(1),ringBase(1)],[pinkyBase(2),
            ringBase(2)],'-k','LineWidth',lw)
        plot([ringBase(1),middleBase(1)],[ringBase(2),
            middleBase(2)],'-k','LineWidth',lw)
        plot([middleBase(1),indexBase(1)],[middleBase(2),
            indexBase(2)],'-k','LineWidth',lw)
        plot([indexBase(1),thumbBase(1)],[indexBase(2),
            thumbBase(2)],'-k','LineWidth',lw)
        plot([indexBase(1),thumbBase(1)],[indexBase(2),
            thumbBase(2)],'-k','LineWidth',lw)
    end
```